Real-World Wrist-Derived Digital Mobility Outcomes in People with Multiple Long-Term Conditions: A Comparison of Algorithms

Waterline Pile Cap Footings for Bridges using Large Diameter FRP Reinforcing – Material Characterization and Design

Contract Number: BEE76-977-01

Final Report

Prepared by:

Principal Investigator: Antonio Nanni, Ph.D., P.E.
Co-Principal Investigator: Francisco De Caso, Ph.D., LEED A.P.
Postdoctoral Associate: Alvaro Ruiz Emparanza, Ph.D., P.E.
Research Associate: Juan Manuel Palacios
Graduate Student: Mattia Mairone
Graduate Student: Khashayar Heydarpour

University of Miami
Department of Civil & Architectural Engineering
1251 Memorial Drive, McArthur Engineering Building, Rm. 325
Coral Gables, FL 33146-0630
nanni@miami.edu; (305) 284-3461

Project Manager:

Steven Nolan, P.E.
State Structures Design Office
605 Suwannee St, Tallahassee, FL 32399
steven.nolan@dot.state.fl.us; (850) 414-4272

Date: May 13, 2025

Disclaimer page

The opinions, findings, and conclusions expressed in this publication are those of the authors and not necessarily those of the Florida Department of Transportation.

Technical Report Documentation Page

1. Report No.	2. Government Accession No.	3. Recipient's Catalog No.
4. Title and Subtitle **Waterline Pile Cap Footings for Bridges using Large Diameter FRP Reinforcing – Material Characterization and Design**		5. Report Date March 2025 6. Performing Organization Code 55220000977
7. Author(s) Antonio Nanni, Ph.D., P.E. Francisco De Caso, Ph.D., LEED A.P. Alvaro Ruiz Emparanza, Ph.D., P.E. Juan Manuel Palacios Mattia Mairone Khashayar Heydarpour		8. Performing Organization Report No.
9. Performing Organization Name and Address University of Miami Department of Civil & Architectural Engineering 1251 Memorial Drive, McArthur Engineering Building, Rm. 325 Coral Gables, FL 33146-0630		10. Work Unit No. (TRAIS) 11. Contract or Grant No. BEE76-977-01
12. Sponsoring Agency Name and Address FDOT Research Center Phone: (850) 414-5260 605 Suwannee Street Tallahassee, Florida 32399-0450 research.center@dot.state.fl.us		13. Type of Report and Period Covered Final report July 2024 to April 2025 14. Sponsoring Agency Code
15. Supplementary Notes		

16. Abstract

The durability of coastal bridge structures is significantly impacted by the corrosion of steel reinforcement, particularly in waterline pile cap footings exposed to aggressive marine environments. This study investigates the feasibility of using large-diameter glass fiber-reinforced polymer (GFRP) bars as a corrosion-resistant alternative to traditional steel reinforcement. The research includes a comprehensive literature review, material characterization, and structural analysis to develop design specifications for #11 GFRP bars. Experimental testing, including tensile, bond, and durability assessments, was conducted to establish mechanical properties and ensure compliance with AASHTO and FDOT requirements. Structural performance evaluations were carried out using computational modeling tools to validate the design methodology for GFRP-reinforced pile cap footings. The findings confirm that #11 GFRP bars demonstrate adequate strength, durability, and environmental resistance for bridge applications, offering a sustainable solution to extend service life and reduce maintenance costs. Design examples are provided to facilitate implementation in practice. This research supports the development of material acceptance criteria and refined design guidelines, promoting wider adoption of GFRP reinforcement in marine bridge construction and enhancing infrastructure resilience in coastal regions.

17. Key Word	18. Distribution Statement		
Fiber reinforced plastics (FRP), Pile caps, Footings, Bridge design	No restrictions		
19. Security Classif. (of this report) Unclassified	20. Security Classif. (of this page) Unclassified	21. No. of Pages 146	22. Price

Executive Summary

In Florida, the tidal zone poses a significant risk for corrosion of steel reinforcement in coastal bridges, particularly affecting waterline pile cap footings. The footings, which support bridge piers and columns, are currently not designed with fiber reinforced polymer (FRP) reinforcing bars. Given that corrosion can lead to costly and time-consuming repairs, using corrosion-resistant FRP bars could represent a viable and economic alternative with resulting long-term cost savings.

Traditionally, pile cap footings are reinforced with steel bars up to #11 (1.375 in) in size, but no standards exist for #11 FRP bars. The AASHTO LRFD Bridge Design Guide Specifications for GFRP-Reinforced Concrete [1] allow for the design of pile cap footings with GFRP bars, offering a solution to corrosion concerns. To implement this, we need to demonstrate the practicality of using current maximum bar sizes and develop design guidance and material acceptance criteria for larger FRP bars.

The objectives of this project included identifying further research needed for using larger FRP bars in waterline pile cap footings, developing material acceptance and design specifications for #11 glass FRP bars, and creating design examples to aid implementation. Additionally, recommendations for future research will be provided to extend the use of larger FRP bars to other structural components, considering the limitations of GFRP compared to steel.

This project aimed to enhance the durability and longevity of coastal bridge structures by using larger diameter FRP reinforcing bars, reducing maintenance costs and extending service life. It will result in material acceptance criteria, design specifications, and practical design examples, promoting wider adoption of FRP reinforcement in bridge construction.

Final Report

The final report consolidates the findings from Tasks 1-5 into a comprehensive document. It includes an introduction outlining the need for research on large-diameter FRP bars and the team's methodological approach. The main chapters detail the literature review, experimental testing, and structural design analyses, while the conclusion summarizes key findings and recommendations for the implementation of #11 GFRP bars in bridge footings. Additionally, the appendices provide two completed design examples for potential publication on the FDOT Structures Design Office website, along with an electronic design tool worksheet to aid engineers in practical applications.

Table of Contents

List of Figures

List of Tables

1. Introduction

The design and durability of pile cap footings in marine environments, particularly in the tidal zones of Florida, present unique challenges due to the accelerated structural deterioration caused by exposure to saltwater and harsh environmental conditions. Corrosion of steel reinforcement in these settings leads to significant maintenance costs and long-term structural risks. Despite the advantages of fiber reinforced polymer (FRP) bars, particularly their corrosion resistance, existing design standards do not provide full specifications for large-diameter FRP reinforcement, particularly #11 (1.375 in) bars. The AASHTO LRFD Bridge Design Guide Specifications for glass fiber reinforced polymer (GFRP)-Reinforced Concrete offer a general framework for designing pile cap footings with GFRP reinforcement, but additional testing, verification, and material acceptance criteria are necessary to support the broader adoption of large-diameter FRP bars in bridge foundations.

This project aimed to investigate the feasibility of using large-diameter GFRP bars in waterline pile cap footings for bridges through experimental testing, structural analysis, and design optimization. Task 1 involved a comprehensive literature review to assess the current state of research, identifying key challenges such as testing complexities, manufacturing constraints, and the size-dependent mechanical properties of large-diameter FRP bars. The review also highlighted the need for updated design specifications, as current standards primarily extrapolate data from smaller bars rather than relying on empirical evidence.

To bridge this gap, Task 2 outlined a detailed testing plan for #11 FRP bars to establish their Physico-mechanical properties. This plan adhered to ASTM standards and FDOT specifications, ensuring that the results would be consistent, reliable, and applicable for structural design. Task 3 then executed this plan, conducting tensile strength, bond strength, and durability tests to assess the performance of #11 FRP bars under conditions representative of marine bridge foundations. The test results confirmed that the evaluated FRP bars met most of the FDOT material requirements, demonstrating adequate mechanical performance and environmental durability for long-term use in pile cap footings.

The structural analysis phase, covered in Tasks 4 and 5, focused on redesigning an existing FDOT steel-RC bridge foundation using large-diameter GFRP bars. The case study selected was the Eastbound Bridge in the north western part of Florida, where ULS and SLS verifications were performed according to AASHTO LRFD Bridge Design Guide Specifications and the FDOT Structures Manual. Altair® software and customized MathCAD® worksheets were utilized for numerical modeling and finite element analysis (FEA), allowing for a detailed evaluation of stress distributions, reinforcement detailing, and pile cap behavior under various loading conditions. This computational approach ensured that the GFRP-reinforced pile cap design met structural performance requirements while optimizing the geometry and reinforcement layout.

By integrating experimental testing, computational modeling, and structural validation, this project established a foundation for the practical implementation of large-diameter FRP

bars in bridge pile cap footings. The findings contribute to refining design codes, improving material acceptance criteria, and advancing sustainable infrastructure solutions in coastal bridge construction.

2. Literature Review – Research and Design Applications of Large (greater than #10) FRP Reinforcing Bars

The corrosion of steel reinforcement in coastal bridges threatens structural integrity and increases long-term maintenance costs, especially in waterline pile cap footings exposed to saltwater. Despite their potential to mitigate corrosion-related issues, FRP reinforcing bars are not yet utilized in these critical components due to the absence of specifications for #11 FRP bars. While the AASHTO LRFD Bridge Design Guide provides a framework for GFRP-reinforced concrete, implementing large-diameter FRP bars requires experimental validation and the development of design guidance. The literature review conducted highlights the scarcity of studies on FRP bars exceeding #8 in diameter, with limited experimental data on #11 bars. While manufacturing feasibility exists, no manufacturer currently produces bars larger than #8 in standard pultrusion lines due to testing challenges and a lack of commercial demand. The primary obstacles to widespread adoption are the complexity of tensile testing for larger bars and the insufficient market incentives, though this may change as new structural applications emerge.

FRP reinforcement for concrete structures includes GFRP, BFRP, and AFRP, with GFRP being the most widely used due to its proven durability and well-documented properties. BFRP offers higher mechanical strength and sustainability benefits but faces manufacturing challenges, especially for large-diameter bars, due to difficulties in temperature control during production and the lower density basalt fiber rovings commercially available compared to glass fiber, which leads to the use of additional fiber bobbins in production. GFRP bars are easier to produce in larger sizes, making them more feasible for high-load applications. Thermosetting resins, such as vinyl esters and epoxies, are preferred for durability, while thermoplastics offer flexibility for post-curing bending but may reduce strength, requiring stronger fibers to compensate. FRP bars using thermoplastic resin are being developed under R&D and are not commercially available yet. Bent FRP bars must be shaped before curing, limiting commercially available sizes to #8, but thermoplastic resins like Elium® [2] allow for post-curing bending, though at increased cost and complexity.

This section will expand on the key aspects of large-diameter FRP reinforcing bars, beginning with an analysis of dimensional effects, including tensile properties such as strength, ultimate strain, durability, and testing challenges. It will then address bonding to concrete, highlighting bond strength and performance under various loading conditions, followed by a discussion on creep and relaxation, particularly the effects of sustained loading and long-term deterioration. Next, experimental evidence will be reviewed from studies conducted at Sultan Qaboos University, the University of Sherbrooke, and the University of Miami, focusing on the mechanical performance of large FRP bars, specifically sizes #10, #11, and #16, and identifying trends in ultimate strength. The section will also explore the commercial

availability of large FRP bars, detailing products from ATP and MST manufacturers and their applications in both permanent and temporary structures. Lastly, design guides and material specifications will be examined, covering material acceptance criteria, design methodologies, and construction practices in the United States, Canada, and internationally, ensuring a comprehensive understanding of the structural feasibility and implementation of large-diameter FRP bars.

2.1. Large FRP Bars: Characteristics

2.1.1. Tensile properties

The tensile behavior of FRP bars is linear-elastic until failure, exhibiting higher tensile strength but lower strain capacity than steel. Unlike steel, FRP bars show size-dependent strength reductions due to the shear-lag effect [3], [4]. Studies confirm that tensile strength decreases by up to 40% between 10 mm and 20 mm bars, while the elastic modulus remains constant [5]. Liu et al. [6] verified this trend experimentally, using Weibull distribution to correlate tensile strength with bar diameter (see Figure 1). Van et al. [7], [8] further analyzed the shear-lag effect in AFRP rods, demonstrating that stress distribution varies across the bar cross-section, affecting tensile capacity (Figure 2, Figure 3).

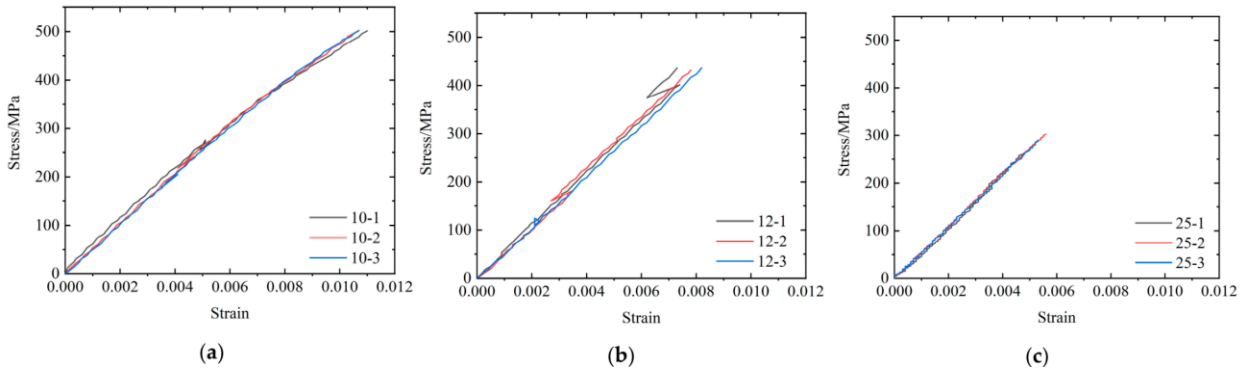

Figure 1. Stress–strain curves of GFRP tendons with different diameters GFRP tendon of (a) 10-mm diameter (b) 12-mm diameter and (c) 25-mm diameter *[6]*

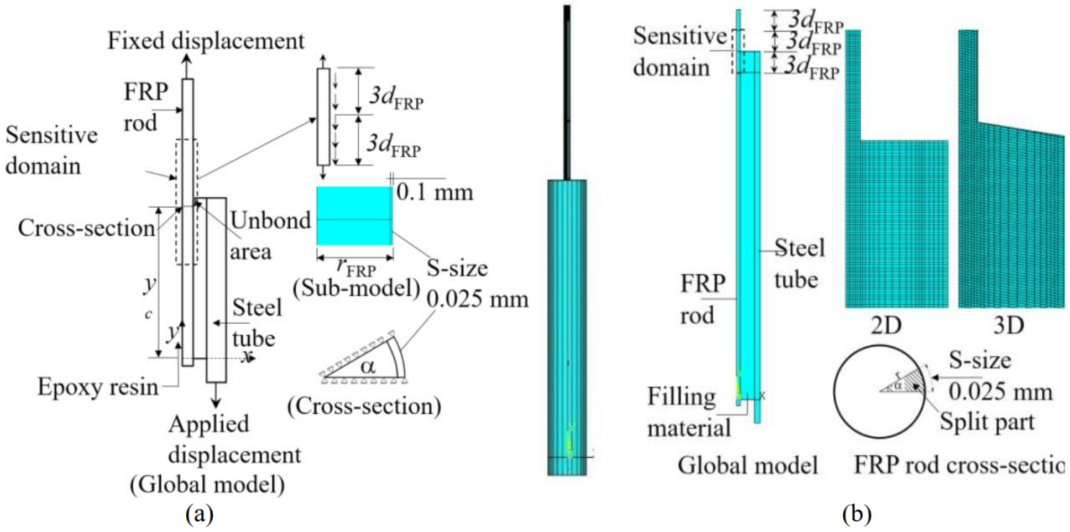

Figure 2. Boundary condition of the (a) analytical model and (b) numerical model *[8]*

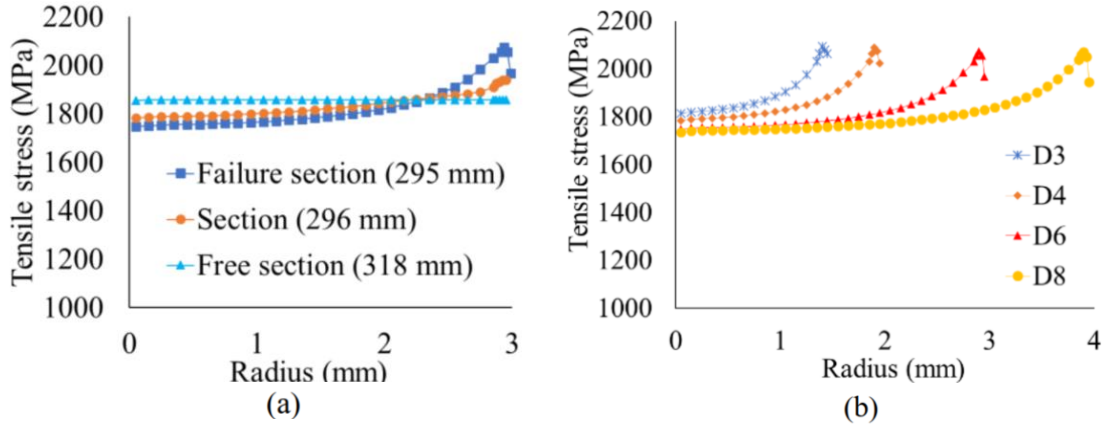

Figure 3. (a) Axial tensile stress distribution in cross-sections and (b) distribution of axial tensile stress on the failure sections separated curves of diameters *[8]*

Ultimate strain studies show that larger GFRP bars exhibit lower strain at similar stress levels, indicating a higher modulus of elasticity [9], [10]. The Weibull theory predicts the rupture of brittle FRP bars by modeling failure propagation within the fiber matrix [7]. Daniels' bundle of fibers model expands this theory, demonstrating progressive fiber failure through singlets, doublets, and triplets until total rupture (see Figure 4) [11].

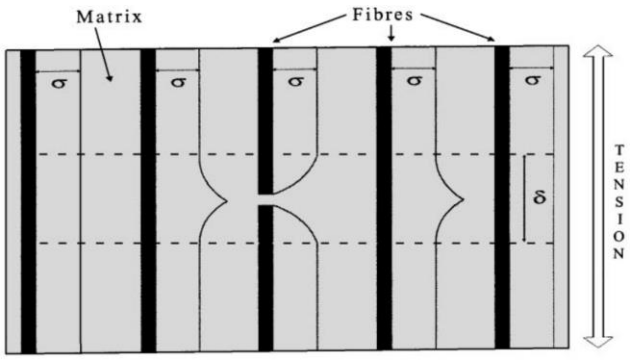

Figure 4. Illustration of load-sharing fiber rapture [6]

Regarding durability, results for large-diameter FRP bars that have been in service in real conditions are lacking, but Arrhenius theory predicts long-term degradation based on temperature exposure after accelerated aging exposure. Existing studies indicate larger bars degrade slower than smaller ones, yet visible manufacturing defects in larger bars may reduce interlaminar shear and flexural strength [12], [13], [14], [15] (see Figure 5). Alkaline exposure negatively impacts FRP bars [13], [16], while other environmental factors such as moisture, freeze-thaw, and seawater exposure also influence durability [17].

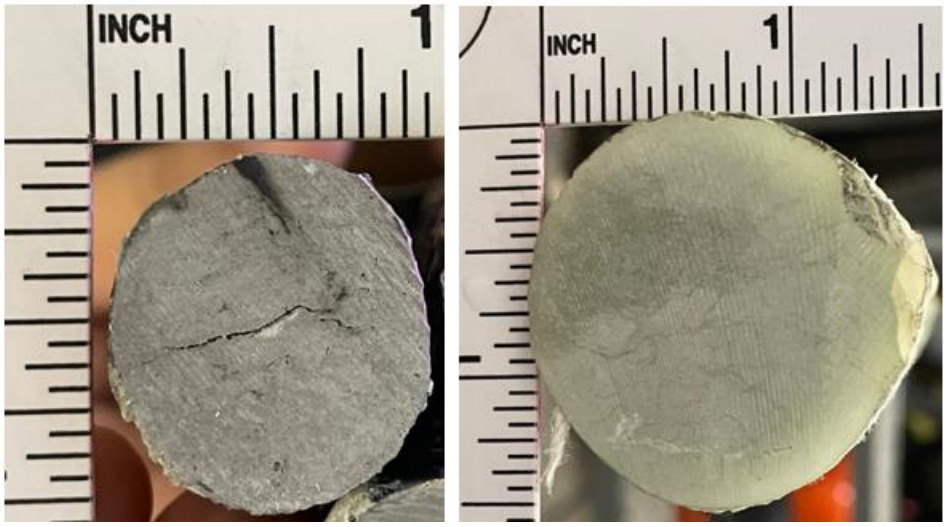

Figure 5. Close up of the cross-section of a #8 BFRP (basalt FRP) bar (left) and #11 GFRP bar (right)

Tensile testing of large FRP bars faces challenges in secure anchoring. ASTM D7205 suggests long anchoring lengths, making large bar testing difficult. University of Miami researchers developed optimized gripping methods, significantly reducing anchor length requirements [18]. Carvelli et al. [19] introduced a conical polymeric anchoring system, enhancing radial pressure and adhesion (Figure 6, Figure 7). Additionally, tensile loading rates influence ultimate strength and elongation, with rates below 6 mm/min reducing tensile properties [20]. Testing large FRP bars at higher loading rates ensures accurate results.

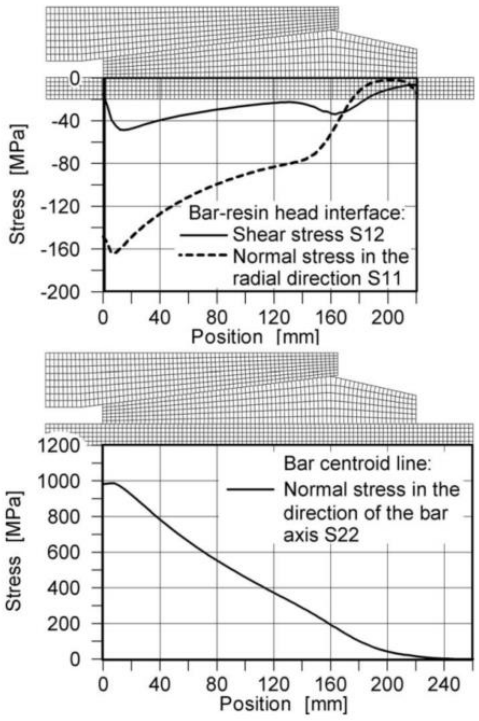

Figure 6. Stress distribution in the resin head (bar diameter=28 mm; tensile force applied=616 kN) [18]

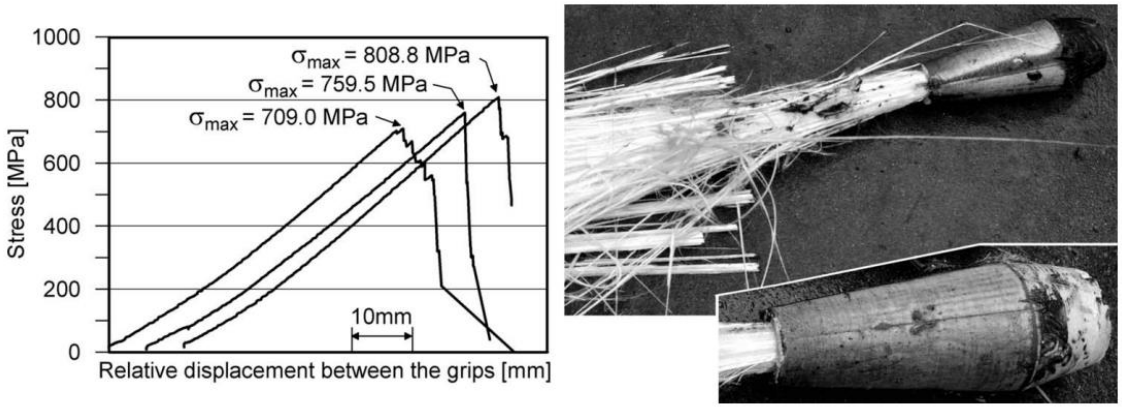

Figure 7. Tensile tests: bar diameter 32 mm [18]

2.1.2. Bond to concrete

Bond strength between FRP bars and concrete decreases as bar diameter increases, at a greater rate than in steel bars. In high-strength concrete, the reduction is less pronounced [21]. Lee et al. [22] identified three key factors affecting bond strength: shear-lag effect, increased water accumulation under larger bars, and Poisson's effect. The shear-lag effect

arises from slip between the outer and core fibers, due to weak epoxy-fiber bonding under axial tension (Figure 8) [23], [24], [25].

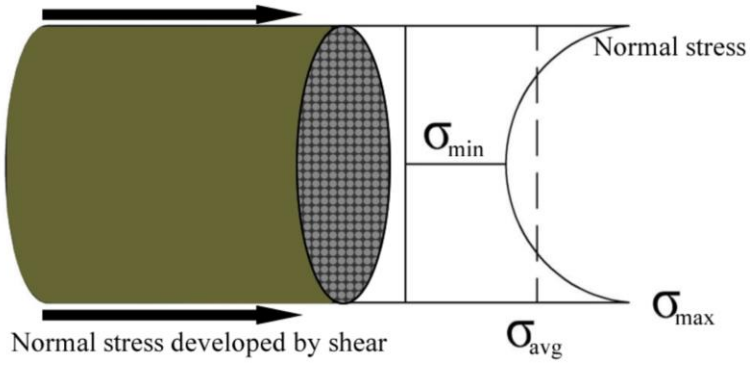

Figure 8. Shear lag effect in bars subjected to tension [15]

Additionally, larger FRP bars trap more water and air during concrete curing, reducing effective bond strength [25]. The Poisson's effect in large bars causes greater volume reduction, weakening mechanical interlock at the bar-concrete interface [26], [27], [28], [29]. Surface resin and fiber tension properties also influence slip resistance and overall bond strength [5]. However, when bond strength is normalized by concrete compressive strength, bar diameter has minimal influence [25] (Figure 9).

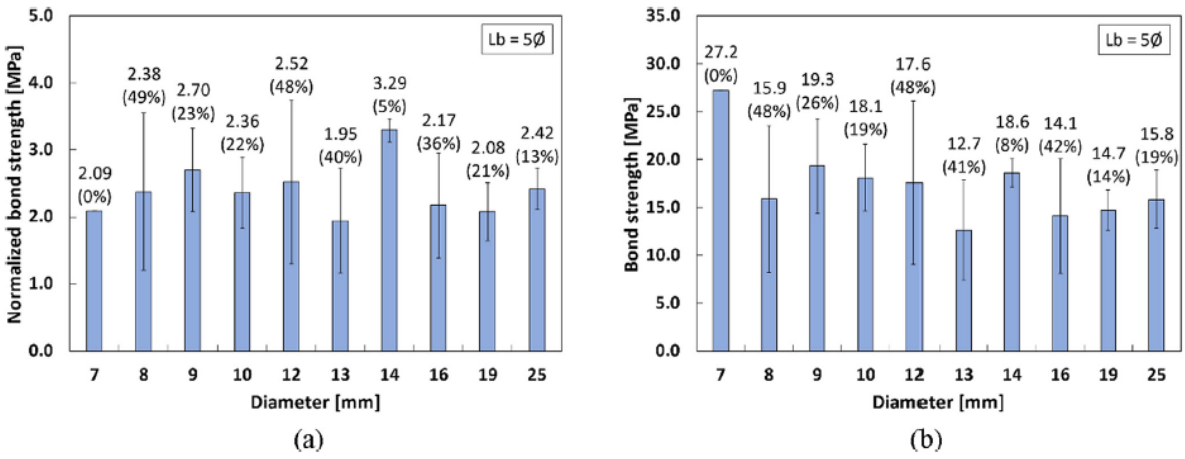

Figure 9. Influence of the FRP bar diameter on the (a) normalized bond strength and (b) bond strength. Note: values near the bars are the mean values and the coefficients of variation (the latter in percentage) [24]

Regarding durability, FRP bar surface resins degrade under aggressive environments, reducing bond strength over time [27]. A study of 1,244 test results from 35 studies found that larger diameter FRP bars degrade slower, particularly at lower temperatures [28]. This is attributed to the thicker resin layers on large bars, which improve alkali resistance and limit environmental damage [16]. Another review confirmed minimal bond degradation across various exposure conditions, including acid, alkali, salt, water immersion, and thermal

cycles [25]. However, long-term bond strength predictions for large FRP bars require further validation for reinforced concrete (RC) applications.

Surface characteristics significantly affect FRP-concrete bond strength, with sand-coated and ribbed bars showing varying performance based on texture, size, dispersion, and material quality [29], [30]. Studies suggest rib modifications and sand coatings can double bond strength, but the behavior of large-diameter bars remains under-researched.

Concrete cover also plays a role, as high cover delays stress concentrations and splitting failures [21]. Early FRP-RC design recommended a minimum cover of twice the bar diameter for pullout resistance [31]. Eccentric pull-out tests suggest higher bond strength, lower slip, and improved progressive bond failure compared to typical tests, but these studies are mainly on smaller bars [32]. Further evaluation of concrete cover requirements for large-diameter FRP bars is necessary to confirm scaling trends observed in smaller bars.

2.1.3. Creep and relaxation

Lack of data exists on the time-dependent mechanical properties of large-diameter FRP bars, particularly regarding creep and relaxation effects [17]. Existing research focuses primarily on small-diameter bars, as current test methods struggle to apply sustained loading to larger bars. Long-term studies indicate that tensile strength and elastic modulus remain unaffected when sustained stress is below 60% of ultimate tensile strength [33], [34]. The only known study on large-diameter FRP bars in this context was conducted by Guo-wei et al. [35], who examined stress relaxation behavior of hybrid basalt-glass FRP (B-GFRP) bars using fiber Bragg grating (FBG) strain sensors. These 1 in. (25 mm) B-GFRP bars, contained 65% glass fiber, 10% basalt fiber, 19% resin, and 6% fine sand, with detailed mechanical properties listed in Table 1.

Table 1. Properties of B-GFRP Bars

Diameter	Basalt	2.1	mm
	Glass	25.35	mm
Ratio of fiber weight of basalt to total fiber		13.16	%
Density		2.07	g/cm^3
Content (weight ratio%)	Basalt	10	%
	Glass	65	%
	Resin	19	%
	Fine sand	6	%
Ultimate tensile load	$p_{u,ave}$	536.29 ± 6.74	kN
Ultimate tensile strength	$f_{u,ave}$	906.40 ± 11.29	MPa
Guaranteed tensile strength	$f_{fu}^{*} = f_{u,ave} - 3\sigma$	872.53	MPa
Design tensile strength	$f_{fu} = (C_E = 0.7) \cdot f_{fu}^{*}$	610.77	MPa
Modulus of elasticity	$E_{f,ave}$	52.26 ± 0.87	GPa
Ultimate tensile strain	$\varepsilon_{f,ave}$	1.73 ± 0.04	%
Guaranteed strain	$\varepsilon_{fu}^{*} = \varepsilon_{u,ave} - 3\sigma$	1.62	%
Design strain	$\varepsilon_{fu} = C_E \cdot \varepsilon_{fu}^{*}$	1.13	%
Allowable strain for creep	$20\%\ \varepsilon_u$	0.23	%

To improve stress relaxation testing, a seamless steel pipe gripping system was used, avoiding issues associated with traditional wedge-shaped grips and improving test accuracy [35]. The loading system, as shown in Figure 10, included a hollow jack, bearing plates, and a load cell. The stress-strain relationship during stress relaxation exhibited three phases: rapid reduction (AB), slower relaxation (BC), and stabilization (CD), highlighting the nonlinear nature of relaxation (Figure 11).

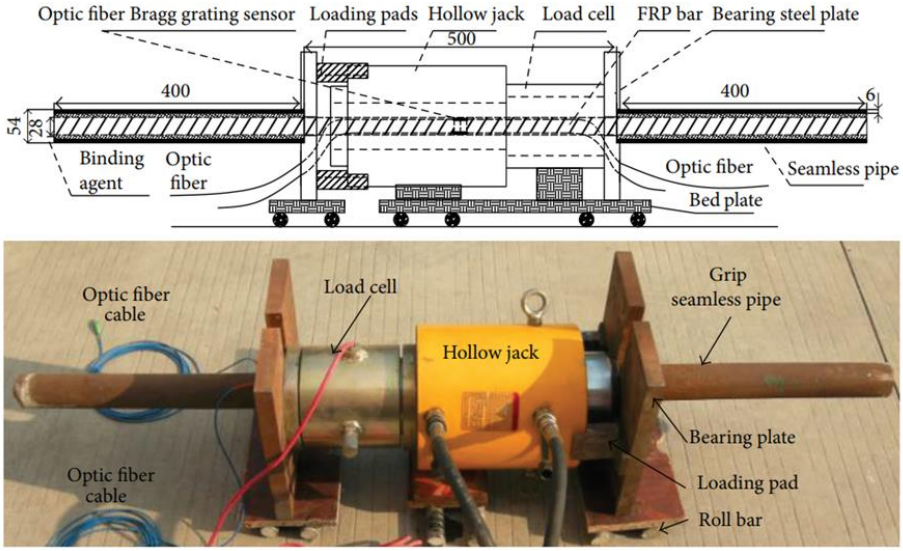

Figure 10. Loading system for stress relaxation test [2]

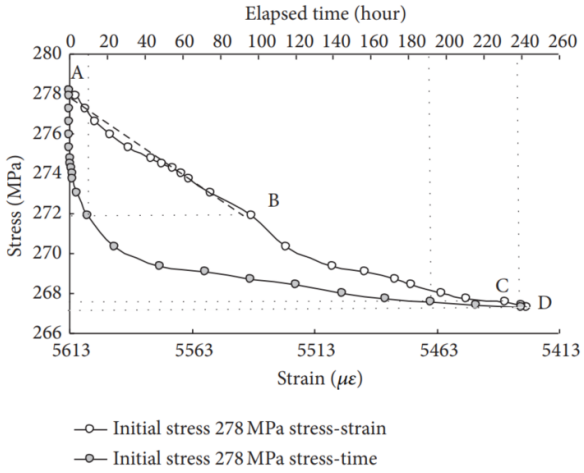

Figure 11. Relaxation process for B-GFRP (basalt-glass) bar gripped with seamless pipe [2]

The combined effects of sustained loading and environmental exposure significantly influence FRP bar deterioration. For low-stress levels (25%-30% of ultimate strength), degradation was dominated by ion diffusion, while medium-stress levels (30%-50%) induce crack propagation. At high-stress levels (above 50%), a brittle fracture occurred [17].

Li et al. [36] investigated stress relaxation of large-diameter sand-coated B-GFRP bars under acidic and alkaline conditions over seven months. Acid-exposed bars exhibited 9.2% stress relaxation, while alkaline-exposed bars showed 13.4%, indicating greater degradation in alkaline environments. The study used a seamless steel pipe gripping device and applied cyclic loading in 10 kN increments before maintaining prestress for seven days. Findings confirmed that acid and alkaline ingress through surface cracks contributed to stress relaxation.

Key conclusions from Li et al.'s study [36] include:

- Alkaline conditions cause greater stress relaxation than acidic conditions.
- Acidic environments, though less corrosive, still induce significant relaxation.
- Surface cracks allow aggressive ion penetration, accelerating degradation.
- Relaxation in acid-exposed bars was influenced more by anchorage limitations than material properties.
- Further research is needed on anchorage design and grout selection to optimize stress relaxation resistance in large-diameter FRP bars.

2.2. Large FRP Bars: Experimental Evidence

This section compiles experimental studies on large-diameter FRP bars, offering key insights into their mechanical performance and applicability. Although existing research is limited, the testing evidence from three universities represents the latest advancements in understanding these materials. The results reveal critical gaps in material characterization, particularly in areas such as bond strength, creep behavior, and durability. While these studies serve as a foundation for developing design specifications and guidelines for reinforced concrete (RC) applications, further research is essential to fully characterize the behavior of large FRP bars and establish comprehensive design standards for their widespread implementation.

2.2.1. Sultan Qaboos University

Under the supervision of Prof. Sherif El-Gamal, 23 GFRP Mateenbar specimens from Pultron were tested at Sultan Qaboos University according to ASTM D7205. The study assessed the tensile properties of GFRP bars of #10 (32 mm), #11 (37.5 mm), and #16 (50 mm) diameters, providing critical data on their ultimate load capacity, tensile strength, modulus of elasticity, and failure modes.

The #10 GFRP bars (32 mm) were tested using 108-in.- long (2750 mm) samples with a 29.5-in. (750 mm) gauge length and 39.4-in. (1000 mm) anchors filled with expanding mortar. The results, detailed in Table 2, showed an average tensile strength of 872 MPa, with failure occurring due to rupture. A 7.9-in. (200 mm) extensometer was used to measure the modulus of elasticity.

Table 2. Test results - Pultron Mateenbar 32.0 mm diameter (10)

Sample ID	Measured Outside Diameter [mm]	Measured Minor Diameter [mm]	Standard diameter [mm]	Standard Cross section area [mm^2]	Ultimate Load [kN]	Tensile Strength [MPa]	Tensile Modulus of Elasticity [GPa]	Ultimate Elongation [%]	Mode of Failure
MVX-BAR32-Sample#1	31.38	28.85	28.7	645	471	730	57.8	1.30%	Rupture
MVX-BAR32-Sample#2	31.52	28.83	28.7	645	592	918	54.9	1.70%	Rupture
MVX-BAR32-Sample#3	31.47	28.88	28.7	645	603	935	54.4	1.70%	Rupture
MVX-BAR32-Sample#4	31.44	28.91	28.7	645	596	925	54.8	1.70%	Rupture
MVX-BAR32-Sample#5	31.51	28.91	28.7	645	550	853	57.2	1.50%	Rupture
Average	**31.46**	**28.88**	**28.7**	**645**	**562**	**872**	**55.8**	**1.60%**	
Number of Samples					5	5	5	5	
Standard deviation					55.1	85.5	1.6	0.19%	
COV%					9.8%	9.8%	2.8%	12.2%	

#11 GFRP bars (37.5 mm) followed the same test setup as #10 bars, with results summarized in Table 3. The average tensile strength was 692 MPa, with failure occurring through rupture. These results confirmed a trend of decreasing tensile strength with increasing bar diameter, primarily due to the shear-lag effect.

Table 3. Test results - Pultron Mateenbar 37.5mm diameter (#11)

Sample ID	Measured Outside Diameter [mm]	Standard diameter [mm]	Standard Cross section area [mm^2]	Ultimate Load [kN]	Tensile Strength [MPa]	Tensile Modulus of Elasticity [GPa]	Ultimate Elongation [%]	Mode of Failure
MVX-BAR38-Sample#1	37.75	36.93	1071	842	786	56.5	1.4	Rupture
MVX-BAR38-Sample#2	37.89	36.93	1071	689	643	57	1.1	Rupture
MVX-BAR38-Sample#3	37.78	36.93	1071	836	780	53.1	1.5	Rupture
MVX-BAR38-Sample#4	37.97	36.93	1071	657	614	54.6	1.1	Rupture
MVX-BAR38-Sample#5	37.91	36.93	1071	681	636	51.6	1.2	Rupture
Average	**37.86**	**36.93**	**1071**	**741**	**692**	**54.56**	**1.26%**	
Number of Samples				5	5	5	5	
Standard deviation				90.1	84.1	2.3	0.16%	
COV%				12.2%	12.2%	4.2%	12.3%	

#16 GFRP bars (50 mm) were tested using 118 in. (3000 mm) long samples with a 39.4 in. (1000 mm) free length and expanding mortar anchors. Test results, summarized in Table 4, revealed an average tensile strength of 569 MPa. Two samples exhibited slipping failure, so they were excluded from the average calculations.

Table 4. Test results - Pultron Mateenbar 50.0mm diameter (#16)

Sample ID	Measured Outside Diameter	Standard diameter	Standard Cross section area	Ultimate Load	Tensile Strength	Tensile Modulus of Elasticity	Ultimate Elongation	Mode of Failure
	[mm]	[mm]	[mm^2]	[kN]	[MPa]	[GPa]	[%]	
MVX-BAR50-Sample#1	50.21	49.73	1943	1190	613	56.5	1.1	Rupture
MVX-BAR50-Sample#2	50.20	49.73	1943	763	393	54.1	0.7	Slipped
MVX-BAR50-Sample#3	50.28	49.73	1943	1146	590	52.5	1.1	Rupture
MVX-BAR50-Sample#4	50.25	49.73	1943	980	504	52.4	1.0	Rupture
MVX-BAR50-Sample#5	50.24	49.73	1943	802	413	56.8	0.7	Slipped
Average	**50.24**	**49.73**	**1943**	**1106**	**569**	**54.0**	**1.06%**	
Number of Samples				5	5	5	5	
Standard deviation				110.91	57.08	2.37	0.08%	
COV%				10.0%	10.0%	4.4%	8.0%	

As expected, the tensile strength of GFRP bars decreased with increasing diameter, following a predictable trend attributed to shear-lag effects. The best-fitting curve summarizing these results is shown in Figure 12, providing initial prediction values for large-diameter FRP bars up to 50 mm (2 in.). These findings contribute to the development of design specifications for large-diameter FRP reinforcement in structural applications.

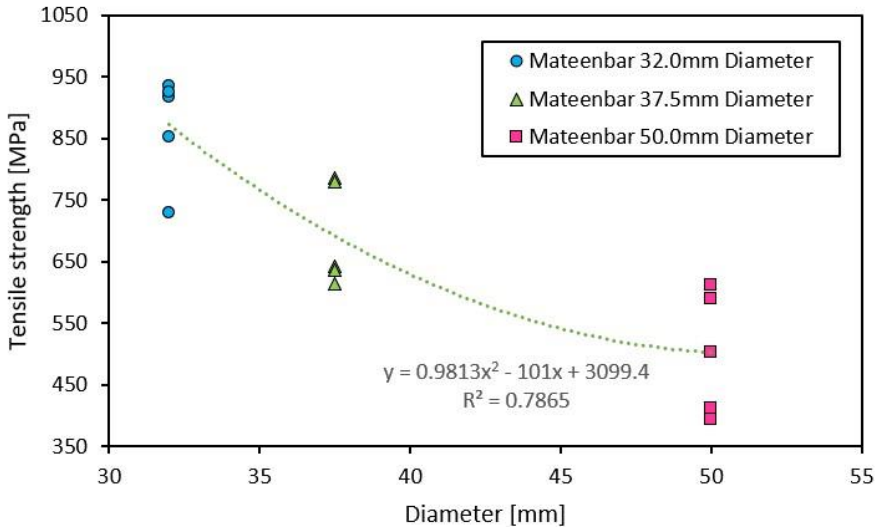

Figure 12. Results of the Mateenbar GFRP bars tested

2.2.2. University of Sherbrooke

Under the supervision of Prof. Brahim Benmokrane, the University of Sherbrooke conducted tensile testing on a sand-coated GFRP #12 (38.1 mm) bar, manufactured by Pultrall Inc., following CSA S807-19 [37] and ASTM D7205/D7205M-06 [38]. The mechanical properties are presented in Table 5.

Table 5. Test results - Pultrall

Sample ID	Ultimate Load	Tensile Strength	Tensile Modulus of Elasticity	Ultimate Tensile Strain
	[kN]	[MPa]	[GPa]	[%]
#1	1203	1055	63	1.70%

The test specimen was instrumented with an LVDT over a 7.9 in. (200 mm) gauge length to capture elongation. A computerized data acquisition system recorded the applied load and strain, and the tensile modulus of elasticity (EL) was determined from stress-strain curve values between 25% and 50% of the tensile capacity, based on a nominal cross-sectional area of 1256 mm^2. The ultimate load was 1203 kN, with a tensile strength of 1055 MPa and elastic modulus of 63 GPa.

The test setup is illustrated in Figure 13, and failure occurred due to longitudinal splitting, as shown in Figure 14. These results provide valuable insights into the tensile behavior of large-diameter GFRP bars, contributing to design specifications and performance evaluation for structural applications.

Figure 13. Test setup

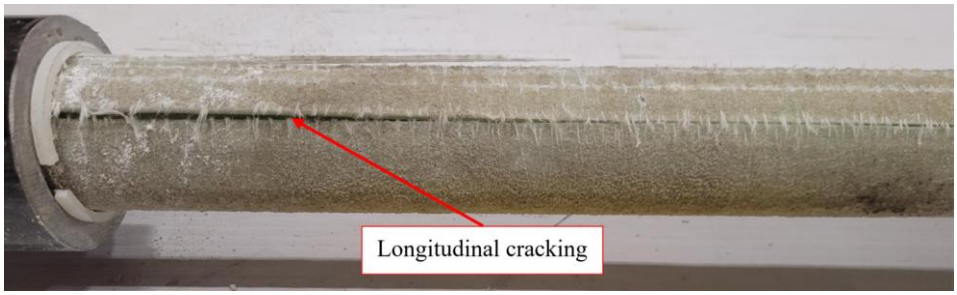

Figure 14. Close view of the tensile failure

2.2.3. University of Miami, Structures and Materials Lab

The Structures and Materials Lab (SML) at the University of Miami, accredited under ISO 17025-2017, IAS TL-478, and FDOT ISM028, conducted tensile testing on #11 GFRP bars following ASTM D7205-21. The study aimed to: (i) ensure proper anchorage, (ii) achieve full cross-section failure (explosive/broom' mode), and (iii) evaluate the effect of gauge length (20D vs. 40D).

In collaboration with MST Rebar Inc., specimens were prepared with a reduced anchor length based on previous research [39]. Figure 15 illustrates the test setup, where bars were tested at displacement rates of 5.0 mm/min (0.20 in./min) with gauge lengths of 27.5 in. (699 mm) and 55 in. (1400 mm). The total specimen lengths were 75.5 in. (1918 mm) and 103 in. (2616 mm).

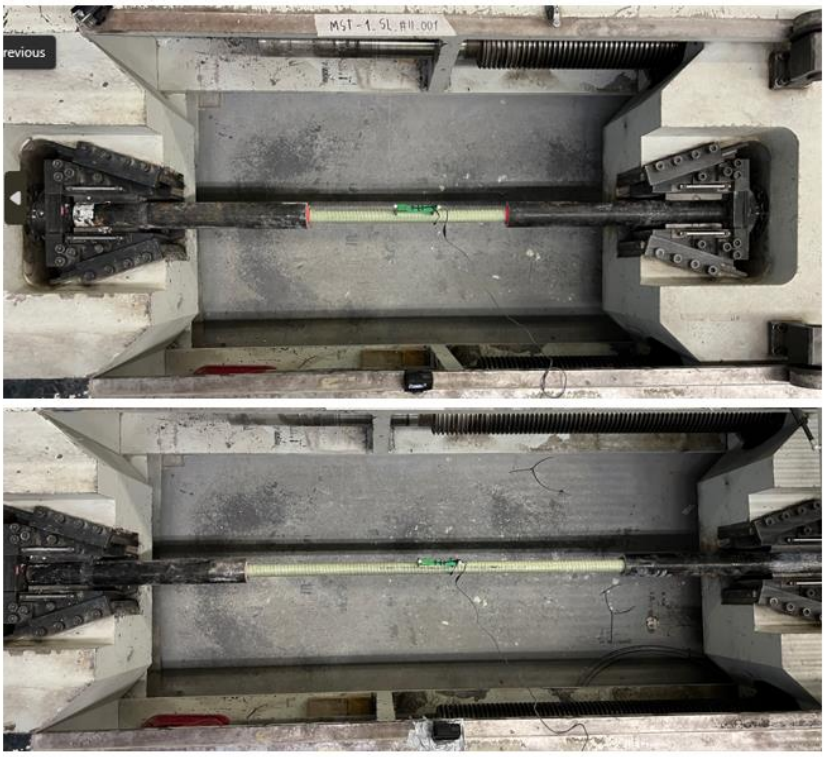

Figure 15. Test setup for each FRP bar at both gauge lengths

Results, summarized in Table 6, confirmed that shorter anchorage lengths (24 in. steel pipe) were feasible, producing consistent full cross-section failure (explosive/broom mode) (Figure 16). This aligns with prior studies, suggesting ASTM D7205 anchorage recommendations may be conservative. Additionally, tensile properties remained statistically consistent between 20D and 40D gauge lengths, supporting existing findings that gauge length does not significantly impact tensile behavior [40].

Table 6. Test results of #11 FRP bars at both gauge lengths

Specimen ID	Tensile Force P_{max}		Nominal Area A_{nom}		Ultimate Strength F^{tu}_{nom}		Modulus of elasticity E_{nom}		Coeff. Of Determination	Strain ε
	kN	kips	mm^2	in^2	MPa	ksi	GPa	Msi	r^2	%
TNS-01	1005.54	226.1			999.1	144.9	53.6	7.77	0.9999	1.86
TNS-02*	1007.26	226.4			1000.8	145.2	58.2	8.45	1.0000	1.72
TNS-03*	944.04	212.2	1006	1.56	938.0	136.0	57.4	8.33	0.9999	1.63
TNS-04	936.90	210.6			930.9	135.0	55.0	7.98	0.9996	1.69
TNS-05	936.32	210.5			930.3	134.9	57.8	8.38	1.0000	1.61
Average	**966.01**	**217.2**			**959.8**	**139.2**	**56.4**	**8.18**		**1.70**
S_{n-1}	37.00	8.3			36.8	5.3	2.0	0.29		0.10
CV (%)	3.8	3.8			3.8	3.8	3.6	3.6		5.9

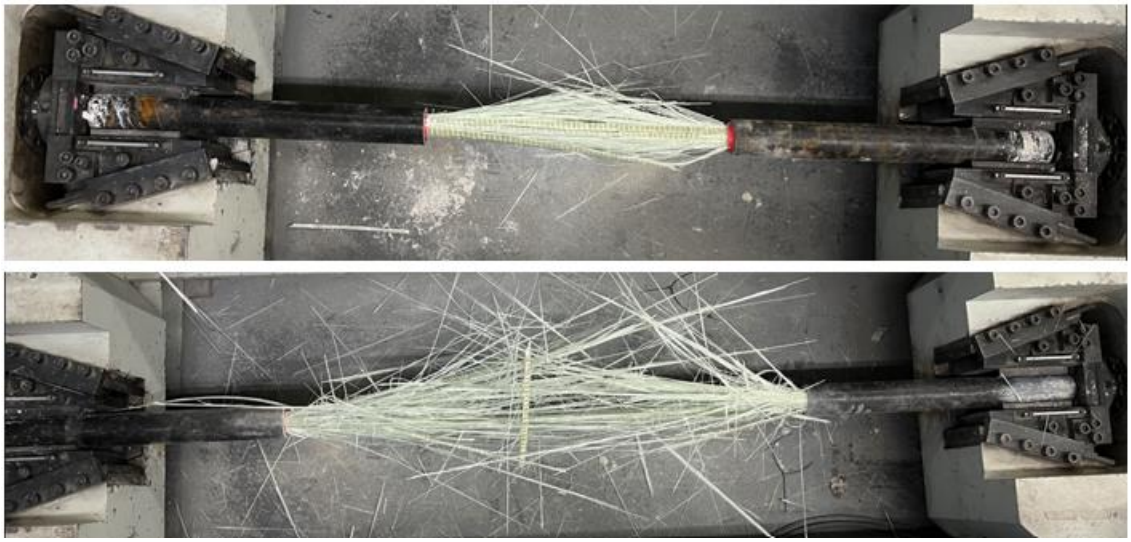

Figure 16. Representative FRP bar explosive or broom type failure mode at both gage lengths

The stress-strain response for both gauge lengths, presented in Figure 17, demonstrates that extensometer removal midway through testing did not influence results. These findings contribute to refining tensile test procedures for large-diameter FRP bars, ensuring practical and efficient testing methodologies for structural applications.

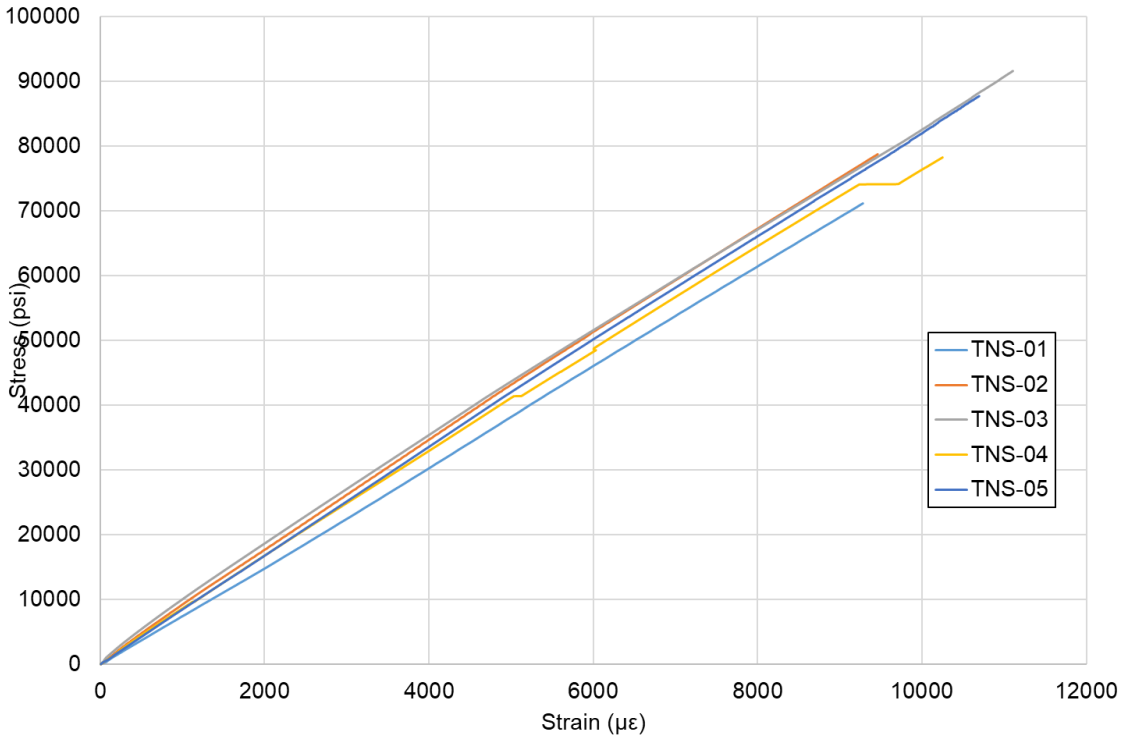

Figure 17. Stress vs. stain of #11 FRP bars at both gauge lengths (extensometer removed halfway during the test)

2.3. Large FRP Bars: Commercial Availability

Currently, ASTM D7957 and ASTM D8505 specify the minimum requirements for FRP bars up to #10. However, some manufacturers, including ATP S.r.l. [41] and MST Rebar Inc. [42], have successfully commercialized FRP bars larger than #10. Other manufacturers, such as Sireg, Mateenbar, and Pultrall, have produced large-diameter FRP bars primarily for research and development purposes.

This chapter presents the Physico-mechanical properties of ATP and MST bars, including straight and bent bars, as reported by manufacturers for structural and temporary applications. Additionally, examples of practical applications for large-diameter FRP bars are provided. This information is intended to highlight the commercial availability of large FRP bars and support their wider adoption in design specifications and applications.

2.3.1. ATP FRP bars

This section presents the material specifications of ATP's FRP bars, particularly large-diameter bars greater than #10, as reported by the manufacturer. ATP offers both straight and bent bars, distinguishing between permanent and temporary applications.

For permanent reinforced concrete (RC) structures, ATP uses vinyl ester resin, ensuring durability for a minimum service life of 50 years. Currently, commercially available permanent-use FRP bars are limited to #10. The RWB-A rebar (vinyl ester resin-based)

exhibits high tensile strength, modulus of elasticity, and ultimate strain, with detailed properties listed in Table 7. The physical and mechanical characteristics, including glass content, glass transition temperature (T_g), transverse shear strength, and bond strength, are tested per ASTM D2584, ASTM E1640, ASTM D7617, and ACI 440.3R.

Table 7. ATP-RWB-A GFRP bars

Size	Diameter		Area		Tensile Strength		Tensile Modulus of Elasticity		Ultimate Strain
	[mm]	[in]	[mm²]	[in²]	[MPa]	[ksi]	[GPa]	[ksi]	[%]
#2	6	0.24	28	0.04	900	131	46	6670	1.96
-	8	0.31	50	0.08	850	123	46	6670	1.85
#3	10	0.39	79	0.12	830	120	46	6670	1.80
#4	13	0.51	133	0.21	760	110	46	6670	1.65
#5	16	0.63	201	0.31	725	105	46	6670	1.58
#6	20	0.79	314	0.49	690	100	46	6670	1.50
#7	22	0.87	380	0.59	655	95	46	6670	1.42
#8	25	0.98	491	0.76	620	90	46	6670	1.35
#9	29	1.14	660	1.02	590	86	46	6670	1.28
#10	32	1.26	804	1.25	550	80	46	6670	1.20

Other physical and mechanical characteristics		**Test method**
Volumetric glass content	>60 %	ASTM D2584
T_g of the resin (glass transition temperature)	≥ 100 °C	ASTM E1640
Transverse shear strength	>150 MPa	ASTM D7617
Bond Strength	>8 MPa	ACI 440.3R (method B3)

For temporary RC structures (typically with a service life of 24 months or less), ATP uses polyester resin. These FRP bars are widely used in soft-eye tunnel construction and as soil nails or soil screws in geotechnical applications. ATP produces ribbed (RWB-N) and standard surface (RWB-S) polyester FRP bars, with sizes up to #16 commercially available. Additionally, bent bars up to #10 are available for temporary applications. The mechanical properties of RWB-N and RWB-S FRP bars, including diameter, tensile strength, modulus of elasticity, and ultimate strain, are detailed in Table 8 and Table 9, with test methods specified under CNR DT203 standards.

Table 8. ATP-RWB-N GFRP bars

Size	Diameter		Area		Tensile Strength		Tensile Modulus of Elasticity		Ultimate Strain
	[mm]	[in]	[mm²]	[in²]	[MPa]	[ksi]	[GPa]	[ksi]	[%]
-	16	0.63	201	0.31	725	105	40	5800	1.81
-	19	0.75	283	0.44	690	100	40	5800	1.73
-	20	0.79	314	0.49	655	95	40	5800	1.64
-	22	0.87	380	0.59	655	95	40	5800	1.64
-	25	0.98	491	0.76	620	90	40	5800	1.55
-	28	1.10	615	0.95	590	86	40	5800	1.48
-	30	1.18	707	1.10	570	83	40	5800	1.43
#10	32	1.26	804	1.25	560	81	40	5800	1.40
-	36	1.42	1017	1.58	560	81	40	5800	1.40
-	40	1.57	1256	1.95	550	80	40	5800	1.38
-	50	1.97	1963	3.04	500	73	40	5800	1.25

Other physical and mechanical characteristics		**Test method**
Volumetric glass content	>60 %	App. B CNR DT203
T_g of the resin (glass transition temperature)	≥ 80 °C	-

Table 9. ATP-RWB-S GFRP bars

Size	Diameter		Area		Tensile Strength		Tensile Modulus of Elasticity		Ultimate Strain
	[mm]	[in]	[mm²]	[in²]	[MPa]	[ksi]	[GPa]	[ksi]	[%]
-	12	0.47	113	0.18	750	109	40	5800	1.88
-	14	0.55	154	0.24	755	109	40	5800	1.89
-	16	0.63	201	0.31	725	105	40	5800	1.81
-	19	0.75	283	0.44	690	100	40	5800	1.73
-	20	0.79	314	0.49	655	95	40	5800	1.64
-	22	0.87	380	0.59	655	95	40	5800	1.64
-	24	0.94	452	0.70	620	90	40	5800	1.55
-	25	0.98	491	0.76	620	90	40	5800	1.55
-	28	1.10	615	0.95	590	86	40	5800	1.48
-	30	1.18	707	1.10	570	83	40	5800	1.43
#10	32	1.26	804	1.25	560	81	40	5800	1.40
-	36	1.42	1017	1.58	560	81	40	5800	1.40
-	38	1.50	1134	1.76	550	80	40	5800	1.38
-	40	1.57	1256	1.95	500	73	40	5800	1.25
-	50	1.97	1963	3.04	500	73	40	5800	1.25

Other physical and mechanical characteristics		**Test method**
T_g of the resin (glass transition temperature)	≥ 80 °C	-

ATP also manufactures rectangular and circular closed polyester stirrups (STR-RWB and STC-RWB) for temporary structures, with properties summarized in Table 10.

Table 10. ATP STR/STC-RWB GFRP rectangular and circular stirrups

Size	Diameter		Area		Tensile Strength		Tensile Modulus of Elasticity		Ultimate Strain
	[mm]	[in]	[mm²]	[in²]	[MPa]	[ksi]	[GPa]	[ksi]	[%]
-	10	0.39	79	0.12	830	120	40	5800	2.08
-	12	0.47	113	0.18	760	110	40	5800	1.90
-	14	0.55	154	0.24	755	109	40	5800	1.89
-	16	0.63	201	0.31	725	105	40	5800	1.81
-	18	0.71	254	0.39	690	100	40	5800	1.73
-	20	0.79	314	0.49	655	95	40	5800	1.64
-	22	0.87	380	0.59	655	95	40	5800	1.64
-	24	0.94	452	0.70	620	90	40	5800	1.55
-	25	0.98	491	0.76	620	90	40	5800	1.55
-	28	1.10	615	0.95	590	86	40	5800	1.48
-	30	1.18	707	1.10	570	83	40	5800	1.43
#10	32	1.26	804	1.25	560	81	40	5800	1.40

Other physical and mechanical characteristics		**Test method**
T_g of the resin (glass transition temperature)	≥ 80 °C	Not reported

A notable real-world application of large-diameter FRP bars and bends is the Venice Metro Station (Line C) in Rome, Italy, currently under construction (summer 2024). The

underground facility spans eight levels, utilizing GFRP reinforcement in the soft-eye diaphragm walls to facilitate Tunnel Boring Machine (TBM) excavation.

The main diaphragm panels measure 1.50 x 2.80 meters, with excavation from +20.00 meters to -66.50 meters above sea level. GFRP reinforcement was implemented from -21.15 meters to -65.90 meters, ensuring maximum versatility in the metro line layout. Five GFRP cages were constructed for perimeter and central diaphragms, shown in Figure 18, with installation in Figure 19.

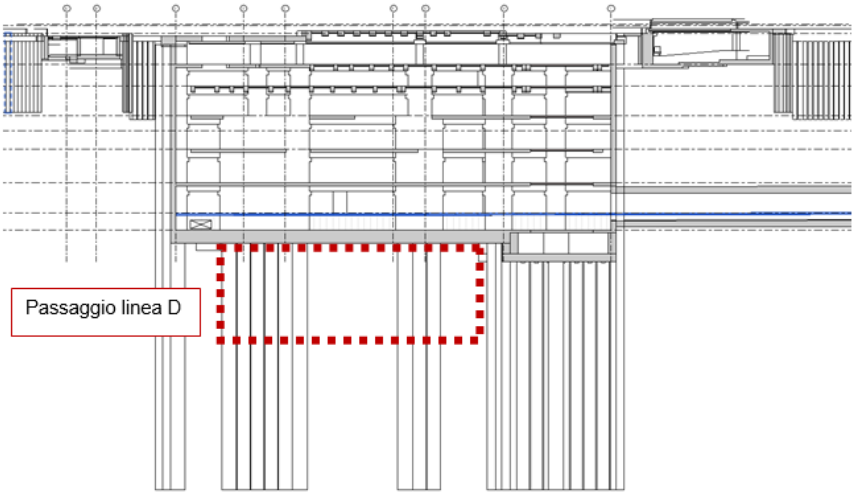

Figure 18. Transverse cross-section – Venezia Station, Rome (Italy)

Figure 19. Installation of a GFRP cage

The mechanical characteristics of the GFRP bars used in the project, including diameter, characteristic strength (f_{fk}), modulus of elasticity (Ef), and characteristic tensile failure strain (ε_{fk}), are provided in Table 11. A 50/90-mm elliptical longitudinal GFRP bar and a 32-mm closed stirrup are shown in Figure 20, demonstrating ATP's capability to manufacture and implement large-diameter GFRP bars in major infrastructure projects.

Table 11. Table 3 ASTM D7957/D7957M-22 – Geometric and mechanical property requirements

Diameter [mm]	**f_{fk} [MPa]**	**E_f [MPa]**	**ε_{fk} [-]**	**A_f [mm^2]**
20	655	40,000	0.0164	310
32	560	40,000	0.014	800
40	500	40,000	0.0125	1250
50/90	500	40,000	0.0125	3920

Where:

- f_{fk} is the characteristic strength of the GFRP reinforcement (MPa)
- E_f is the normal modulus of elasticity (MPa)
- ε_{fk} is the characteristic tensile failure strain
- A_f is the area (mm^2).

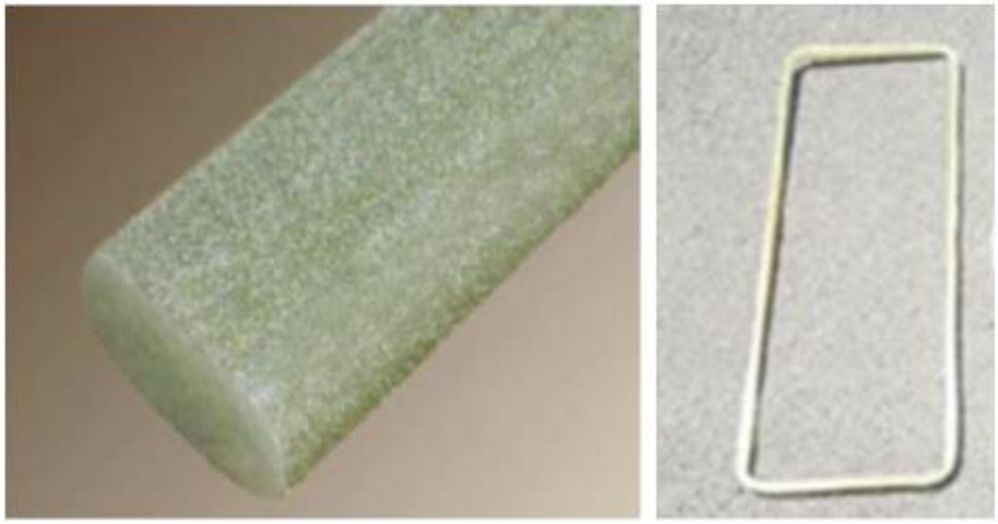

Figure 20. 50/90-mm GFRP bar (left), and 32-mm closed stirrup (right)

2.3.2. MST FRP bar

MST Rebar Inc. manufactures MST-BAR, offering straight bars (sizes #2 to #11) and bent bars (sizes #3 to #8) for various structural applications. These bars are commonly used in concrete slabs, shear walls, bridge foundations, highways, and highly corrosive environments, including underwater structures, coastal areas, and industrial sites. MST-BAR has also been used for hybrid steel-GFRP reinforced concrete solutions, such as pier cap retrofitting and pier cage reinforcement, as shown in Figure 21.

Figure 21. Pier cap retrofitting (left) and pier cage GFRP reinforcement (right) [40]

The mechanical properties of MST-BAR, including large-diameter bars, are detailed in Table 12. MST-BAR Grade III has an elastic modulus of 60 GPa, and tensile strength values exceeding 1000 MPa for most sizes. However, tensile properties for the #11 bar are not guaranteed, as valid failure conditions could not be achieved per ASTM D7205.

Table 12. MST Rebar GFRP straight bars Grade III (E_f=60 GPa)

Size	Diameter		Min. Tensile Load		Area		Tensile Strength		Tensile Modulus of Elasticity		Ultimate Strain	Unit weight/Length	
	[mm]	[in]	[kN]	[kip]	[mm^2]	[in^2]	[MPa]	[ksi]	[GPa]	[ksi]	[%]	[kg/m]	[lb./ft]
#2	6	0.24	33	7.4	32	0.05	1031	150	60	8700	1.72	0.120	0.081
#3	10	0.39	74	16.6	71	0.11	1042	151	60	8700	1.74	0.220	0.148
#4	13	0.51	132	29.7	132	0.20	1000	145	60	8700	1.67	0.350	0.235
#5	16	0.63	202	45.4	201	0.31	1005	146	60	8700	1.67	0.500	0.336
#6	20	0.79	285	64.1	285	0.44	1000	145	60	8700	1.67	0.700	0.470
#7	22	0.87	390	87.7	387	0.60	1008	146	60	8700	1.68	0.900	0.605
#8	25	0.98	507	114.0	491	0.76	1033	150	60	8700	1.72	0.122	0.082
#9	29	1.14	650	146.1	645	1.00	1008	146	60	8700	1.68	1.400	0.941
#10	32	1.26	819	184.1	819	1.27	1000	145	60	8700	1.67	1.720	1.156
#11*	36	1.42	1000	224.8	1007	1.56	993	144	60	8700	1.66	2.150	1.445

Other physical and mechanical characteristics

Transverse shear strength	>220 MPa (31.9 ksi)
Bond Strength to concrete (min.)	>20 MPa (2900 Psi)
Strength to bend (straight portion)	>900 MPa
Strength to bend (bend portion $R_{max}=4\phi_{bar}$)	>600 MPa
T_g of the resin (glass transition temperature)	≥ 125 °C

*Tensile properties of #11 bar are NOT guaranteed due to the inability to achieve a valid bar break per ASTM D7205.

2.4. Design Guides and Material Specifications

This section presents a comprehensive review of national design guides and material specifications for reinforced concrete (RC) structural elements using FRP bars. It covers material specifications, acceptance criteria, design guidelines, and construction standards from the United States, Canada, and other international sources, with a primary focus on North American standards.

Most existing design specifications are limited to FRP bars up to #10, with only a few standards addressing #11 bars. However, specifications for #11 bars are largely based on theoretical extrapolations or limited experimental data, highlighting the need for further research to refine design recommendations and performance criteria for large-diameter FRP reinforcement. This section outlines the material specifications and acceptance criteria for FRP bars, detailing standards from the United States, Canada, and international bodies.

2.4.1. United States

This section outlines the national standards and design specifications governing the use of FRP bars in reinforced concrete (RC) structures, including those from ASTM and FDOT. These specifications primarily cover FRP bars up to #10, with #11 bars included only through extrapolation from smaller bars.

ASTM D7957/D7957M-22 [43] is the first ASTM standard for GFRP bars, referenced in ACI 440.11-22. It specifies requirements for solid round GFRP bars up to #10, with a minimum modulus of elasticity of 44.8 GPa (Table 13). ASTM D8505/D8505M-23 [44] expands coverage

to include both GFRP and BFRP bars, with a higher minimum modulus of 60.0 GPa, but still limits the largest size to #10 (Table 14).

Table 13. Table 3 ASTM D7957/D7957M-22 – Geometric and mechanical property requirements

Bar Size Designation	Designated diameter	Standard Cross section area	Measured Cross-Sectional Area mm² [in²]		Minimum Guaranteed Strength
	mm [in]	mm² [in²]	Min.	Max.	kN [kip]
M6 [2]	6.3 [0.250]	32 [0.049]	30 [0.046]	55 [0.085]	27 [6.1]
M10 [3]	9.5 [0.375]	71 [0.110]	67 [0.104]	104 [0.161]	59 [13.2]
M13 [4]	12.7 [0.500]	129 [0.200]	119 [0.185]	169 [0.263]	96 [21.6]
M16 [5]	15.9 [0.625]	199 [0.310]	186 [0.288]	251 [0.388]	130 [29.1]
M19 [6]	19.1 [0.750]	284 [0.440]	268 [0.415]	347 [0.539]	182 [40.9]
M22 [7]	22.2 [0.875]	387 [0.600]	365 [0.565]	460 [0.713]	241 [54.1]
M25 [8]	25.4 [1.000]	510 [0.790]	476 [0.738]	589 [0.913]	297 [66.8]
M29 [9]	28.7 [1.128]	645 [1.000]	603 [0.934]	748 [1.159]	365 [82.0]
M32 [10]	32.3 [1.270]	819 [1.270]	744 [1.154]	950 [1.473]	437 [98.2]

Table 14. Table 3 ASTM D8505/D8505M-23 – Geometric and mechanical property requirements

Bar Size Designation	Designated diameter	Standard Cross section area	Measured Cross-Sectional Area mm² [in²]		Minimum Guaranteed Strength	Minimum Bond Strength
	mm [in]	mm² [in²]	Min.	Max.	kN [kip]	MPa [psi]
M6 [2]	6.3 [0.250]	32 [0.049]	30 [0.046]	55 [0.085]	33 [7.4]	
M10 [3]	9.5 [0.375]	71 [0.110]	67 [0.104]	104 [0.161]	71 [16.0]	
M13 [4]	12.7 [0.500]	129 [0.200]	119 [0.185]	169 [0.263]	124 [27.9]	9.6
M16 [5]	15.9 [0.625]	199 [0.310]	186 [0.288]	251 [0.388]	181.5 [40.8]	[1400]
M19 [6]	19.1 [0.750]	284 [0.440]	268 [0.415]	347 [0.539]	254.9 [57.3]	
M22 [7]	22.2 [0.875]	387 [0.600]	365 [0.565]	460 [0.713]	337.2 [75.3]	
M25 [8]	25.4 [1.000]	510 [0.790]	476 [0.738]	589 [0.913]	422.1 [94.9]	
M29 [9]	28.7 [1.128]	645 [1.000]	603 [0.934]	748 [1.159]	511.5 [115.0]	7.6 [1100]
M32 [10]	32.3 [1.270]	819 [1.270]	744 [1.154]	950 [1.473]	617.0 [138.7]	

FDOT Standard Specifications, Section 932-3 [45], outline material requirements for GFRP and BFRP bars in highway and bridge construction, as referenced in the FDOT Structures Manual, Vol. 4. Unlike ASTM standards, FDOT specifications include bars up to #11 (Table 15). However, #11 bar properties are derived from extrapolated data using a conservative best-fit trend, rather than extensive experimental testing. The cross-sectional area and ultimate capacity of FRP reinforcing bars #11 and smaller conform to the requirements listed in §932-4.2 of FDOT FY2024-25 specifications [46].

Table 15. Table 932-8 FDOT FY2024-25 – Sizes and tensile loads of FRP reinforcing bars

Bar Size Designation	Nominal Bar Diameter [in]	Nominal Cross Sectional Area [in²]	Measured Cross-Sectional Area [in²] Min.	Measured Cross-Sectional Area [in²] Max.	Minimum Guaranteed Tensile Load [kips] BFRP & GFRP Bars (Type 0)	Minimum Guaranteed Tensile Load [kips] BFRP & GFRP Bars (Type III)	Minimum Guaranteed Tensile Load [kips] CFRP (Type II) Single & 7-Wire Strands	Minimum Guaranteed Tensile Load [kips] CFRP Bars (Type I)	Minimum Nominal Ultimate Tensile Stress [ksi] BFRP & GFRP Bars (Type 0)	Minimum Nominal Ultimate Tensile Stress [ksi] BFRP & GFRP Bars (Type III)	Minimum Nominal Ultimate Tensile Stress [ksi] CFRP * (Type II) Single & 7-Wire Strands	Minimum Nominal Ultimate Tensile Stress [ksi] CFRP Bars (Type I)
2.1-CFRP	0.21	0.028	0.026	0.042	-	-	7.1	-	-	-	273.1	-
2	0.25	0.049	0.046	0.085	6.1	7.4	-	10.3	132.6	160.9	-	223.9
2.8-CFRP	0.28	0.051	0.048	0.085	-	-	13.1	-	-	-	272.9	-
3	0.375	0.11	0.104	0.161	13.2	16	-	20.9	126.9	153.8	-	201.0
3.8-CFRP	0.38	0.09	0.087	0.134	-	-	23.7	-	-	-	272.4	-
4	0.5	0.2	0.185	0.263	21.6	27.9	-	33.3	116.8	150.8	-	180.0
5	0.625	0.31	0.288	0.388	29.1	40.8	-	49.1	101.0	141.7	-	170.5
6	0.75	0.44	0.415	0.539	40.9	57.3	-	70.7	98.6	138.1	-	170.4
6.3-CFRP	0.63	0.19	0.184	0.242	-	-	49.8	-	-	-	270.7	-
7	0.875	0.6	0.565	0.713	54.1	75.8	-	-	95.8	134.2	-	-
7.7-CFRP	0.77	0.29	0.274	0.355	-	-	74.8	-	-	-	273.0	-
8	1	0.79	0.738	0.913	66.8	94.9	-	-	90.5	128.6	-	-
9	1.128	1	0.934	1.159	82	115	-	-	87.8	123.1	-	-
10	1.27	1.27	1.154	1.473	98.2	138.7	-	-	85.1	120.2	-	-
11	1.41	1.56	1.5	1.7	105.8	160	-	-	70.5	106.7	-	-

* large-tow carbon fiber

The trend of tensile strength for Type 0 and Type III bars (low and high modulus, respectively) demonstrates that ultimate strength decreases with increasing cross-sectional area, as illustrated in Figure 22. This trend highlights the need for further experimental validation to refine design specifications for large-diameter FRP reinforcement in structural applications.

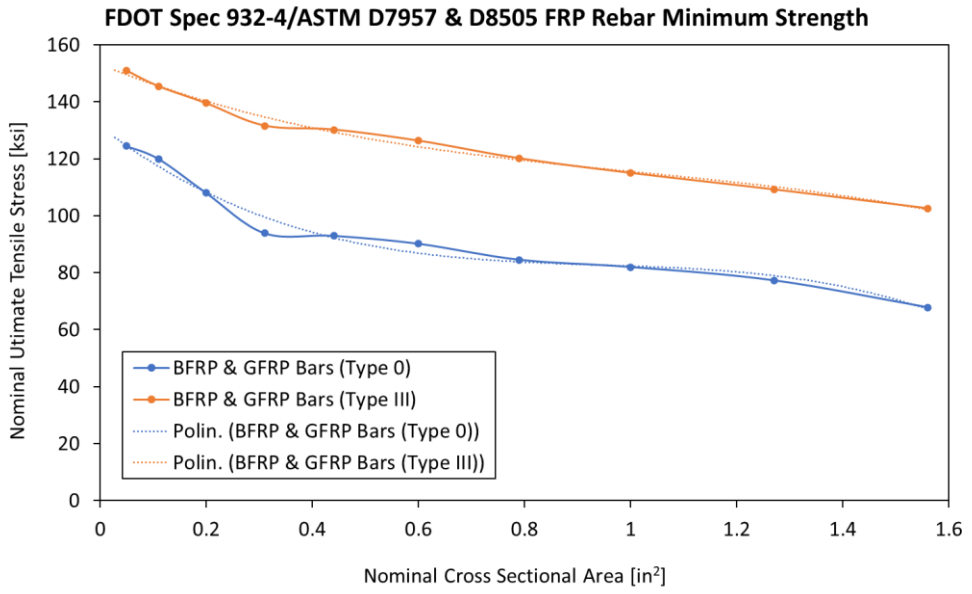

Figure 22. Ultimate stress trend vs. FRP bars area

ACI 440.11-22 [47] is the primary building code for designing concrete structures reinforced with GFRP bars. It references ASTM D7957 for material specifications and follows a structure similar to ACI 318, allowing designers familiar with steel reinforcement to transition more easily to GFRP design.

ACI PRC-440.1-15 [48] was the first design guide developed by ACI 440 for GFRP-reinforced concrete structures. It is currently under review by the ACI 440-H Sub-Committee to align with ACI 440.11-22 and potentially incorporate new topics, such as BFRP bars (per ASTM D8505), shear friction provisions, and updated development length requirements. Unlike ACI 440.11-22, this guide is advisory and does not use mandatory language.

AASHTO LRFD Bridge Design Guide Specifications for GFRP-Reinforced Concrete [1] serves as the primary design guide for infrastructure projects, particularly bridges reinforced with GFRP bars. The second edition (2018) enables the comprehensive design of all bridge elements using GFRP reinforcement.

The FDOT Design Manual 2024 V.4 [45] outlines state-specific methodologies for designing transportation structures reinforced with GFRP and BFRP bars, ensuring compliance with Florida Department of Transportation (FDOT) requirements.

ACI 440.5-08 [49] is the standard specification for construction procedures involving FRP reinforcing bars. It establishes the necessary procedures and quality control measures to ensure that concrete structures reinforced with FRP bars meet the required standards for structural integrity and performance. This document serves as a guideline for contractors and engineers, ensuring that FRP reinforcement is properly installed and that construction practices align with industry standards.

2.4.2. Canada

CSA S807:19 [37] is a Canadian specification covering FRP bars made from aramid, basalt, carbon, or E-CR glass fibers. The largest bar size included is #11 (36 mm), as shown in Table 16. However, the values provided are based on limited testing data, so users should exercise caution when applying them in structural design.

Table 16. Table 1 CSA S807:19 – Designated bar diameter and nominal area

Designated Diameter [mm]	Nominal Cross Sectional Area [mm^2]	Measured Cross-Sectional Area [mm^2]	
		Min.	Max.
6	32	30	55
8	50	48	79
10	71	67	104
13	129	119	169
15	199	186	251
20	284	268	347
22	387	365	460

Designated Diameter [mm]	Nominal Cross Sectional Area [mm²]	Measured Cross-Sectional Area [mm²]	
		Min.	Max.
25	510	476	589
30	645	603	733
32	819	744	894
36	1006	956	1157

Notes:
(1) *The nominal cross-sectional area is not based on designated diameter. These designated diameters shall be used for the calculation of the bond strength and the apparent horizontal shear strength.*
(2) *These nominal cross-sectional area values shall be used for the determination of properties.*

The nominal cross-sectional area for FRP bars is not directly based on the designated diameter, meaning that bond strength and apparent horizontal shear strength calculations must use specific designated diameters. Additionally, these nominal cross-sectional area values are required for determining mechanical properties of FRP bars.

This specification represents one of the few design documents that extends coverage to #11 bars, though further research and validation are necessary to confirm the reliability of the provided values.

CSA S806:12 (R2021) [50] provides design and construction guidelines for building structures reinforced with various types of FRP materials, including aramid (AFRP), carbon (CFRP), and glass (GFRP) fibers. Unlike ACI 440.11-22, which is limited to GFRP bars, this Canadian standard covers a broader range of FRP materials, allowing for more diverse reinforcement applications in building construction.

CSA S6:19 Canadian Highway Bridge Design Code [51] serves as Canada's primary standard for transportation infrastructure, including bridges reinforced with FRP bars. Chapter 16 specifically outlines design provisions for FRP-reinforced structures, ensuring that FRP materials are integrated safely and effectively into Canadian transportation projects.

2.4.3. International

AC454 [52], issued by the ICC Evaluation Service, establishes the test methods and evaluation criteria for GFRP and BFRP bars used in internal reinforcement of concrete members. This criterion references ASTM D7957 and applies to bars up to size #10, ensuring compliance with industry standards for structural applications.

AC521 [53] serves a similar purpose but is tailored for non-structural concrete elements. It also references ASTM D7957 and applies to FRP bars and meshes up to size #10. These criteria help standardize the performance assessment of FRP reinforcement, though they do not extend to larger bar sizes beyond #10.

3. Test Plan for #11 FRP Bar Mechanical Characterization

This report presents a comprehensive testing plan for #11 FRP bars intended for waterline pile cap footings in bridges. The physico-mechanical characterization of these bars is essential for ensuring structural performance and long-term reliability. Accurate and standardized testing assesses tensile strength, bond strength, shear strength, and other critical properties necessary for their implementation in bridge design.

All tests are conducted following ASTM standards, ensuring consistency and reliability in the results. The testing protocols align with Florida Department of Transportation (FDOT) specifications, particularly Section 932-4 Fiber Reinforced Polymer (FRP) Reinforcing Bars and Materials Manual Section 12.1 Volume II Fiber Reinforced Polymer Composites [1]. These standardized procedures help establishing material acceptance criteria and support the safe adoption of large-diameter FRP bars in transportation infrastructure.

This document provides a test plan to meet Task 2: Test Plan for #11 Bar Mechanical Characterization under the task work order titled 'Waterline Pile Cap Footings for Bridges Using Large Diameter FRP Reinforcing - Material Characterization and Design.' The document is developed in accordance with applicable references from the Florida Department of Transportation (FDOT) Section 932-4 Fiber Reinforced Polymer (FRP) Reinforcing Bars and Materials Manual Section 12.1 Volume II Fiber Reinforced Polymer Composites, as well as the task work order needs and current research practices. The goal is to establish a test plan to evaluate large diameter glass fiber reinforced polymer (GFRP) bars with a nominal size of #11 (1.375 in.). The tests methods used for the qualification test program are summarized in Table 17.

Table 17. Summary of standard test methods for the qualification test program

Test Description	ID Test Method	ASTM Standard Test Reference
Fiber Mass Fraction	FC	ASTM D2584-18 Standard Test Method for Ignition Loss of Cured Reinforced Resins [54]
Moisture Absorption	MA	ASTM D570-22, Standard Test Method for Water Absorption of Plastics. Section 8.1 for short term and Section 8.4 for long term [55]
Glass Transition Temperature	TG	ASTM E1356-23, Standard Test Method for Assignment of the Glass Transition Temperatures by Differential Scanning calorimetry [4]
		ASTM D7028-07(2015), Standard Test Method for Glass Transition Temperature (DMA) of Polymer Matrix Composites by Dynamic Mechanical Analysis (DMA) [56]
Degree of Cure	DC	ASTM E2160-04 (2018), Standard Test Method for Heat of Reaction of Thermally Reactive Materials by Differential Scanning Calorimetry [57]
Measured Cross-Sectional Area	MXA	ASTM D7205/D7205M-21, Standard test method for Tensile Properties of Fiber Reinforced Polymer Matrix Composite Bars, Section 11.2.4.1. ASTM D792-20, Standard Test Methods for Density and Specific Gravity (Relative Density) of Plastics by Displacement [58]
Tensile Properties (Load and Modulus)	TNS	ASTM D7205/D7205M-21, Standard test method for Tensile Properties of Fiber Reinforced Polymer Matrix Composite Bars [59]

Test Description	ID Test Method	ASTM Standard Test Reference
Alkaline Resistance with no Load	AR	ASTM D7705/D7705M-12(2019), Standard Test Method for Alkali Resistance of Fiber Reinforced Polymer (FRP) Matrix Composite Bars used in Concrete Construction, Procedure A [60]
Transverse Shear Strength	TSS	ASTM D7617/D7617M-11(2017), Standard Test Method for Transverse Shear Strength of Fiber–Reinforced Polymer Matrix Composite Bars [61]
Horizontal Shear Strength	HSS	ASTM D4475-21, Standard Test Method for Apparent Horizontal Shear Strength of Pultruded Reinforced Plastics Rods by Short-Beam Method [62]
Bond Strength to Concrete, Block Pull-Out	BS	ASTM D7913/D7913M – 14(2020), Standard Test Method for Bond Strength of Fiber-Reinforced Polymer Matrix Composite Bars to Concrete by Pullout Testing [63] ASTM C39-20, Standard Test Method for Compressive Strength of Cylindrical Concrete Specimens [64]

Testing of the proposed plan is carried out by the University of Miami, Structures and Materials Laboratory (SML). All tests are performed by and under the supervision of SML. SML is a qualified laboratory by the Florida Department of Transportation (FDOT) under laboratory number ISM028 and has met the requirements of the International Accreditation Service (IAS) AC89 (Accreditation Criteria for Testing Laboratories). This demonstrates compliance with ANS/ISO/IEC Standard 17025-2017, "General requirements for the competence of testing and calibration laboratories," and the laboratory has been accredited for the test methods listed in the approved scope of accreditation under Testing Laboratory #TL-478.

Initially, the project included the characterization of one GFRP and one BFRP #11 bar type. However, due to the difficulty in finding a BFRP manufacturer capable of producing bars in the #11 size, two GFRP #11 bar types were evaluated, as agreed with FDOT. The selected manufacturers are MST and Pultrall. Figure 23 and Figure 24 show typical rebars made by the two different manufacturers.

The comprehensive test plan outlines the specific Physico-mechanical properties to be evaluated, the ASTM standards to be adhered to, and the detailed procedures to be followed to ensure accurate and reliable results.

Figure 23. FRP bar manufactured by Pultrall

Figure 24. FRP bar manufactured by MST

3.1. Specimen ID Nomenclature

All proposed test specimens including mechanical, physical and durability tests will be uniquely labeled and identified for quality and traceability purposes using the format described below. The detailed specimen identification (ID) nomenclature is summarized in Table 18Table 18:

CCC-PP_TTT_EE_XX

where,

CCC, refers to company reference;

PP, refers to the product / sample under evaluation;

TTT, refers to the test type or mechanical property;

EE, refers to the type of exposure; and

XX, is the specimen repetition number.

Table 18. Specimen identification (ID) nomenclature

Nomenclature	Reference Definition Detail	ID
CCC, Company Reference	V-Rod/Pultrall	PUL
	MST-Bar	MST
PPP, Product / Sample	Straight Glass FRP straight bar – Nominal Size 11	11S
TTT, Test Type	Fiber Content	FC
	Glass Transition Temperature	TG
	Degree of Cure (Total Enthalpy of Polymerization)	DC
	Measured Cross Sectional Area	MXA
	Tensile Properties	TNS
	Transverse Shear Strength	TSS
	Horizontal Shear Strength	HSS
	Bond Strength to Concrete	BS
	Moisture Absorption	MA
EE, Exposure	Control/benchmark tests (laboratory conditions) if applicable	CC
	Alkaline Resistance without Load	AR
XX, Specimen no.	Specimen Repetition Number	as applicable

3.2. Test Program

The following section provides a detailed test program for the approval and qualification of the products under evaluation, which is summarized from Table 20 to Table 21. The test program is developed, and in compliance, with the sampling and test requirements referenced within per FDOT's Materials Manual Section 12.1 Volume II Fiber Reinforced Polymer Composites and FDOT's specification Section 932 for Nonmetallic Accessory Materials for Concrete Pavement and Concrete Structures, sub-section 932-4.3, Table 932-8. The specimen ID nomenclature is used within the tables (refer to Table 17 for definitions. Table 20 to Table 21include: the product type, the test type, the exposure/aging condition, the number of test repetitions per lot; as well as the specification requirement (i.e. pass/fail acceptance criteria) for each test method and product as applicable. Note that the number of test repetition reported herein, is equal to or exceeds the requirements set forth within Materials Manual Section 12.1 Volume II. Results are based on the reported results.

Table 19. Test program for physical properties

Company-Product-Shape ***CC-PP***	**Test ID MMM**	**TYPE of exposure EE**	**Minimum Repetitions per Manufacturer (Single Lot)**	**Materials Manual Section 12.1 Table 1**
Fiber Mass Content ASTM D2584, Standard Test Method for Ignition Loss of Cured Reinforced Resins				
PUL-11S	FC	CC	5	≥ 70 %
MST-11S				
Glass Transition Temperature ASTM E1356, Standard Test Method for Assignment of the Glass Transition Temperatures by Differential Scanning Calorimetry				
PUL-11S	TG	CC	5	≥ 100°C (212°F) *based on DSC*
MST-11S				
Degree of Cure ASTM E2160, Standard test method for heat of reaction of thermally reactive materials by differential scanning calorimetry				
PUL-11S	DC	CC	5	≥ 95 %
MST-11S				
Cross-Sectional Area ASTM D7205/D7205M, Standard test method for Tensile Properties of Fiber Reinforced Polymer Matrix Composite Bars ASTM D792, Standard Test Methods for Density and Specific Gravity (Relative Density) of Plastics by Displacement				
PUL-11S	MXA	CC	5	> 968 mm^2 (1.500 in^2) <1097 mm^2 (1.700 in^2)
MST-11S				

Table 20. Test program for mechanical properties

Company-Product-Shape ***CC-PP***	**Test ID MMM**	**TYPE of exposure EE**	**Minimum Repetitions per Manufacturer (Single Lot)**	**Materials Manual Section 12.1 Table 1**
Guaranteed Tensile Load and Tensile Modulus ASTM D7205/D7205M, Standard test method for Tensile Properties of Fiber Reinforced Polymer Matrix Composite Bars				
PUL-11S	TNS	CC	10	Type 0 bars ≥470 kN (105.8 kip) ≥ 44.8 GPa (6.5 Msi)
MST-11S				Type III bars ≥712 kN (160.0 kip) ≥ 58.6 GPa (8.5 Msi)
Transverse Shear Strength ASTM D7617/D7617M, Standard Test Method for Transverse Shear Strength of Fiber-Reinforced Polymer Matrix Composite Bars				
PUL-11S	TSS	CC	5	≥ 152 MPa (22 ksi)
MST-11S				
Horizontal Shear Strength ASTM D4475, Standard Test Method for Apparent Horizontal Shear Strength of Pultruded Reinforced Plastic Rods By the Short-Beam Method				
PUL-11S	TSS	CC	5	≥38 MPa (5.5 ksi)
MST-11S				
Bond Strength ASTM D7913/D7913M, Standard Test Method for Bond Strength of Fiber-Reinforced Polymer Matrix Composite Bars to Concrete by Pullout Testing				
PUL-11S	BS	CC	5	Type 0 bars ≥7.6 MPa (1.1 ksi) Type III bars ≥ 9.7 MPa (1.4 ksi)
MST-11S				

Table 21. Test program for durability properties

Company-Product-Shape ***CC-PP***	**Test ID MMM**	**TYPE of exposure EE**	**Minimum Repetitions per Manufacturer (Single Lot)**	**Materials Manual Section 12.1 Table 1**
Moisture Absorption ASTM D570, Standard Test Method for Water Absorption of Plastics, PROCEDURE 7.1 and 7.4				
PUL-11S	MA	CC	5	≤ 0.25 % post 24 hrs. at 50°C (122°F)
MST-11S				≤ 1.0 % saturation at 50°C (122°F)
Alkaline Resistance with no Load ASTM D7705/D7705, Standard test method for Alkali Resistance of Fiber Reinforced Polymer (FRP) Matrix Composite Bars used in Concrete Construction. PROCEDURE A ASTM D7205/D7205, Standard test method for Tensile Properties of Fiber Reinforced Polymer Matrix Composite Bars				
PUL-11S	TNS	AR	5	≥ 70% of tensile strength retention
MST-11S				

3.3. Testing of Representative Products

Sampling for the V-Rod/Pultrall and MST Bar FRP bars under evaluation was conducted under the supervision of FDOT personnel per FDOT specifications.

Upon arrival of the products for evaluation to the testing laboratory, the packages were acknowledged and identified to account for all the products and their batch numbers for quality assurance purposes. All products were then individually inspected to ensure validity for testing, free of damage, contamination, or other criteria deviating from being representative of the standard manufactured products as initially sampled based on SML standard operating procedures.

Table 22 provides a summary of the products under evaluation and the identification provided by the manufacturer for quality and traceability purposes.

Table 22. FRP product manufacturing traceability references

Product Identification	Manufacture Production Reference
Pultrall #11 Glass FRP Straight Bar	2414002-11-60
MST Bar #11 Glass FRP Straight Bar	15M.GRADEIII.25368.S.204.2024

3.4. Test Data

All the test results presented herein are linked through unbroken chain to the raw data files recorded on the day of the test. Details regarding raw data can be found in the technical test record completed at the time of the tests.

Analyzed data is obtained directly from the raw data obtained during testing, from which the test results are presented. This report contains analyzed tabulated data results of each test. Additionally, as part of the standard operating procedures and quality assurance of the SML, intermediate checks of the data analysis are performed at various stages of the data analysis process reducing the possible analysis errors.

4. Physico-mechanical Testing of #11 Bars

This section provides the tests results to meet Task 3 of the project: Physico-mechanical testing for #11 Bars under the task work order titled 'Waterline Pile Cap Footings for Bridges Using Large Diameter FRP Reinforcing - Material Characterization and Design.'

The FRP bars manufactured by V-Rod/Pultrall had a sand coated surface finish and the FRP bars manufactured by MST-Bar had a grooved surface finish. Table 23 summarizes the bar product/s under evaluation, including the identification (ID) within this report.

Table 23. Products under evaluation

Product No.	Product Size	Product Description	Report ID
1	#11	V-Rod/ Pultrall Glass FRP straight bar #11 with sand coated surface	PUL_11S
2	#11	MST-Bar Glass FRP straight bar #11 with grooved surface	MST_11S

Figure 25 and Figure 26 show the #11 FRP bars from Pultrall and MST as received by the manufacturers to be tested at University of Miami.

Figure 25. FRP straight bar #11 manufactured by Pultrall.

Figure 26. FRP straight bar #11 manufactured by MST-Bar.

The following sub-sections, summarize the testing results for each of the Physico-mechanical testing that was conducted as part of the testing plan summarized in Section 3.2.

4.1. Fiber Content – ASTM D2584

To determine the fiber content by mass of the products under evaluation based on ASTM D2584.

The specimens were cut from different randomly selected locations from sample bar to the prescribed dimensions using a high precision blade saw and conditioned under laboratory ambient conditions for at least 40 hr. at room temperature, 23 ± 3°C (73 ± 6°F) and 50±10% relative humidity. Refer to Table 24, which includes the test specimen nominal length, test location, and date. Representative pictures of specimens before and after testing are provided in Figure 28.

Table 24. Specimen summary information

Specimen ID	Specimen Nominal Length	Test Date mm/dd/yy	Test Location
PUL_11S_FC_01 to 05	25 mm (1.0 in.).	10/28/24 to 10/29/24	SML
MST_11S_FC_01 to 05		10/31/24 to 11/01/24	

Tests were conducted under laboratory ambient conditions by qualified personnel. The date of each test, technical personnel, variations to the test method as applicable, calibration information for instruments and equipment used in all measurements, identification of the material tested, temperature and humidity of testing laboratory, and other applicable test data or details are provided in the technical data sheet: TDS-FC-FDOT that can be found online per request.

Specimens were placed in pre-heated crucibles and placed in a furnace at 565 ± 28°C (1050 ± 50°F) until all carbonaceous material disappeared, as shown in Figure 27 and Figure 28. Weight measurements in a high precision microscale were taken to the nearest 0.0001 g (2.2×10^{-7} lb.) before and after to determine the fiber content as per ASTM D2584, where a desiccator was used to place the specimens while cooling down to avoid absorption of air moisture by the dry fibers.

The results reported herein have been computed per ASTM D2584 using the parameters defined in Table 25. Note that sand granules (as applicable) were separated from the calculation, so that only the dry fiber weight after ignition was measured in order to obtain the actual fiber content.

Table 25. Fiber content parameter definitions and calculations

Symbol	Parameter	Description
W_1	Weight	Weight of bar specimen
W_2		Weight of residue, fibers only
RC	Resin content	Ignition loss = $[(W1 - W2)/W1]*100$
FC	Fiber content	$100 - [(W1 - W2)/W1]*100$

Based on the experimental tests presented herein the fiber content by mass results are summarized in Table 26. Tabulated test results are reported in appendix A.

Table 26. Average summary results for fiber content by mass tests

Test ID	Number of Tested Specimens	Fiber Content FC %	Materials Manual Section 12.1 Table 1 Specification (% by weight)	Acceptance Criteria
PUL_11S_FC	5	84	≥ 70%	PASS
MST_11S_FC	5	81		

Glass FRP bars with nominal size #11 for manufacturers V-Rod/Pultrall and MST-Bar, comply with the requirements established in Table 1 Physical and Mechanical Property Requirements for Straight FRP Reinforcing Bars of the FDOT's Materials Manual Section 12.1 Volume II Fiber Reinforced Polymer Composites by having an average Fiber Content by weight greater or equal to 70% and a coefficient of variance less or equal to 15%.

Figure 27. Fiber content furnace test setup

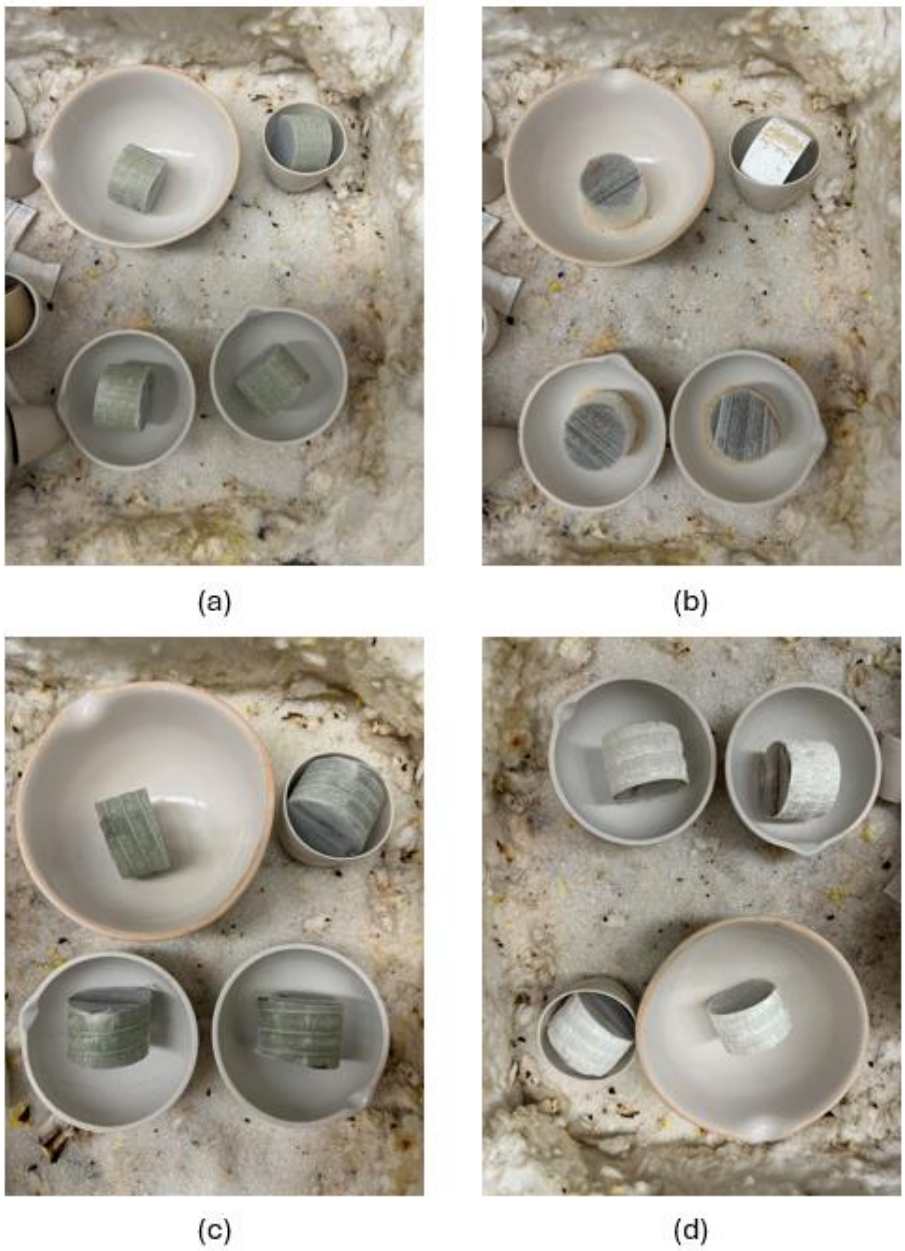

Figure 28. Fiber content representative test samples (a) pre-testing and (b) post-test (ignition) for Pultrall and (c) pre-testing and (d) post-test (ignition) for MST-Bar

4.2. Glass Transition Temperature – ASTM E1356

To determine the glass transition temperature based on differential scanning calorimetry (DSC) method for the products under evaluation, based on ASTM E1356.

A disk specimen was extracted with a high precision blade saw from the cross-section of the bar, avoiding grinding to reduce the thermal effects that may affect the specimen's thermal history properties, to then extract a portion of the disk with a high precision blade to provide a specimen with a minimum mass of 5 mg. All specimens were conditioned under laboratory ambient conditions for at least 40 hrs. at room temperature 23 ± 3°C (73 ± 6°F) and 50 ± 10% relative humidity. Refer to Table 27 which includes the test specimen size (weight), test location and date.

Table 27. Specimen summary information

Specimen ID	Specimen Nominal Size	Test Date mm/dd/yy	Test Location
PUL_11S_TG_01 to 05	10 mg	11/06/24 to 11/13/24	SML
MST_11S_TG_01 to 05		10/04/24	

Tests were conducted under laboratory ambient conditions by qualified personnel. The date of each test; technical personnel; variations to the test method as applicable; calibration information for instruments and equipment used in all measurements; identification of the material tested; temperature and humidity of testing laboratory; and other applicable test data or details is provided in the technical data sheet: TDS-TG-FDOT.

A differential scanning calorimeter (DSC) capable of programming, measuring, and recording heat flow as a function of temperature and time with a dedicated test was used, as seen in Figure 29. The specimen was placed in the chamber and programmed as needed for the temperature rate heating and cooling.

A heating/cooling rate of 10°C/min was applied until the glass transition temperature was determined. An initial thermal program was done prior testing flowing nitrogen in the chamber at a rate of 10°C/min to laboratory conditions to remove potential environmental thermal history.

The results reported herein have been computed per ASTM E1356 using the parameters defined in . The Tg is extrapolated numerically by the DSC from the heat flow versus temperature reaction curve, corresponding to range at which the observed material transitions from the hard, brittle region to the soft, rubbery region.

Table 28. Parameter definitions and calculations for glass transition temperature

Symbol	Parameter	Description
T_g	Temperature	Glass Transition Temperature

Based on the experimental tests presented herein the mean Glass Transition Temperature is summarized in Table 29. Tabulated test results are reported in appendix A.

Table 29. Average summary results for glass transition temperature tests

Specimen ID	Number of Tested Specimens	Glass Transition Temperature T_g °C	°F	Materials Manual Section 12.1 Table 1 Specification	Acceptance Criteria
PUL_11S_TG	5	118	244	≥100°C (212°F)	PASS
MST_11S_TG	5	114	238		

Glass FRP bars with nominal size #11 for manufacturers V-Rod/Pultrall and MST-Bar, comply with the requirements established in Table 1 Physical and Mechanical Property Requirements for Straight FRP Reinforcing Bars of the FDOT's Materials Manual Section 12.1 Volume II Fiber Reinforced Polymer Composites by having an average Glass Transition Temperature greater than 100 °C (212 °F) and a coefficient of variance less or equal to 15%.

Figure 29. Test setup showing DSC in operation

4.3. Degree of Cure – ASTM E2160

To determine the exothermic heat of reaction of thermally reactive chemicals or chemical mixtures of the products under evaluation based on ASTM E2160.

A disk specimen with nominal thickness of 1 mm (0.04 in.) was extracted with a high precision blade saw from the cross-section of the bar. A wedge portion of this disk was then extracted with a high precision blade to provide a specimen with a total minimum mass of 5 mg. The specimens were cut to the prescribed dimensions avoiding grinding to reduce the thermal effects that may affect the specimen's thermal history properties. All specimens were conditioned under laboratory ambient conditions for at least 40 hrs. at room temperature 23 ± 3°C (73 ± 6°F) and 50 ± 10% relative humidity. Refer to Table 30 which includes the test specimen size (weight), test location and date.

Table 30. Specimen summary information

Specimen ID	Specimen Nominal Size	Test Date mm/dd/yy	Test Location
PUL_11S_DC_01 to 05	10 mg	11/06/24 to 11/13/24	SML
MST_11S_DC_01 to 05		10/04/24	

Tests were conducted under laboratory ambient conditions by qualified personnel. The date of each test; technical personnel; variations to the test method as applicable; calibration information for instruments and equipment used in all measurements; identification of the material tested; temperature and humidity of testing laboratory; and other applicable test data or details is provided in the technical data sheet: TDS-DC-FDOT.

A differential scanning calorimeter (DSC), capable of programming, measuring and recording heat flow as a function of temperature and time with a dedicated sealed test chamber was used, as seen in Figure 29. The specimen was placed in the chamber, weighted and programmed as needed for the temperature rate heating. A heating rate of 10 ± 0.1°C/min to provide uniform controlled heating of the specimen and reference to a constant temperature within the temperature range of 25 to 250°C (77 to 482°F) was applied.

The results reported herein have been computed per ASTM E2160 using the parameters defined in Table 32. The degree of cure, DC is computed percentage of the fraction reacted, given by the difference between the total heat of reaction, H_t, and the normalized heat, H. The total heat of reaction and the normalized heat, where computed with the integrated thermal analysis software of the DSC. Note that the total heat of reaction (H_t), which is derived from the unreacted resin system (neat resin), is conservatively assumed value of 100 J/g to compute the degree of cure.

Table 31. Parameter definitions and calculations for total enthalpy of polymerization (degree of cure)

Symbol	Parameter	Description
A	Reaction	Heat of reaction of bar sample
M	Mass	Specimen mass
H	Normalized heat of reaction	H = A/M
H_t	Reaction	Total heat of reaction of unreacted sample = 100 J/g
DC	Degree of Cure	Fraction reacted = $(1 – H/H_t)*100\%$

Based on the experimental tests presented herein the average degree of cure is summarized in Table 32. Tabulated test results are reported in appendix A.

Table 32. Average summary results for degree of cure tests

Specimen ID	Number of Tested Specimens	Degree of Cure DC %	Materials Manual Section 12.1 Table 1 Specification	Acceptance Criteria
PUL_11S_DC	5	99	≥ 95%	PASS
MST_11S_DC	5	98		

Glass FRP bars with nominal size #11 for manufacturers V-Rod/Pultrall and MST-Bar, comply with the requirements established in Table 1 Physical and Mechanical Property Requirements for Straight FRP Reinforcing Bars of the FDOT's Materials Manual Section 12.1 Volume II Fiber Reinforced Polymer Composites by having an average Degree of Cure greater than 95% and a coefficient of variance less or equal to 15%.

4.4. Cross-sectional Area – ASTM D7205/D792

To determine the measured cross-sectional area of the products under evaluation by immersion method based on ASTM D7205 and ASTM D792.

The specimens were cut to the prescribed dimensions using a high precision blade saw and conditioned, under laboratory ambient conditions for at least 40 hrs. at room temperature 23 ± 3°C (73 ± 6°F) and 50 ± 10% relative humidity. Refer to Table 33 which includes the test specimen size (length), test location and date. Representative pictures of the test set up are provided in Figure 30.

Table 33. Specimen summary information

Specimen ID	Specimen Nominal Size	Test Date mm/dd/yy	Test Location
PUL_11S_MXA_01 to 05	19 mm (0.75 in.)	10/23/24	SML
MST_11S_MXA_01 to 05	19 mm (0.75 in.)	10/23/24	SML

Tests were conducted under laboratory ambient conditions by qualified personnel. The date of each test; technical personnel; variations to the test method as applicable; calibration information for instruments and equipment used in all measurements; identification of the material tested; temperature and humidity of testing laboratory; and other applicable test data or details is provided in the technical data sheet: TDS-MXA-FDOT.

A precision analytical balance was used to determine of the specific gravity, an internal frame holds the specimen, and then immersed into distilled water, where additionally the container with the distilled water rests on a support that spans over the scale so that the weight of the container is dismissed, as seen in Figure 30.

The results reported herein have been computed as per ASTM D792, as referenced by ASTM D7205, using the parameters defined in Table 34.

Table 34. Parameter definitions and calculations for cross-sectional

Symbol	Parameter	Description
L	Length	Average length of specimen based on three measurements
ρ_s	Density	Density of specimen
V	Volume	Volume of specimen
A	Area	Measured (experimental) cross-sectional Area of specimen
Weight/unit length	Weight per unit length	Mass per unit length

Based on the experimental tests presented herein the average measured cross-sectional area is summarized in Table 35. Tabulated test results are reported in Appendix A.

Table 35. Average summary results for measured cross-sectional area tests

Specimen ID	Number of Tested Specimens	Measured Area A		Materials Manual Section 12.1 Table 1 Specification	Acceptance Criteria
		mm^2	in^2		
PUL_11S_MXA	5	1108	1.717	>968 mm^2 (1.500 in^2)	FAIL
MST_11S_MXA	5	1118	1.734	<1097mm^2 (1.700 in^2)	

Glass FRP bars with nominal size #11 for manufacturers V-Rod/Pultrall and MST-Bar, do not comply with the current requirements established in Table 1 Physical and Mechanical Property Requirements for Straight FRP Reinforcing Bars of the FDOT's Materials Manual Section 12.1 Volume II Fiber Reinforced Polymer Composites and in Table 932-8 of FDOT's specification Section 932 for Nonmetallic Accessory Materials for Concrete Pavement and Concrete Structures. It is recommended to adjust the range of acceptance for bars with nominal size #11 based on these results.

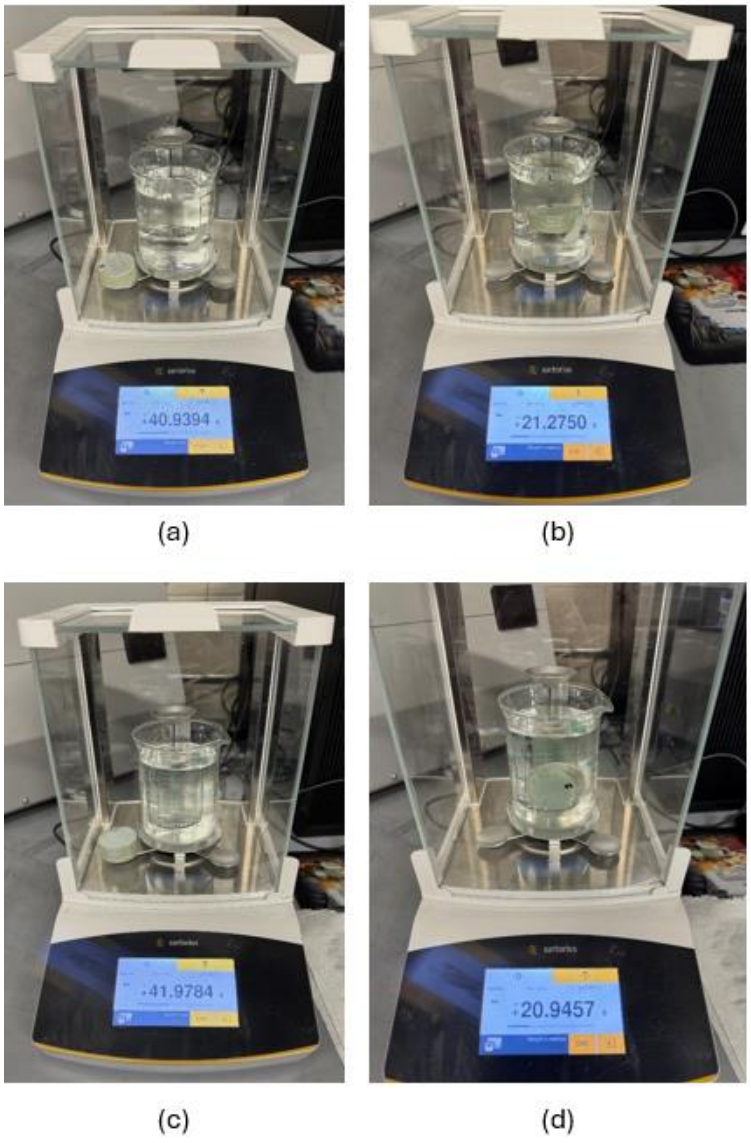

Figure 30. Test setup for measurement of cross-sectional area; (a) specimen weight and (b) immersed specimen for Pultrall; (c) Specimen weight and (b) immersed specimen for MST-Bar

4.5. Tensile Properties – ASTM D7205

To determine the ultimate and guaranteed tensile load carrying capacity, mean tensile modulus of elasticity and mean ultimate tensile strain of the products under evaluation based on ASTM D7205.

The specimens were cut to the prescribed dimensions using chop saw. Steel pipe-type anchors were installed using expansive grout by laboratory personnel after machining the ends of the specimens to center the bar within the anchors and fixtures. All specimens were left to cure for a minimum period of 7 days to ensure the grout reached its maximum internal pressure, ensuring proper anchorage. Refer to Table 36 and Figure 31, for the test specimen size, test date, and location. Considering that L_a=610 mm (24 in.), L=699 mm (27.5 in.), and, Ø=71.1 mm (2.80 in.).

Table 36. Specimen summary information

Specimen ID	Specimen Nominal Size	Test Date mm/dd/yy	Test Location
PUL_11S_TNS_01 to 09	Ø=71.1 mm (2.80 in.)	11/15/24 to 11/19/24	SML
MST_11S_TNS_01 to 10		11/04/24 to 11/19/24	

Tests were conducted under laboratory ambient conditions by qualified personnel. The date of each test, technical personnel, variations to the test method as applicable, calibration information for instruments and equipment used in all measurements, identification of the material tested, temperature and humidity of testing laboratory, and other applicable test data or details are provided in the technical data sheet: TDS-TNS-FDOT that can be found online per request.

Uniaxial tensile load was applied to all specimens. Tensile testing was performed using a universal test frame Tensile load was measured with the internal frame load cell in compliance with ASTM E4-21 (Standard Practice for Force Verification of Testing Machines), while the extension (elongation) of the specimen was measured using a Class B-2 clip-on extensometer in accordance to ASTM E83-16 (Standard Practice for Verification and Classification of Extensometer Systems), with a 100-mm (4.0 in.) gauge length, placed at mid-length of the free length between the anchors, as seen in Figure 32. The extensometer was removed approximately halfway during the test to avoid damage to the instrument. Specimens' anchors were gripped with mechanical wedge-type grips. All data were gathered using a National Instruments data acquisition system at a rate of 100 Hz.

Load was applied in displacement control to effect a near constant strain rate in the gauge section, producing failure within 1 to 10 minutes, as per ASTM D7205 requirements.

The results reported herein have been computed per ASTM D7205 based on the nominal area of the bar. Refer to Table 37 for definitions and calculations.

Table 37. Definitions of calculations for tensile tests

Symbol	Parameter	Description
P_{max}	Maximum force at failure	Peak load recorded during test
P_G	Guaranteed ultimate tensile force	Mean Peak load minus three standard deviations of the average test results.
A_{nom}	Nominal cross-section area	Cross-section area FDOT 932-4, Table 932-8
F^{tu}_{nom}	Nominal ultimate tensile strength	$F^{tu}_{nom} = P_{max} / A_{nom}$
$\varepsilon_{u\text{-}nom}$	Computed ultimate strain based on linear elastic behavior	$\varepsilon_u = F^{tu}_{nom} / E_{nom}$
E_{nom}	Tensile modulus of elasticity	As per Section 13.3.1 ASTM D7205 – computed by fitting a straight line to the data using the method of linear least squares regression analysis. The data range selected goes between 1000 and 6000 με. $E_{nom} = \frac{\sum_{i=1}^{K}(\varepsilon_i \sigma_i) - n\,\bar{\sigma}\,\bar{\varepsilon}}{\sum_{i=1}^{K}\varepsilon_i^2 - n\,\bar{\varepsilon}^2}$

All specimens behaved linear elastically until failure. Based on the experimental tests presented herein the guaranteed ultimate tensile force (P_G), mean tensile modulus (E), the mean computed ultimate tensile strain (ε_u) as summarized in Table 38, where the condition of acceptance is provided below. The mode of failure for all bars was by tensile rupture of the rebar as seen in Figure 33. Tabulated test results are reported in Appendix A.

- #11 Type 0 bars: minimum guaranteed tensile force ≥ 470 kN (105.8 kip)
- #11 Type 0 bars: minimum E shall be ≥ 44.8 GPa (6.5 Msi)
- #11 Type III bars: minimum guaranteed tensile force ≥ 712 kN (160.0 kip)
- #11 Type III bars: minimum E shall be ≥ 58.6 GPa (8.5 Msi)
- All bar sizes: Mean Ultimate Tensile Strain shall be ≥ 1.1 %

Table 38. Average summary results for tensile tests

Specimen ID	Number of Tested Specimens	Guaranteed Ultimate Tensile Force P_G kN	kip	Mean Tensile Modulus of Elasticity E GPa	Msi	Mean Ultimate Tensile Strain ε_u %	Materials Manual Section 12.1 Table 1 **Specification** P_G, & E	Acceptance Criteria
PUL_11S_TNS	9	1098	246.9	59.9	8.7	2.0	Type 0 Bars ≥470 kN (105.8 Kip) ≥44.8 GPa (6.5 Msi)	PASS Refer to Section 9.7
MST_11S_TNS	10	824	185.3	57.8	8.4	1.6	Type III Bars ≥712 kN (160.0 Kip) ≥58.6 GPa (8.5 Msi)	

Based on the current specification established in Table 1 Physical and Mechanical Property Requirements for Straight FRP Reinforcing Bars of the FDOT's Materials Manual Section 12.1 Volume II Fiber Reinforced Polymer Composites and in Table 932-8 of FDOT's specification Section 932 for Nonmetallic Accessory Materials for Concrete Pavement and Concrete Structures:

Glass FRP bars with nominal size #11 for manufacturer V-Rod/Pultrall would be classified as a Type III bar meeting both the requirements of Minimum Guaranteed Tensile Load and Minimum Modulus of Elasticity and a coefficient of variance less or equal to 15%.

Glass FRP bars with nominal size #11 for manufacturer MST-Bar would be classified as a Type 0 bar meeting both the requirements of Minimum Guaranteed Tensile Load and Minimum Modulus of Elasticity and a coefficient of variance less or equal to 15%.

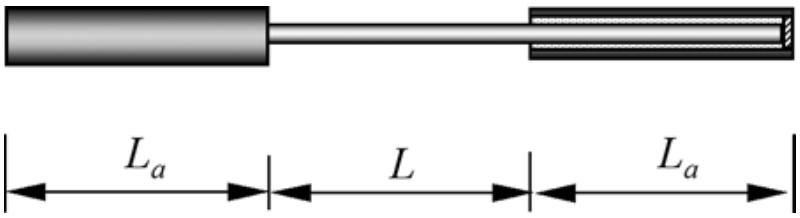

Figure 31. Tensile specimen geometry

Figure 32. Tensile test setup for (a) Pultrall and (b) MST-Bar

Figure 33. Representative failure mode of tensile test for (a) Pultrall and (b) MST-Bar

4.6. Transverse Shear Strength – ASTM D7617

To determine the ultimate transverse shear strength of the products under evaluation based on ASTM D7617.

The specimens were cut from different randomly selected locations from sample bar to the prescribed dimensions using a high precision blade saw and conditioned, under laboratory ambient conditions for at least 40 hrs. at room temperature 23 ± 3°C (73 ± 6°F) and 50 ± 10% relative humidity. Refer to Table 39, which includes the test specimen size (length), test location and date.

Table 39. Specimen summary information

Specimen ID	Specimen Nominal Size	Test Date mm/dd/yy	Test Location
PUL_11S_TSS_01 to 05	229 mm (9.0 in.)	11/04/24	SML
MST_11S_TSS_01 to 05	229 mm (9.0 in.)	11/04/24	SML

Tests were conducted under laboratory ambient conditions by qualified personnel. The date of each test; technical personnel; variations to the test method as applicable; calibration information for instruments and equipment used in all measurements; identification of the material tested; temperature and humidity of testing laboratory; and other applicable test data or details is provided in the technical data sheet: TDS-TSS-FDOT.

Transverse compressive load was applied to the bar using a fixture as per ASTM D7617, providing an evenly distributed load applied to the bar in a double shear configuration. The load was applied using a screw-driven universal test frame with a maximum capacity of 130 kN (30 kip). The load was measured with the internal load cell of the frame in compliance with ASTM E4-21. The test set-up is shown is Figure 34.

The results reported herein have been computed per ASTM D7617 using the parameters defined in Table 40.

Table 40. Parameter definitions and calculations

Symbol	Parameter	Description
P_{max}	Maximum failure force	Peak load recorded during test
A_{nom}	Nominal cross-section area	Area per FDOT 932-4, Table 932-8
$T_{u\text{-}nom}$	Nominal Transverse shear strength	$T_u = P_{max} / (2*A_{nom})$

Based on the experimental tests presented herein the guaranteed transverse shear strength of the bars are summarized in Table 41. The mode of failure was by double shear, as reflected in Figure 35 for all specimens. Tabulated test results are reported in appendix A.

Table 41. Average summary results for transverse shear strength tests

Specimen ID	Number of Tested Specimens	Transverse Shear Strength T		Materials Manual Section 12.1 Table 1 Specification	Acceptance Criteria
		MPa	ksi		
PUL_11S_TSS	5	163	23.6	≥ 151 MPa, (22.0 ksi)	PASS
MST_11S_TSS	5	172	25.0		

Glass FRP bars with nominal size #11 for manufacturers V-Rod/Pultrall and MST-Bar, comply with the requirements established in Table 1 Physical and Mechanical Property Requirements for Straight FRP Reinforcing Bars of the FDOT's Materials Manual Section 12.1 Volume II Fiber Reinforced Polymer Composites by having an average Transverse Shear Strength greater than 22.0 ksi and a coefficient of variance less or equal to 15%.

Figure 34. Transverse shear strength test setup (a) Pultrall and (b) MST-Bar

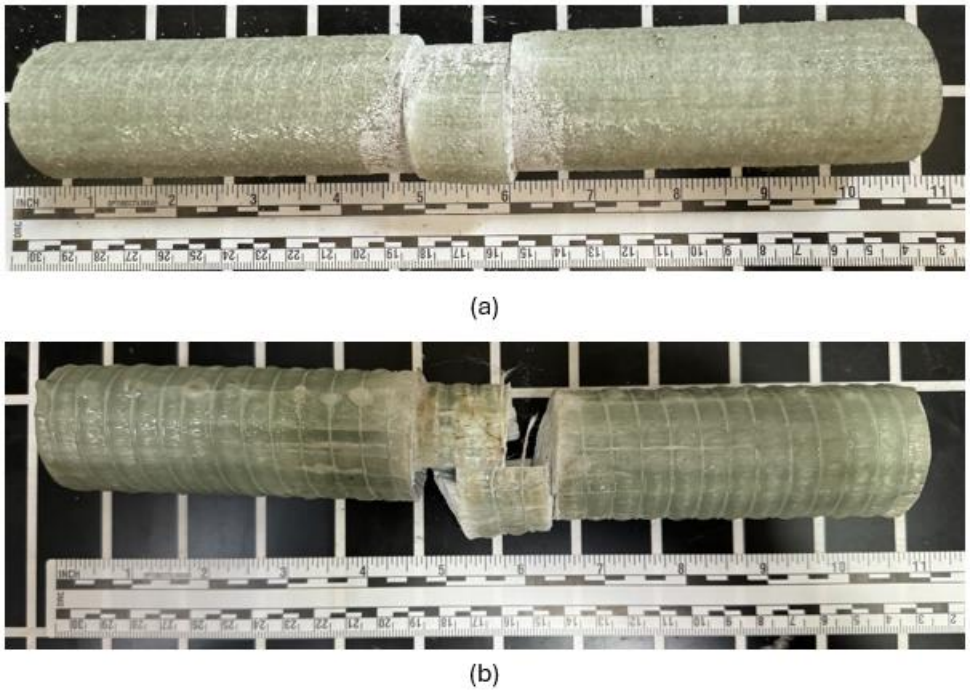

Figure 35. Transverse shear strength representative double shear failure mode; (a) Pultrall and (b) MST-Bar

4.7. Horizontal Shear Strength – ASTM D4475

To determine the ultimate horizontal shear strength of the products under evaluation based on ASTM D4475.

The specimens were cut from different randomly selected locations from sample bar to the prescribed dimensions using a high precision blade saw and conditioned, under laboratory ambient conditions for at least 40 hrs. at room temperature 23 ± 3°C (73 ± 6°F) and 50 ± 10% relative humidity. Refer to Table 42, which includes the test specimen size (length), test location and date.

Table 42. Specimen summary information

Specimen ID	Specimen Nominal Size	Test Date mm/dd/yy	Test Location
PUL_11S_HSS_01 to 05	210 mm (8.25 in.)	10/24/24	SML
MST_11S_HSS_01 to 05		10/25/24	

Tests were conducted under laboratory ambient conditions by qualified personnel. The date of each test; technical personnel; variations to the test method as applicable; calibration information for instruments and equipment used in all measurements; identification of the

material tested; temperature and humidity of testing laboratory; and other applicable test data or details is provided in the technical data sheet: TDS-HSS-FDOT.

An axial load was applied to the center of the bar using a dedicated fixture as per ASTM D4475, providing a support that allow the specimen to bend. The load was applied using a screw-driven universal test frame. The load was measured with the internal load cell of the frame in compliance with ASTM E4-21. The test set-up is shown in Figure 36.

The results reported herein have been computed per ASTM D4475 using the parameters defined in Table 43.

Table 43. Parameter definitions and calculations

Symbol	Parameter	Description
P_{max}	Maximum failure force	Peak load recorded during test
d_{nom}	Diameter of specimen	Nominal diameter
S	Apparent shear strength	$S = 0.849 * P_{max} / d^2_{nom}$

Based on the experimental tests presented herein the apparent horizontal shear strength of the bars are summarized in Table 44. The mode of failure was by double shear. Tabulated test results are reported in Appendix A.

Table 44. Average summary results for horizontal shear strength tests

Specimen ID	Number of Tested Specimens	Apparent Horizontal Shear Strength S		Materials Manual Section 12.1 Table 1 Specification	Acceptance Criteria
		MPa	ksi		
PUL_11S_HSS	5	40.56	5.9	> 37.92 MPa (5.5 ksi)	PASS
MST_11S_HSS	5	39.47	5.7		

Glass FRP bars with nominal size #11 for manufacturers V-Rod/Pultrall and MST-Bar, comply with the requirements established in Table 1 Physical and Mechanical Property Requirements for Straight FRP Reinforcing Bars of the FDOT's Materials Manual Section 12.1 Volume II Fiber Reinforced Polymer Composites by having an average Horizontal Shear Strength greater than 5.5 ksi and a coefficient of variance less or equal to 15%.

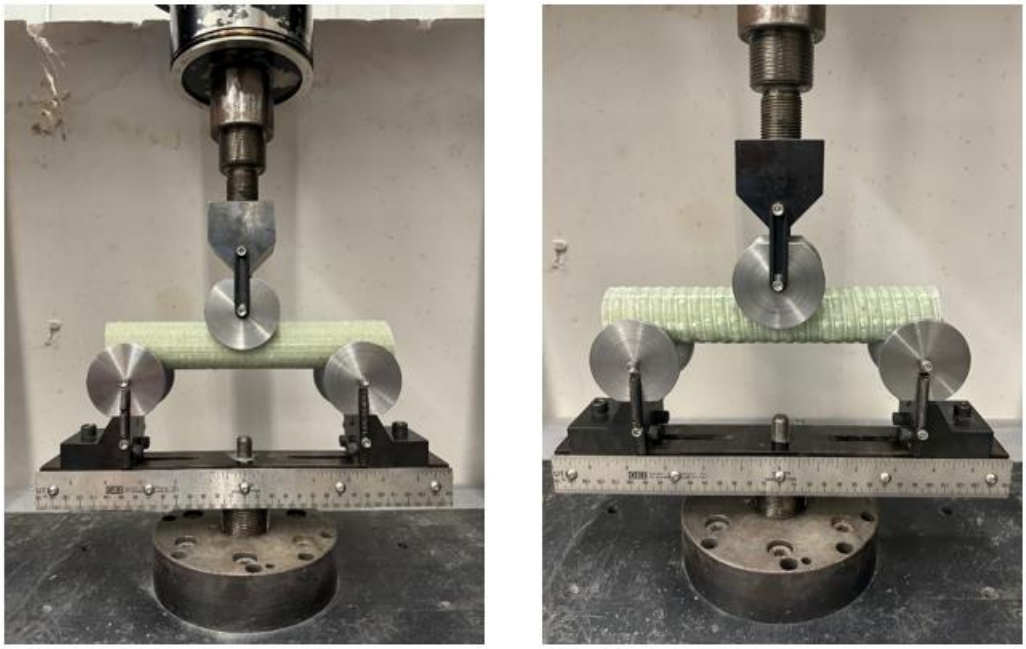

Figure 36. Horizontal shear strength test setup: (a) Pultrall and (b) MST-Bar

Figure 37. Horizontal shear strength representative interlaminar shear failure mode: (a) Pultrall; (b) MST-Bar

4.8. Bond Strength – ASTM D7913

To determine the bond strength to concrete by pullout test method evaluation based on ASTM D7913.

The specimens were cut from different randomly selected locations from sample bar to the prescribed dimensions using a high precision blade saw and conditioned, under laboratory ambient conditions for at least 40 hrs. at room temperature 23 ± 3°C (73 ± 6°F) and 50 ± 10% relative humidity. Refer to Table 45 which includes the test specimen bonded length, test location and date.

Table 45. Specimen summary information

Specimen ID	Specimen Nominal Bonded Length	Test Date mm/dd/yy	Test Location
PUL_11S_BS_01 to 05	174.6 mm (6.875 in.)	02/12/25 to 02/14/25	SML
MST_11S_BS_01 to 05		01/29/25 to 02/05/25	

The bar specimens were placed in solid plain concrete cubes 205 mm (8.00 in.), after applying a steel pipe anchor per ASTM D7205 to one end of the bar. The specimen layout is presented in Figure 38 and Figure 39, where specimens had a de-bonded length to the concrete, so that the total bonded length to concrete was equivalent to five times the diameter of the bar per ASTM D7913. A total of 6 stirrups #3 spaced 2.0 inches on center were installed per block to ensure adequate confinement.

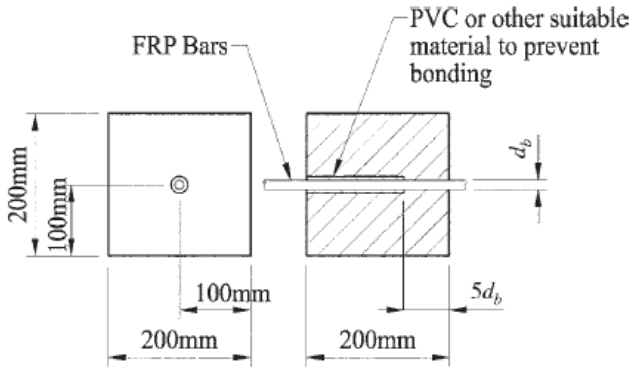

Figure 38. Concrete pullout bond specimen layout

Figure 39. Concrete pullout bond specimen for Pultrall (left) and MST (right)

Specimens were prepared simultaneously from one single batch of concrete following ASTM C192/C192M-13a, Practice for Making and Curing Concrete Test Specimens in the Laboratory; while lot 2 and lot 3 was prepared together in a second batch. The concrete compressive strength at the time of testing was then tested as per ASTM C39, (Standard Test Method for Compressive Strength of Cylindrical Concrete Specimens). Summary results of the compressive strength are provided in Table 46.

All specimens were conditioned post curing under laboratory ambient conditions at room temperature 23 ± 1°C (73 ± 3°F) and 60 ± 5% relative humidity, for at least 28 days prior testing.

Table 46. Concrete compressive strength results at time of testing (ASTM C39) for bond pullout tests

Specimen ID	Cylinder Diameter d		Area A		Peak force P_{max}		Compressive Strength f'_c		Failure Mode
	mm	in.	mm²	in²	kN	lbf	MPa	psi	
B1-C1	101.9	4.01	8159	12.65	218.9	49200	26.82	3891	2
B1-C2	101.9	4.01	8149	12.63	217.1	48800	26.64	3863	2
B1-C3	101.2	3.98	8037	12.46	232.6	52300	28.95	4198	2
B1-C4	103.2	4.06	8366	12.97	237.5	53400	28.39	4118	2
B1-C5	102.2	4.02	8197	12.71	230.0	51700	28.06	4069	2
Average	**102.1**	**4.02**	**8182**	**12.68**	**227.2**	**51080**	**27.77**	**4028**	
S_{n-1}	0.7	0.03	119	0.18	8.9	1999	1.00	146	
CV (%)	0.7	0.7	1.5	1.5	3.9	3.9	3.6	3.6	

Tests were conducted under laboratory ambient conditions by qualified personnel. The date of each test, technical personnel, variations to the test method as applicable, calibration

information for instruments and equipment used in all measurements, identification of the material tested, temperature and humidity of testing laboratory, and other applicable test data or details are provided in the technical data sheet: TDS-BS-FDOT that can be found online per request.

A uniaxial tensile load was applied to all specimens. Testing was performed using a screw-driven universal test frame. Tensile load was measured a dedicated donut-type load cell in compliance with ASTM E4-21 (Standard Practice for Force Verification of Testing Machines), while the extension (elongation) of the loaded and free end of the specimen was measured using a linear voltage displacement transducers (LVDTs) in accordance to ASTM E83-16 (Standard Practice for Verification and Classification of Extensometer Systems). The test setup is shown in Figure 40.

Load was applied in displacement control to effect a near constant strain rate in the gauge section until failure at a constant frame head displacement of 1.3 mm/min (0.05 in./min), producing failure within 1 to 10 minutes.

The results reported herein have been computed per ASTM D7913 using the parameters defined in Table 47.

Table 47. Definitions of calculations for bond strength

Symbol	Parameter	Description
d_b	Diameter	Nominal dimeter of bar based on bar nominal size
C_p	Circumference	Circumference of bar based on nominal dimeter
L	Length	Length of bar bonded to concrete
Fu	Tensile load	Tensile load applied with the load device
A_L	Bar Bond Area to Concrete	Lateral Area = Cp x L
T^B	Bond Strength	$T^B = F / A_L$

Based on the experimental tests presented herein, the guaranteed bond strength, T^B_G, of the bars under evaluation is summarized in Table 48. The primary mode of failure was loss of bond via slippage between the bonded bar and the concrete substrate due to pullout from concrete block, as represented from the posttest evaluation in Figure 41.

Table 48. Guaranteed bond strength results

Specimen ID	Number of Tested Specimens	Bond Strength, T^B_G		Materials Manual Section 12.1 Table 1 Specification	Acceptance Criteria
		MPa	ksi		
PUL-11S_BS	5	4.9	0.71	Type 0 bars >1.1 ksi	FAIL
MST-11S_BS	5	9.2	1.33	Type III bars >1.4 ksi	PASS

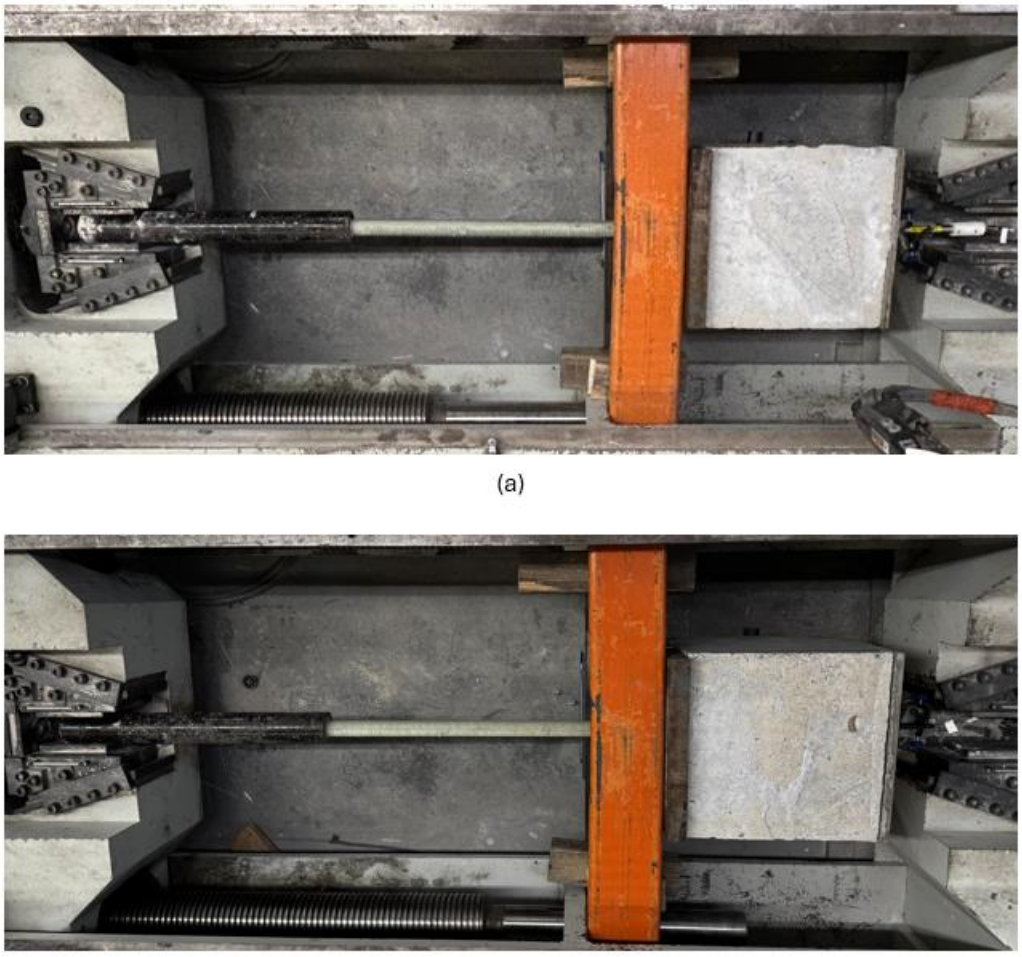

Figure 40. Bond strength test setup: (a) Pultrall; (b) MST-Bar

Figure 41. Bond strength representative slippage failure mode

Based on the current specification established in Table 17 Physical and Mechanical Property Requirements for Straight FRP Reinforcing Bars of the FDOT's Materials Manual Section 12.1 Volume II Fiber Reinforced Polymer Composites and in Table 932-8 of FDOT's specification Section 932 for Nonmetallic Accessory Materials for Concrete Pavement and Concrete Structures:

- Glass FRP bars with nominal size #11 for manufacturer V-Rod/Pultrall fail the current specification for minimum bond strength.
- Glass FRP bars with nominal size #11 for manufacturer MST-Bar would be classified as a Type 0 bar meeting the minimum requirement for bond strength. However, the requirement of a coefficient of variance less or equal to 15% was not met.

4.9. Moisture Absorption – ASTM D570

To determine the short term (24 hr.) and long term (saturation) level of moisture absorption when immersed in at 50°C (122°F) of the products under evaluation based on ASTM D570.

The specimens were cut to the prescribed dimensions using a high precision blade saw. Refer to Table 49 for the test specimen size, test date and location.

Table 49. Specimen summary information

Specimen ID	Specimen Nominal Size	Test Date mm/dd/yy	Test Location
PUL_11S_MA_01 to 05	25 mm (1.0 in.)	09/24/24 to 11/12/24	SML
MST_11S_MA_01 to 05		09/24/24 to 11/12/24	

Tests were conducted under laboratory ambient conditions by qualified personnel. The date of each test; technical personnel; variations to the test method as applicable; calibration information for instruments and equipment used in all measurements; identification of the material tested; temperature and humidity of testing laboratory; and other applicable test data or details is provided in the technical data sheet: TDS-MA-FDOT.

The short and long-term moisture specimens tested in accordance with ASTM D570. They were conditioned and immersed in water for a 24-hour period at a temperature of 50°C (122°F). Similarly, the long-term specimens, were tested and immersed in water at a temperature of 50°C (122°F) until moisture equilibrium was reached per ASTM D570, until saturation. An analytical balance with an accuracy of 0.0001 g was used to take readings of the specimens at the desired intervals, while a chamber capable of maintaining uniform temperatures of 50°C ± 3°C (122°F ± 6°F) was checked periodically proximally every 200 hrs. for quality purposes. All specimens had their surface wiped off with a dry cloth prior weighing.

The results reported herein have been computed per ASTM D570 using the parameters defined in Table 50.

Table 50. Definitions of calculations for moisture absorption tests

Symbol	Parameter	Description
W_d	Weight	Weight of condition specimen, prior immersion in water
W_w	Weight	Weight of specimen, post immersion in water
W_{24}	%	% Increase in weight of specimen, post 24 hrs. period, $W_{24} = [W_w - W_d / W_d] * 100$
W_s	%	% Increase in weight of specimen, post saturation period $W_s = [W_w - W_d / W_d] * 100$

Based on the experimental tests presented herein the average short moisture absorption and saturation content is summarized in Table 51, where the condition of acceptance for the short term and long-term (saturation) moisture absorption shall not exceed 0.25 % and 1.00 % increase in mass, respectively. Tabulated test results are reported in appendix A.

Table 51. Summary results for moisture absorption tests

Specimen ID	Number of Tested Specimens	Short Term Immersion (24 hrs.) W_{24} %	Long Term Immersion (Saturation) W_s %	Materials Manual Section 12.1 Table 1 Specification	Acceptance Criteria
PUL-11S_MA	5	0.14	0.48	≤ 0.25% (24 hrs.) ≤ 1.0% (Saturation)	24 hrs. PASS
MST-11S_MA	5	0.17	0.67		Saturation PASS

Glass FRP bars with nominal size #11 for manufacturers V-Rod/Pultrall and MST-Bar, comply with the requirements established in Table 17 Physical and Mechanical Property Requirements for Straight FRP Reinforcing Bars of the FDOT's Materials Manual Section 12.1 Volume II Fiber Reinforced Polymer Composites by having a short term saturation less than 0.25% and a long-term saturation less than 1.0%

4.10. Alkaline Resistance – ASTM D7705-A

To determine the mean alkaline resistance (tensile load retention) of the products under evaluation per ASTM D7205, post accelerated aging exposure immersed in a high pH solution without any applied sustained load per ASTM D7705 Procedure A.

All specimens were conditioned by immersion in an aqueous alkaline solution with a pH value between 12.6 and 13.0, as measured by ASTM E70, Standard Test Method for pH of Aqueous Solutions With the Glass Electrode. The alkaline solution was set to have a constant temperature of 60 ± 3°C (140 ± 5°F) for a minimum exposure period of 90 days (2160 hrs.). The specimens and environmental chamber were visually checked periodically proximally every 200 hrs. for quality purposes. Refer to Table 52 which includes exposure period, the test date and location.

Table 52. Specimen summary information

Specimen ID	Aging Exposure *Start* mm/dd/yy	*Finish* mm/dd/yy	Test Date mm/dd/yy	Test Location
PUL_11S_TNS-AR_01 to 05	08/27/24	11/25/24	12/06/24	SML
MST_11S_TNS-AR_01 to 05	08/23/24	11/21/24	12/06/24	

Tests were conducted under laboratory ambient conditions by qualified personnel. The date of each test, technical personnel, variations to the test method as applicable, calibration information for instruments and equipment used in all measurements, identification of the material tested, temperature and humidity of testing laboratory, and other applicable test data or details are provided in the technical data sheet: TDS-TNS-AR-FDOT that can be found online per request.

Uniaxial tensile load was applied to all specimens. Tensile testing was performed using a universal test frame Tensile load was measured with the internal frame load cell in compliance with ASTM E4-21 (Standard Practice for Force Verification of Testing Machines), while the extension (elongation) of the specimen was measured using a Class B-2 clip on extensometer in accordance to ASTM E83-16 (Standard Practice for Verification and Classification of Extensometer Systems), with a 100-mm (4.0 in.) gauge length, placed at mid-length of the free length between the anchors. The extensometer was removed halfway during the test to avoid damage of the instrument. Specimen's anchors were gripped with mechanical wedge-type grips. All data were gathered using a National Instruments data acquisition system at a rate of 100 Hz.

The load was applied in displacement control to effect a near constant strain rate in the gauge section, producing failure within 1 to 10 minutes, as per ASTM D7205 requirements.

The results reported herein have been computed per ASTM D7205 based on the nominal area of the bar. Refer to Table 53 for definitions and calculations.

Table 53. Definitions of calculations for tensile tests

Symbol	Parameter	Description
P_{max}	Maximum force at failure	Peak load recorded during test
A_{nom}	Nominal cross-section area	Cross-section area per ASTM D7957, Table 3
F^{tu}_{nom}	Nominal ultimate tensile strength	$F^{tu}_{nom} = P_{max} / A_{nom}$
$\varepsilon_{u\text{-}nom}$	Computed ultimate strain based on linear elastic behavior	$\varepsilon_u = F^{tu}_{nom} / E_{nom}$
E_{nom}	Tensile modulus of elasticity	As per Section 13.3.1 ASTM D7205 – computed by fitting a straight line to the data using the method of linear least squares regression analysis. The data range selected goes between 1000 and 6000 με. $E_{nom} = \frac{\sum_{i=1}^{K}(\varepsilon_i \sigma_i) - n\,\bar{\sigma}\,\bar{\varepsilon}}{\sum_{i=1}^{K}\varepsilon_i^2 - n\,\bar{\varepsilon}^2}$
P_{ret}	Tensile Capacity Retention	Ratio between the P_{max} post alkaline resistance exposure tests and the benchmark tests, multiplied by 100.

All specimens behaved linear elastically until failure. Based on the experimental tests presented herein the mean tensile load carrying capacity as well as the ultimate strength, mean tensile modulus, the mean computed ultimate tensile strain post alkaline resistance with load, is summarized in Table 54; where the condition of acceptance is a minimum tensile strength retention of 70% compared to the average ultimate tensile force as reported in Section 9. Tabulated test results are reported in appendix A.

Table 54. Average summary results for tensile tests

Specimen ID	Number of Tested Specimens	Ultimate Mean Tensile Force P_{max}		Mean Tensile Modulus of Elasticity E		Mean Ultimate Tensile Strain ε_u	Tensile Capacity Retention P_{ret}	Acceptance Criteria
		kN	kips	GPa	Msi	%	%	
PUL_11S_TNS-AR	5	1094	246.0	62.2	9.0	1.7	90	PASS
MST_11S_TNS-AR	5	816	183.6	56.8	8.2	1.4	88	

Glass FRP bars with nominal size #11 for manufacturers V-Rod/Pultrall and MST-Bar, meets the requirement established in the Characterization Test Plan approved by FDOT where the minimum Tensile Capacity Retention is 70%.

5. Curate and Compare Existing Designs for Pile Footings in Marine Locations

This section reviews the steps carried out for the design of the pile cap footings for the piles of an existing FDOT steel-RC bridge located in a coastal area of Florida as shown in Figure 42.

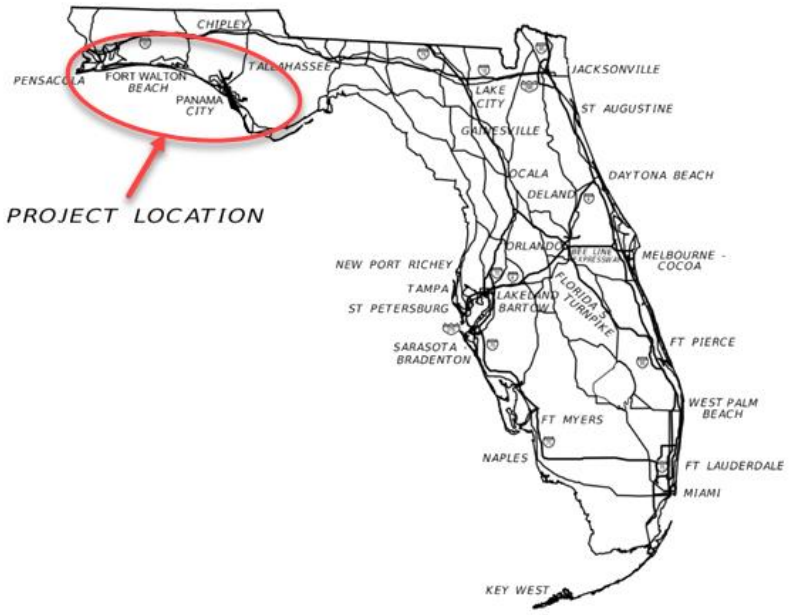

Figure 42. Example bridge location (B1-01)

The Eastbound Bridge is the selected case study with steel-RC foundation. The analysis includes ULS and SLS verifications, with a focus on the large pier foundations of the case study bridge.

5.1. Case Study Bridge Description (Eastbound Bridge)

The waterline pile caps of the selected bridge are located in a Florida marine environment splash zone in accordance with ***SDG 1.3***. The bridge was designed in 2017 and consists of 25 simply supported spans. The structure is rectilinear in plan, and the piers 22 to 26, as well as the last abutment, have a skew angle of approximately 22° with respect to the transverse direction.

The nominal length of the prestressed beams and the pier spacing measured along the centerline are:

- Span 1-20 = 60.0 ft (AASHTO type-II beam, ***Index 450-120***);
- Span 21-22 = 77.6 ft (Florida-I 63 beam, ***Index 450-063***);
- Span 23-24 = 125.0 ft (Florida-I 63 beam, ***Index 450-063***);

- Span 25 = 112.0 ft (Florida-I 63 beam, ***Index 450-063***).

The number of prestressed concrete beams and transverse spacing for each span are listed below:

- Span 1: 7 beams (6 x 8'-3" = 49'-6")
- Span 26: 7 beams (6 x 13'-8$^{1/2}$" = 82'-3$^{1/4}$")
- Span 2-20: 7 beams (6 x 8'-3" = 49'-6")
- Span 21: 5 beams (4 x 12'-0" = 48'-0")
- Span 22: 5 beams (4 x 12'-11$^{1/4}$" = 51'-9$^{1/4}$")
- Span 23: 5 beams (4 x 15'-5$^{1/8}$" = 61'-8$^{1/2}$")
- Span 24: 7 beams (6 x 13'-8$^{1/2}$" = 82'-3$^{1/4}$")
- Span 25: 7 beams (6 x 13'-8$^{1/2}$" = 82'-3$^{1/4}$")

The beams are connected by an RC-slab 8.5" thick. The out-to-out transverse width of the carriage is 55'-8" for the spans 1-24 and 71'-8" for the spans 25-26. Piers are grouped into portal frame structures with different sizes and geometry, depending on the number of beams they support:

- Pier 2÷20: 7 columns (6 x 8'-3" = 49'-6")
- Pier 21: 3 columns (2 x 19'-3" = 38'-6")
- Pier 22: 3 columns (2 x 21'-3" = 42'-6")
- Pier 23: 3 columns (2 x 26'-3" = 52'-6")
- Pier 24-25: 4 columns (3 x 24'-6" = 72'-18")

The bridge abutments are built of conventional bent caps founded on piles, similar to those of the piers. Composite neoprene pads are arranged on the pier-cap and the abutments to support the bridge beams.

Figure 43 and Figure 44 show the overall views of the Eastbound Bridge in plan and elevation.

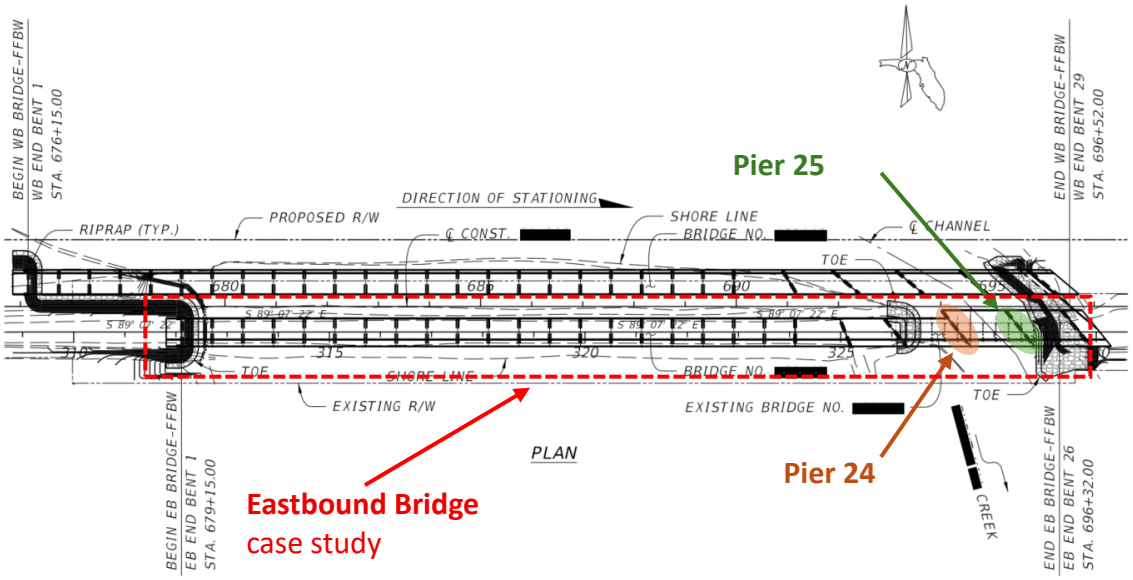

Figure 43. Selected Eastbound Bridge plan (B1-15)

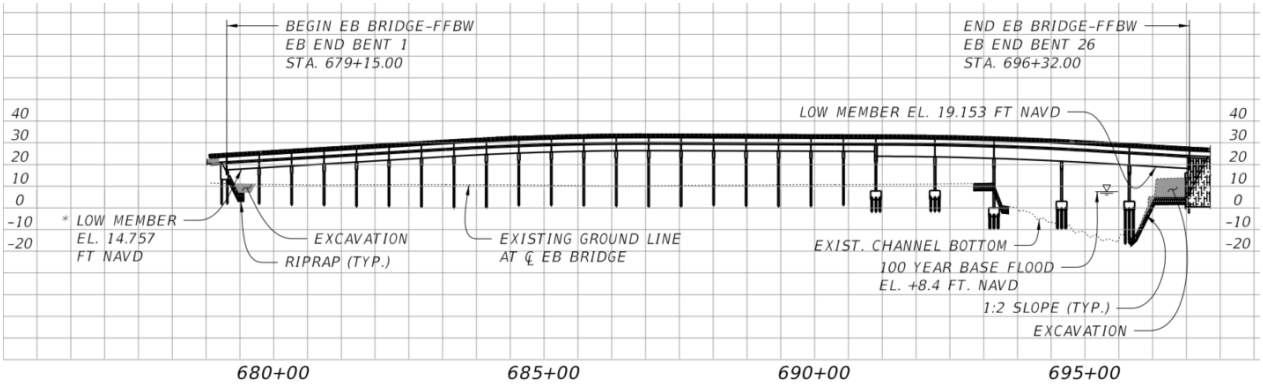

Figure 44. Eastbound Bridge elevation (B1-15)

Specifically, Figure 45 and Figure 46 show in plan view the axis of piers 24 and 25 respectively, for the Eastbound Bridge.

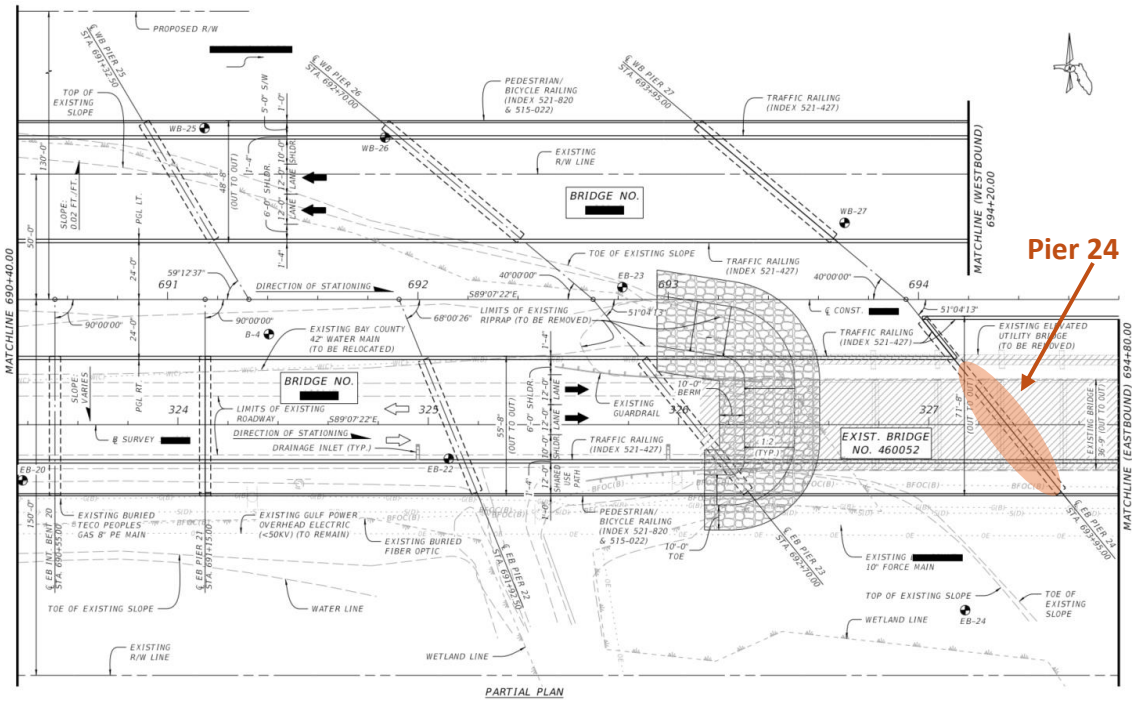

Figure 45. Partial plan – Selected Pier no.24 of the Eastbound Bridge (B1-05)

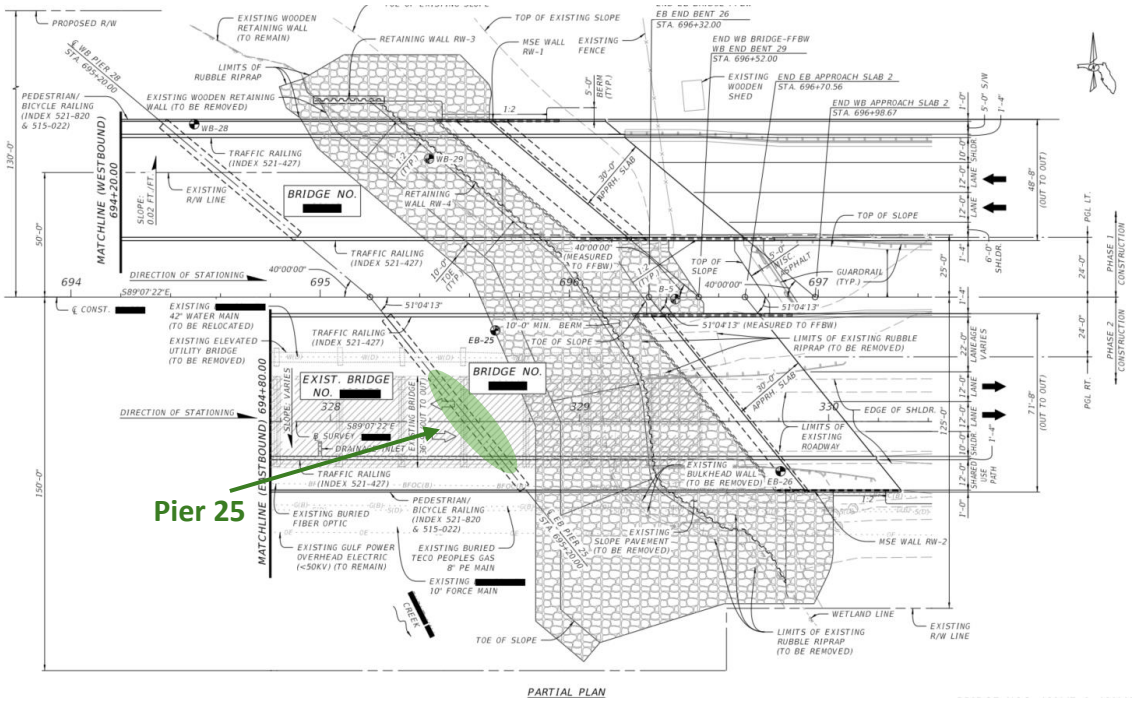

Figure 46. Partial plan – Selected Pier no.25 of the Eastbound Bridge (B1-06)

The elevation views in the longitudinal direction of piers 24 and 25 are shown (without skew) in Figure 47 and Figure 48.

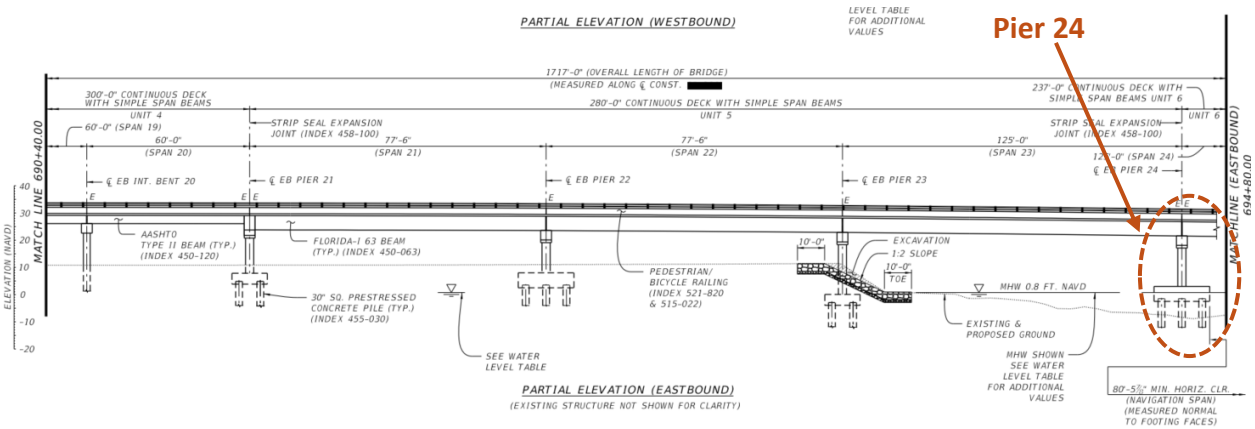

Figure 47. Partial elevation – Selected Pier no.24 of the Eastbound Bridge (B1-11)

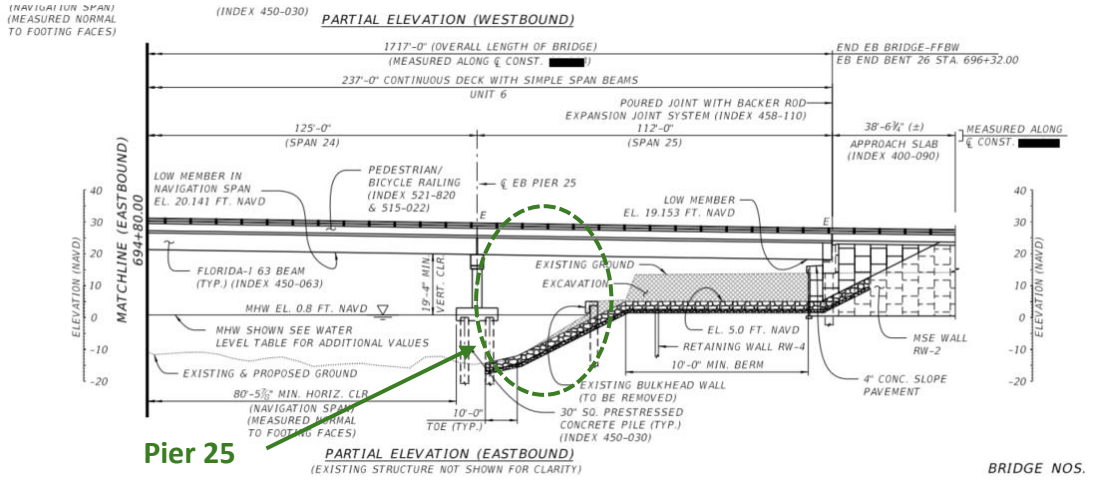

Figure 48. Partial elevation – Selected Pier no.25 of the Eastbound Bridge (B1-12)

The plan view of the pile groups at the individual elevations of piers 24 and 25 are shown in Figure 49 and Figure 50.

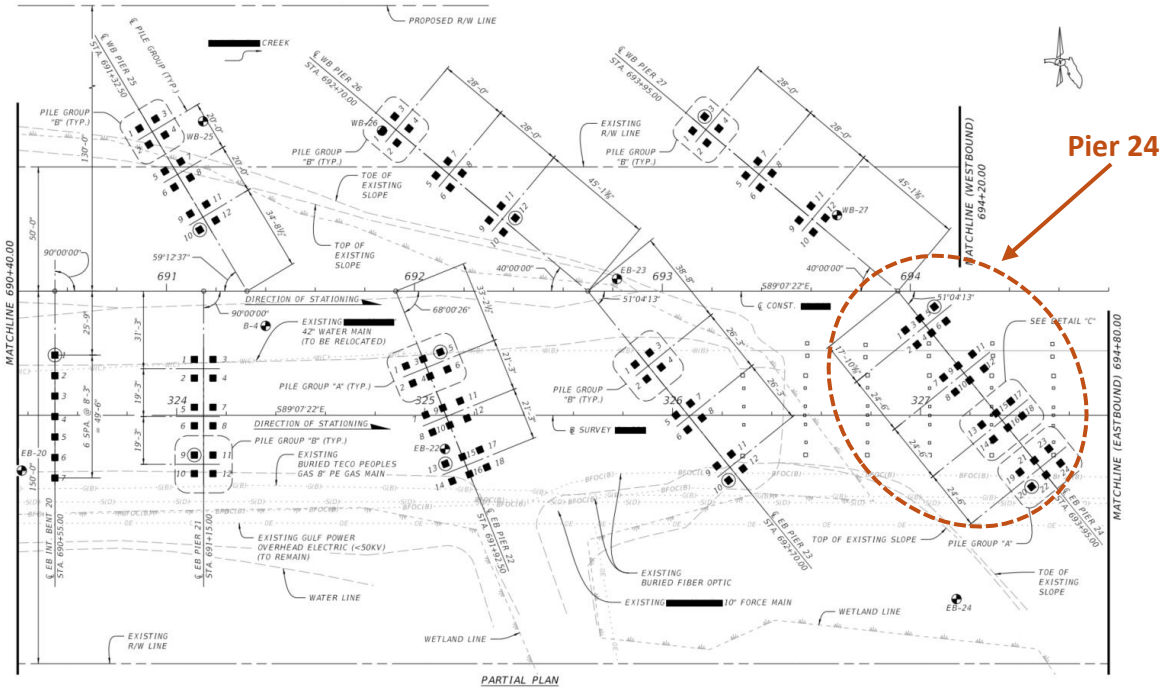

Figure 49. Partial foundation layout plan – Selected Pier no.24 of the Eastbound Bridge (B1-83)

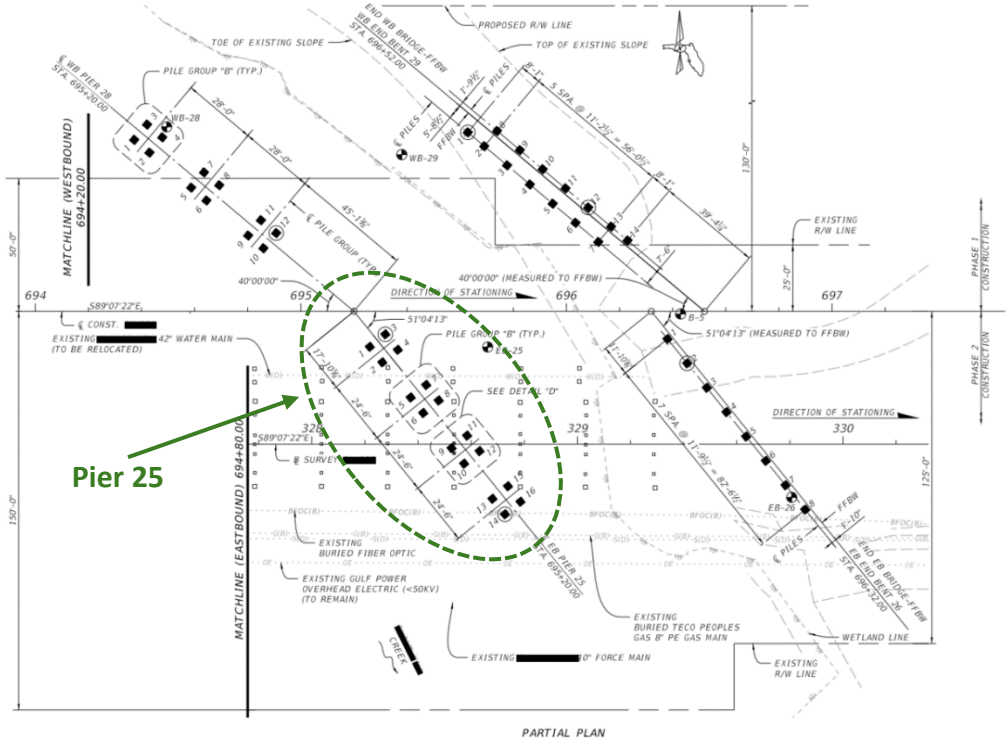

Figure 50. Partial foundation layout plan – Selected Pier no.25 of the Eastbound Bridge (B1-84)

The geometric details of the pile groups are reported below. In particular, Figure 51 shows the 6-pile group “A” of the pier 24 and Figure 52 shows the 4-pile group “B” of and the of pier 25.

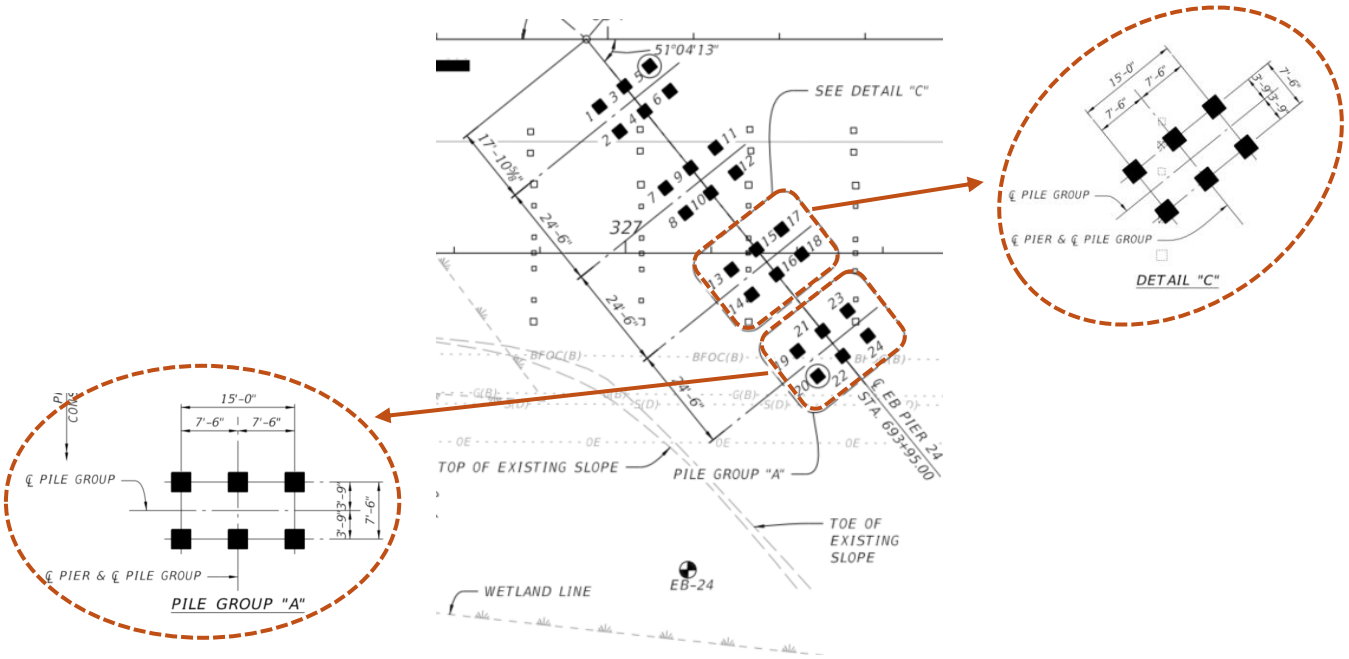

Figure 51. Pile group details – Selected Pier no.24 of the Eastbound Bridge (B1-83, B1-84)

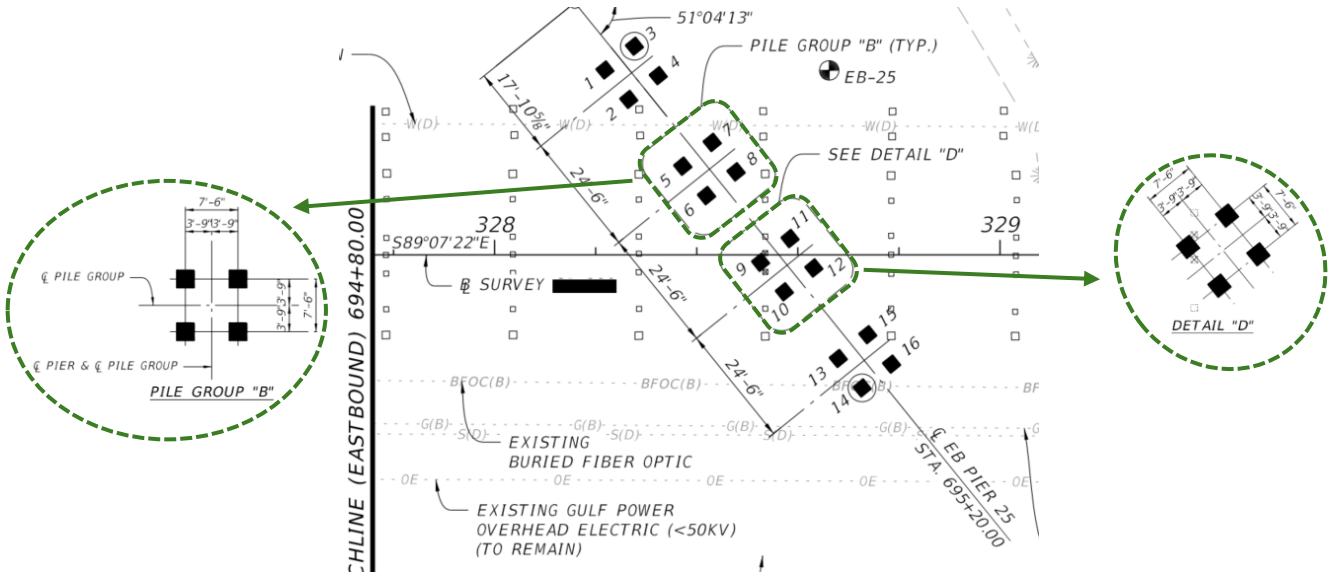

Figure 52. Pile group details – Selected Pier no.25 of the Eastbound Bridge (B1-84)

The bidirectional carbon-steel reinforcement arrangement of the 6-pile cap group “A” (pier 24) is shown in Figure 53, while Figure 54 shows the 4-pile cap group “B” (pier 25).

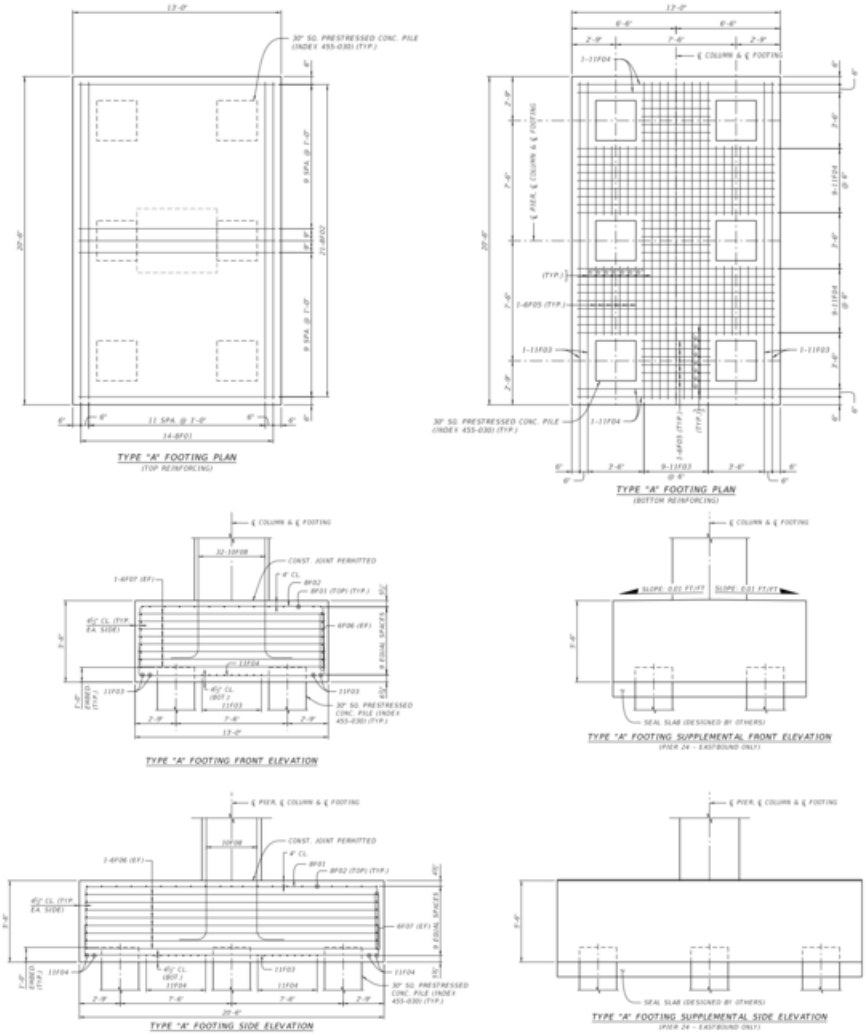

Figure 53. Carbon-steel reinforcement layout – Pile cap 6-pile group “B” of the selected Pier n.24 of the Eastbound Bridge (B1-113, B1-114)

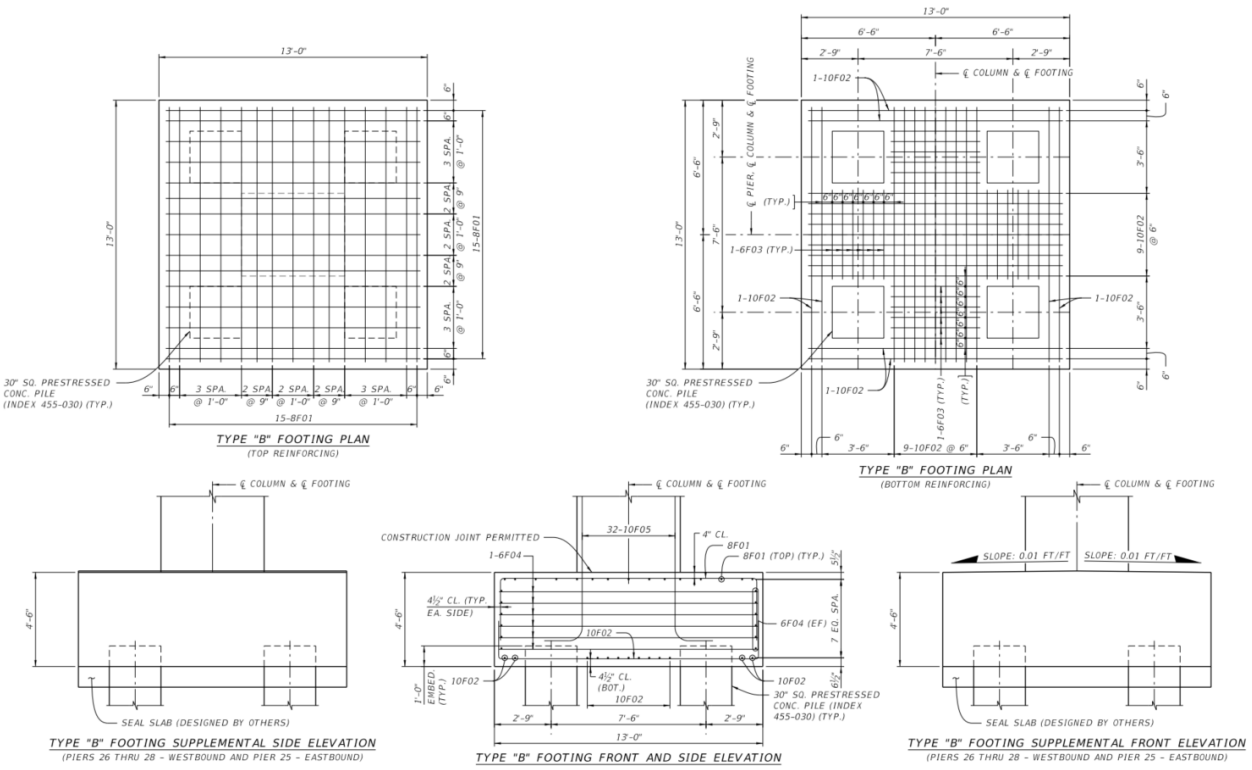

Figure 54. Carbon-steel reinforcement layout – Pile cap 4-pile group "A" of the selected Pier n.25 of the Eastbound Bridge (B1-115)

The geometric details for the carbon-steel reinforcement arrangement of pier caps are shown in Figure 55 for pier 24 and Figure 56 for pier 25.

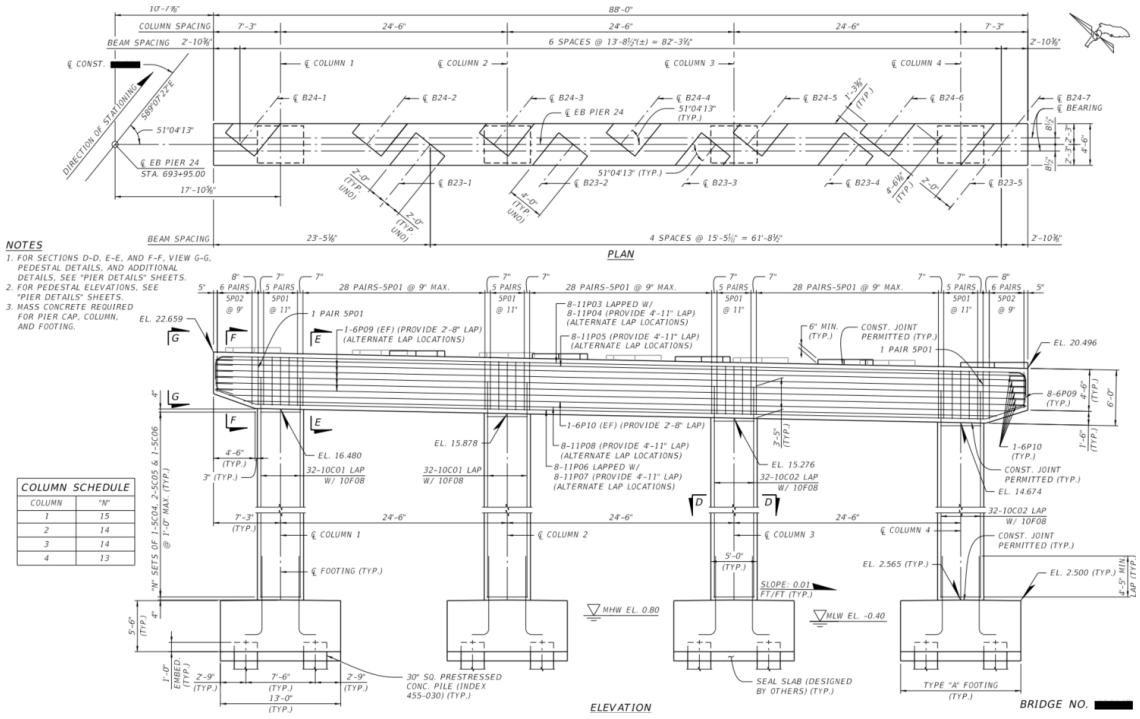

Figure 55. Carbon-steel reinforcement layout – Pier cap of the selected Pier n.24 of the Eastbound Bridge (B1-111)

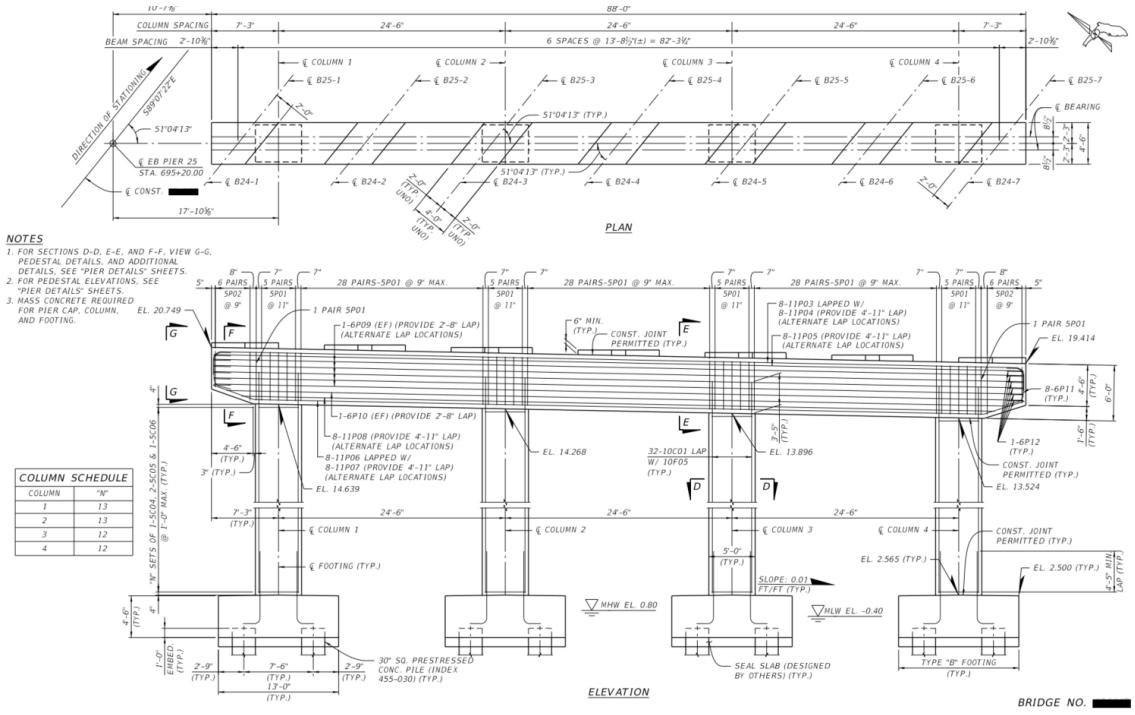

Figure 56. Carbon-steel reinforcement layout – Pier cap of the selected Pier n.25 of the Eastbound Bridge (B1-112)

5.2. Geometry and Material Definition

The parameters assumed for design are listed in Table 55:

Table 55. Concrete parameter AASHTO LRFD

Concrete Compressive Strength	$f_c = 5500\ psi$
Modulus of Elasticity for Concrete (AASHTO LRFD C5.4.2.4-1)	$E_c = 1820\sqrt{f_c ksi} = 4268\ ksi$
Modulus of Rupture (AASHTO LRFD 5.4.2.6)	$f_r = 0.24\sqrt{f_c ksi} = 0.563\ ksi$
Concrete maximum compressive strain	$\varepsilon_{cu} = 0.003$
Rectangular Concrete Stress Block Depth Correction Factor (AASHTO LRFD 5.7.2.2)	$\beta_1 = \begin{cases} 0.85 \text{ if } f_c \le 4\ ksi \\ 0.85 - [0.05\ ksi(f_c - 4\ ksi)] = 0.775 \\ 0.65 \text{ if } f_c \ge 8\ ksi \end{cases}$

The parameters assumed for design are listed in Table 56:

Table 56. Steel parameter AASHTO LRFD

Yield Strength of Steel (carbon-steel grade 60)	$f_y = 60\ ksi$
Modulus of Elasticity for Steel	$E_s = 29000\ ksi$
Yield Strain	$\varepsilon_y = 0.003$

The critical dimensions for the pile cap are listed in Table 57:

Table 57. Pile cap geometry of the selected pier n.24 of the Eastbound Bridge

Footing Height	$h_{ftg} = 5.5ft$
Transverse Footing Width	$b_T = 13.0\ ft$
Longitudinal Footing Width	$b_L = 20.5\ ft$
Footing Design Width (One Foot Design Width)	$b_{ftg} = 12\ inc$
Top Reinforcement Concrete Cover (Extremely Aggressive Substructure)	$cover_{top} = 4.0\ in$
Bottom Reinforcement Concrete Cover (Extremely Aggressive Substructure)	$cover_{bot} = 4.5\ in$
Side Reinforcement Concrete Cover (Extremely Aggressive Substructure)	$cover_{side} = 4.0\ in$

The critical steel reinforcement quantitative design parameters are listed in Table 58:

Table 58. Pile cap reinforcement of the selected Pier no.24 of the Eastbound Bridge

Bar Location/ Direction*	**Bar Size**	**Bar Spacing**	**Number of Bars**
Bottom/ Longitudinal	$bar_{F1B} = 11$	$s_{F1B} = 12\ in$	$n_{F1B} = 13$
Bottom/ Transverse	$bar_{F2B} = 11$	$s_{F2B} = 12\ in$	$n_{F2B} = 22$
Top/ Longitudinal	$bar_{F1T} = 8$	$s_{F1T} = 12\ in$	$n_{F1T} = 14$
Top / Transverse	$bar_{F2T} = 8$	$s_{F2T} = 12\ in$	$n_{F2T} = 21$

The area of bars per one foot design width is generally computed as:

$$A_s = a_{bar} \frac{b_{ftg}}{spacing} \quad (1)$$

5.3. Load Analysis and Combinations

The following design loads are used in superstructure and substructure analysis:

- **Dead loads**
  - Traffic Railing Barrier 32" F-Shape = 420 plf;
  - Pedestrian /Bicycle Railing = 225 plf;
  - Unit Weight of Structural Concrete 150 pcf;
  - AASHTO Type II = 385 plf;
  - Florida-I 36 Beam = 840 plf;
  - Florida-I 45 Beam = 906 plf;
  - Florida-I 54 Beam = 971 plf;
  - Florida-I 63 Beam = 1037 plf;
  - Stay-in-Place Forms = 20 psf;
  - Compacted Soil = 115 pcf;
  - Aluminum Pedestrian/Bicycle = xx plf;
  - Bullet Railing (2 Rails) = 10 plf;
  - Bridge Deck: The minimum thickness of bridge decks cast-in-place (CIP) on beams is 8½". The ½" sacrificial thickness for all alternatives is included in the dead load of the deck slab but omitted from its section properties for structural design.

- **Live loads**
  - Vehicle HL93 Design Truck Models;
  - Pedestrian 75 plf.

- **Wind loads**
  - Wind loads per SDG 2.4, which is a modification of the AASHTO LRFD Bridge Design Specifications.

- **Thermal forces – temperature variation**
  - Movements of bridge RC-structures is calculated assuming the following temperature ranges:

Superstructure material	Mean	High	Low	Range
Concrete Only	70°F	105°F	35°F	70°F

  - The coefficient of thermal expansion for concrete is taken as 6 x 10-6°F.

- **Seismic design**
    - The bridges shall meet the minimum bearing support dimension as specified in AASHTO LRFD 4.7.4.4.

- **Wave and current forces**
    - Design is in accordance with the AASHTO Guide Specifications for Bridges Vulnerable to Coastal Storms. Since the bridge superstructure for all alternatives considered is located in excess of 1-foot above the 100-year plus wave crest elevation, these forces are not considered.

- **Degradation aspects**
    - According to the SDG 1.3.2 both the superstructure and substructure are classified as extremely aggressive due to chlorides in excess of 6000 ppm.
        - Superstructure: Extremely aggressive.
        - Substructure (Concrete): Extremely aggressive.

The following limit states were verified during the design phase:

- Conventional LRFD loadings using load factor combination groups specified in AASHTO LRFD Table 3.4.1-1 in combination with the most severe case of scour up to and including that from a 100-year flood event.
- Stability check during the "super-flood" using the most severe case of scour up to and including that from the 500-year flood event.
- Substructure was designed for an Extreme Event-II vessel collision load by a barge.

Load factors and combination of characteristic loads refer to the AASHTO LRFD Bridge Design Specifications 2014 (7th Edition) [54] paragraph 3.4.1 relative to the limit states:

- Strength I, II, III, IV, & V;
- Extreme Event I & II;
- Service I & III.

5.4. Computational Model

For the purpose of this research project, only loads on the substructure and specifically the forces and stresses in the pile caps' concrete and reinforcing were considered. The structural response of bridge-pier-pile-soil structures was conducted with the help of finite element models based on BSI FB-MultiPier® v5.1 software (see Figure 57).

Figure 57. BSI FB-MultiPier® software

Soil and pile stiffnesses were modeled with nonlinear properties whereas pile cap, column and pier cap stiffnesses were modeled with linear behavior (see Figure 58).

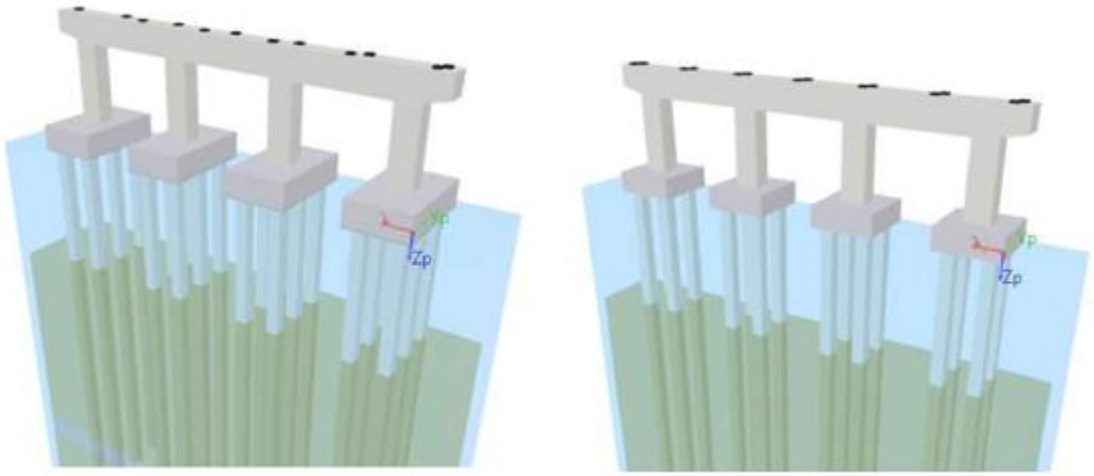

Figure 58. 3D views of the of the selected pier n.24 (left) and n.25 (right) of the Eastbound Bridge

5.5. Verification Criteria

Verifications at ULS and SLS, according to AASHTO LRFD Bridge Design Specifications 2014 (7th Edition) [54], of the carbon steel-RC pile cap foundations were performed externally with personalized calculation sheets coded in Mathcad Professional 14.0® (see Figure 59).

Figure 59. Mathcad® software

5.5.1. Ultimate Limit State (ULS) verification criteria

For the ULS design, a tension-controlled section was first assumed, with the steel being yielded before the concrete crushed. The maximum concrete strain considered for the design was $\varepsilon_{cu} = 0.003$.

Through equilibrium at translation, the depth of the neutral axis is calculated a in which a rectangular stress block distribution equivalent to the real stress distribution is considered:

$$a = \frac{A_s\, f_y}{0.85\, f_c\, b} \tag{2}$$

Where:

- A_s = area of the longitudinal tension steel within width b (typically taken as 12-in.);
- $f_y = 60\ ksi$ is the minimum yield strength of carbon-steel;
- $f_c = 5500\ psi$ is the minimum 28-day concrete compressive strength.

From the equilibrium equation, the nominal resistant moment is computed:

$$M_n = A_s\, f_y \left(d_e - \frac{a}{2}\right) \tag{3}$$

Where:

- d_e = depth of the tensioned reinforcement from the extreme fiber of concrete in compression.

Finally, the resisting design moment $\phi_f M_n$ must be computed and ensure that is greater than the factored ultimate moment:

$$\phi_f\, M_n > M_u \tag{4}$$

Where:

- M_u = the design flexural moment at ULS;
- M_n = the nominal flexural resistance;
- $\phi_f = 0.9$ is the flexural resistance (strength reduction) factor, for tension-controlled RC section (*AASHTO LRFD 5.5.4.2*).

In addition, the initial hypothesis of tension-controlled section should be confirmed, otherwise the flexural resistance factor must be reduced (see *AASHTO LRFD Figure C5.5.4.2-1)*.

The actual depth of the neutral axis *c* is calculated:

$$c = \frac{a}{\beta_1} \tag{5}$$

Where:

- $\beta_1 = \begin{cases} 0.85 \text{ if } f_c \leq 4\ ksi \\ 0.85 - [0.05\ ksi(f_c - 4\ ksi)] \\ 0.65 \text{ if } f_c \geq 8\ ksi \end{cases}$
  is the rectangular concrete stress block coefficient *(AASHTO LRFD 5.7.2.2*)

Assuming that sections remain planar, for strain compatibility, the strain in the tension steel ε_t is calculated to be at least 0.003 greater than the yield strain, which is equal to 0.002 (steel grade 60).

$$\varepsilon_t = \frac{d_{out} - c}{c}\varepsilon_{cu} \geq 0.005 \quad (6)$$

5.5.1.1. Shear

The nominal one-way shear is the minimum between:

$$V_n = \min(V_{n1}, V_{n2}) \quad (7)$$

Where:

$$V_{n1} = V_c + V_s + V_p \quad (8)$$

Because there is neither shear reinforcement (except around the perimeter) nor prestressing reinforcement, assume $V_s = V_p = 0\ kip$.

$$V_{n2} = 0.25\ f_c\ b\ d_v + V_p \quad (9)$$

The resistant shear, offered by the concrete, for unreinforced shear elements V_c is:

$$V_c = 0.0316\ \beta\ \lambda\ \sqrt{f_c}\ b\ d_v \quad (10)$$

Where:

- $\beta = 2$ per *AASHTO LRFD 5.8.3.4.1*
- $\lambda = 1$ for normal-weight concrete
- $d_v = max(0.9d_e; 0.72h_{ftg})$ is the effective shear depth

The two-way shear $\phi_s V_n$ must be greater than the ULS shear action V_u:

$$V_u < \phi_s V_n \quad (11)$$

Where:

- $\phi_s = 0.9$ is the resistance factor, shear and torsion normal weight concrete section (AASHTO LRFD 5.5.4.2.1)

The nominal two-way shear is the minimum between:

$$V_n = \min\left(V_{n1}, V_{n2}\right) \tag{12}$$

Where:

$$V_{n1} = \left(0.063 + \frac{0.126}{\beta_c}\right)\sqrt{f_c}\, b_0\, d_v \tag{13}$$

- β_c is the ratio of long side to short side of the rectangle through which the concentrated load or reaction force is transmitted:

$$\beta_c = \begin{cases} \dfrac{X + b_{pile} + edge}{Y + b_{pile} + edge} & (X > Y) \\ \dfrac{Y + b_{pile} + edge}{X + b_{pile} + edge} \end{cases} \tag{14}$$

$$X = \begin{cases} 0.5d_v & spa_T \geq d_v + b_{pile} \\ \dfrac{spa_T - b_{pile}}{2} \end{cases}$$

$$Y = \begin{cases} 0.5d_v & spa_L \geq d_v + b_{pile} \\ \dfrac{spa_L - b_{pile}}{2} \end{cases}$$

- b_0 is the perimeter of critical section

$$V_{n2} = 0.126\sqrt{f_c} b_0\, d_v \tag{15}$$

- b_0 is the perimeter of critical section

$$b_0 = 2\left(X + b_{pile} + edge\right) + 2\left(Y + b_{pile} + edge\right) \tag{16}$$

5.5.2. Serviceability Limit State (SLS) verification criteria

The tension reinforcement in flexural bending must be sufficient to ensure crack control at the SLS.

It is necessary that the resistant design moment $\phi_f M_n$ developed by the cross section is at least 1/3 greater than the design bending moment at the ULS M_u and that the collapse

condition does not occur just after cracking of the section when the cracking moment M_{cr} is reached:

$$\phi_f M_n < min\left(\frac{4}{3}M_u, 1.2\ M_{cr}\right) \quad (17)$$

The cracking moment of the cross section M_{cr} is calculated as follow:

$$M_{cr} = f_r \frac{I_g}{y_t} \quad (18)$$

Where:

- y_t is the neutral axis depth, distance from neutral axis to the extreme tension fiber:

$$y_t = \frac{h_{ftg}}{2} \quad (19)$$

- I_g is the gross moment of inertia of the uncracked sections:

$$I_g = \frac{1}{12}\ b_{ftg}\ h_{ftg}^3 \quad (20)$$

- f_r Limit tensile stress of concrete exceeded which results in the formation of the first crack (AASHTO LRFD 5.4.2.6):

$$f_r = 0.24\sqrt{f_c} \quad (21)$$

Tensioned reinforcement bars, well distributed in the zone of maximum concrete tension, have the function of being bridge between cracks formed in concrete to control flexural cracking and for this reason the spacing s between bars should not be excessive and must satisfy the following requirement s_{max}:

$$s <= s_{max} = \frac{700\ \gamma_e}{\beta_s\ f_s} - 2d_c \quad (22)$$

Where:

- γ_e = 0.75 is the exposure factor (class 2 exposure condition)
- β_s is the coefficient defined as follows:

$$\beta_s = 1 + \frac{d_c}{0.7\left(h_{ftg} - d_c\right)} \quad (23)$$

- f_s is the stress level in the reinforcement when the cross-section is subjected to the flexural action M_s (equal to the unfactored moment due to all sustained loads: dead loads and the sustained portion of the live load):

$$f_s = \frac{M_s}{A_s\ j\ d_e} \quad (24)$$

- j is the coefficient defined as follows:

$$j = 1 - \frac{k}{3} \quad (25)$$

- k is the ratio of the depth of the elastic cracked section neutral axis to the effective depth:

$$k = \sqrt{2\rho\, n + (\rho\, n)^2} - \rho\, n \quad (26)$$

- ρ is the geometric percentage of tensioned reinforcement:

$$\rho = \frac{A_s}{b_{ftg}\, d_e} \quad (27)$$

The reinforcement to be installed vertically along the sides of the 12" base section considered for foundation sizing, should be the maximum between the skin reinforcement A_{sSK} and temperature and shrinkage reinforcement A_{sTS}:

$$A_{s,face} = \max(A_{sSK};\, A_{sTS}) \quad (28)$$

The skin reinforcement, additional to the reinforcing contributing to flexural resistance, must be provided if:

$$d_e > 3ft \quad (29)$$

The skin reinforcement is calculated with the following equation and must be included in the range A_{sSKmin} to A_{sSKmax}:

$$A_{sSKmin} = 0.012(d_e - 30in) \quad (30)$$

$$A_{sSKmax} = \frac{A_s}{4ft} \quad (31)$$

The maximum spacing s_{SKmax} in vertical direction between each bar is:

$$s_{SKmax} = min\left(\frac{d_e}{6}, 12in\right) \quad (32)$$

Crack formation is influenced by differential thermal stresses, concrete shrinkage, and other time-dependent effects so a minimum reinforcement A_{sTS} must be provided to control cracks.

$$A_{sTS} = 0.11 \leq \frac{1.3\; b\; h_{ftg}}{2(b + h_{ftg})f_y} \leq 0.6 \quad (33)$$

6. Preparation of Design Example and Mathcad Worksheet for Pile Footing Design

6.1. Pile Cap Foundation Material and Geometry Definition

Concrete material parameters assumed for design are listed in Table 59:

Table 59. Concrete parameter AASHTO LRFD

Concrete Compressive Strength	f'_c	5.5	[ksi]
Rectangular Concrete Stress Block Theory	β_1	0.775	[-]
Concrete Ultimate Compressive Strain	ε_{cu}	0.003	[-]
Modulus of Elasticity for Concrete	E'_c	4268.3	[ksi]

GFRP properties assumed for design are listed in Table 60:

Table 60. GFRP bars parameter AASHTO LRFD

GFRP #11 BARS			
Environmental Reduction Factor	C_e	0.7	[-]
Modulus of Elasticity of GFRP	E_f	8700	[ksi]
Diameter	$\phi_{f\#11}$	1.41	[in]
Area	$A_{f\#11}$	1.56	[in^2]
Characteristic Ultimate Guaranteed Rupture Strain	$\varepsilon_{fu\#11}$	0.01179	[-]
Characteristic Ultimate Guaranteed Tensile Strength	$f_{fu\#11}$	102.6	[ksi]
Design Ultimate Guaranteed Rupture Strain	$\varepsilon_{fd\#11}$	0.0083	[-]
Design Ultimate Guaranteed Tensile Strength	$f_{fd\#11}$	71.8	[ksi]
GFRP #8 BARS			
Environmental Reduction Factor	C_e	0.7	[-]
Modulus of Elasticity of GFRP	E_f	8700	[ksi]
Diameter	$\phi_{f\#8}$	1	[in]
Area	$A_{f\#8}$	0.79	[in^2]
Characteristic Ultimate Guaranteed Rupture Strain	$\varepsilon_{fu\#8}$	0.01381	[-]
Characteristic Ultimate Guaranteed Tensile Strength	$f_{fu\#8}$	120.1	[ksi]
Design Ultimate Guaranteed Rupture Strain	$\varepsilon_{fd\#8}$	0.0097	[-]
Design Ultimate Guaranteed Tensile Strength	$f_{fd\#8}$	84.1	[ksi]

GFRP #6 BARS			
Environmental Reduction Factor	C_e	0.7	[-]
Modulus of Elasticity of GFRP	E_f	8700	[ksi]
Diameter	$\phi_{f\#6}$	0.75	[in]
Area	$A_{f\#6}$	0.44	[in^2]
Characteristic Ultimate Guaranteed Rupture Strain	$\varepsilon_{fu\#6}$	0.01497	[-]
Characteristic Ultimate Guaranteed Tensile Strength	$f_{fu\#6}$	130.2	[ksi]
Design Ultimate Guaranteed Rupture Strain	$\varepsilon_{fd\#6}$	0.0105	[-]
Design Ultimate Guaranteed Tensile Strength	$f_{fd\#6}$	91.2	[ksi]
Design Ultimate Guaranteed Tensile Strength (bent bars)	$f_{fd\#6}$	34.8	[ksi]

Importantly, the geometry of the foundation designed with GRP reinforcement remains the same as that of the original design with steel reinforcement. The critical dimensions for the pile cap are listed in Table 61:

Table 61. Pile cap geometry of the selected pier n.24 of the Eastbound Bridge

Footing Height	h_{ftg}	5.5	[ft]
Transverse Footing Width	b_T	20.5	[ft]
Longitudinal Footing Width	b_L	13	[ft]
Footing Design Width (One Foot Design Width)	b_{ftg}	12	[in]
Top Reinforcement Concrete Cover	c_{top}	4	[in]
Bottom Reinforcement Concrete Cover	c_{bot}	4.5	[in]
Side Reinforcement Concrete Cover	c_{side}	4	[in]

6.2. Validation of Analytical Calculations

The selected foundation case study was modelled in Altair S-Foundation® software (see Figure 60).

Figure 60. Altair S-Foundation® software

In this FEM, the applied load represents the maximum axial stress at the base of pile n.24, which produces the maximum axial stress within the piles. The value of the loads was deduced from the output of the substructure model implemented with BSI FB-MultiPier® software.

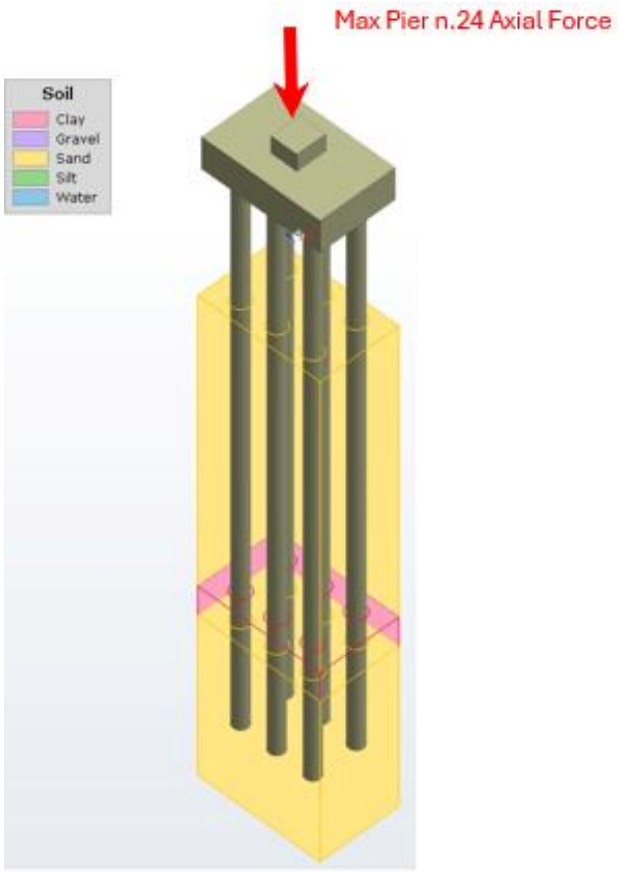

Figure 61. Nodal load applied in Altair S-Foundation® software

The FE model implemented in Altair® is intended to validate flexure, on-way and two-way shear verifications at the ULS. The program does not perform verifications at SLS and does not check construction details.

Figure 62 illustrates the results of the FEM analysis for the selected pile cap, showing the shear distribution in two orthogonal directions (F_{xz} and F_{yz}) in units of [kip/ft].

- **Shear Fxz**: The stress distribution indicates a concentrated load in the central area, with higher values (in red) localized around the column area, loaded with a point load, gradually decreasing toward the outer areas;
- **Shear Fyz**: The stresses in the perpendicular direction show a similar pattern, with high values at the central load point and a gradual transition to less stressed zones.

Note: Fxz is the shear in the Z direction along the face perpendicular to the X axis, similar for Fyz.

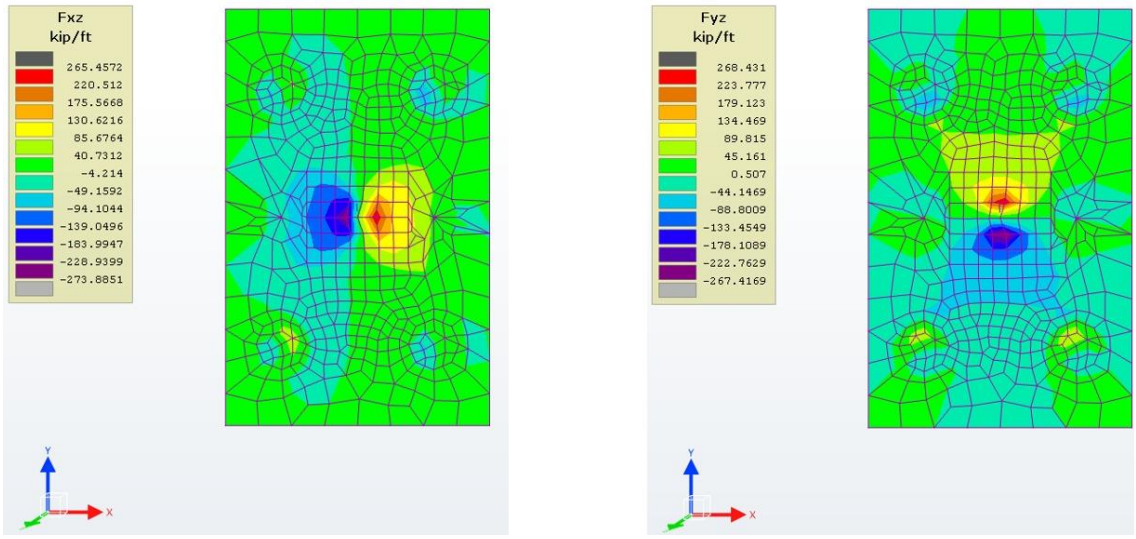

Figure 62. Shear demand distribution of F_{xz} and F_{yz}

Figure 63 of the FEM analysis for the selected pile cap, shows the distribution of bending moments (M_x and M_y) across a structural element in units of [kip-ft/ft].

- **Left (Mx):** The color map illustrates the bending moment distribution in the x-direction. Higher moment values (red) are observed in the pier peripheral regions, while lower moments (blue) are concentrated around the center of the slab, meaning that the slab's central area is less stressed in this direction.
- **Right (My):** This plot displays the bending moment distribution in the y-direction. Similar to the Mx distribution, higher moments (red) are present on the edges, while the central region has lower values (blue).

Note: Mx is the bending moment in the X direction along the face perpendicular to the X axis, similar to My.

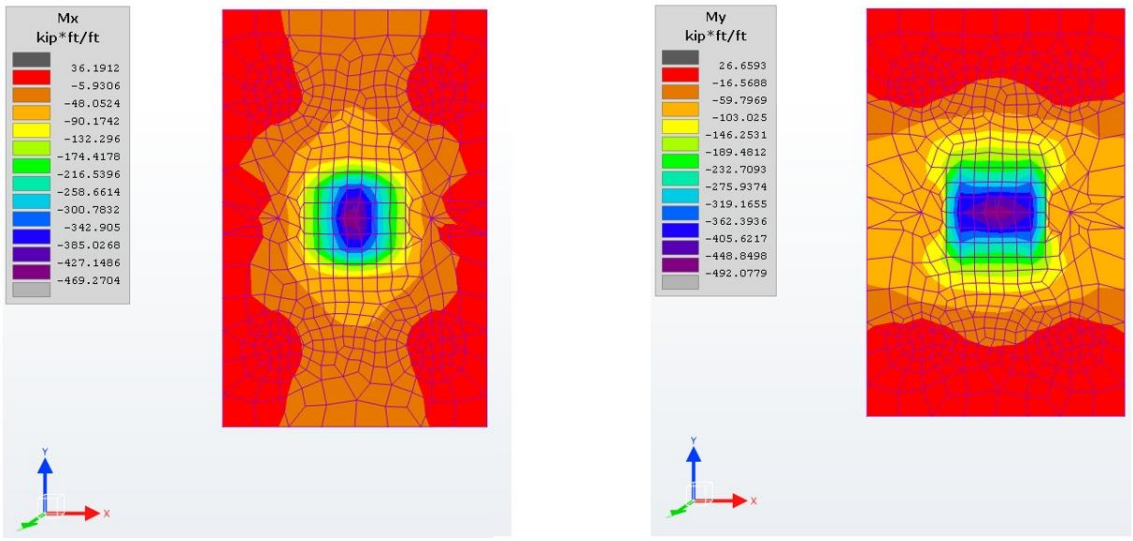

Figure 63. Bending moment demand distribution of M_x and M_y

6.3. Verification Criteria

Verifications at ULS and SLS, according to *AASHTO LRFD Bridge Design Guide Specifications for GFRP-Reinforced Concrete 2018 (2nd Edition)* [1] and *AASHTO LRFD Bridge Design Guide Specifications 2020 (9th Edition)* [55] of the carbon GFRP-RC pile cap foundations were performed externally with personalized calculation sheets coded in Mathcad Professional 14.0® (see Figure 64).

Figure 64. Mathcad® software

The properties for the GFRP #11 bars are extrapolated from data on smaller bars using a conservative best-fit trend based on bar area as shown in Figure 65 and Figure 66.

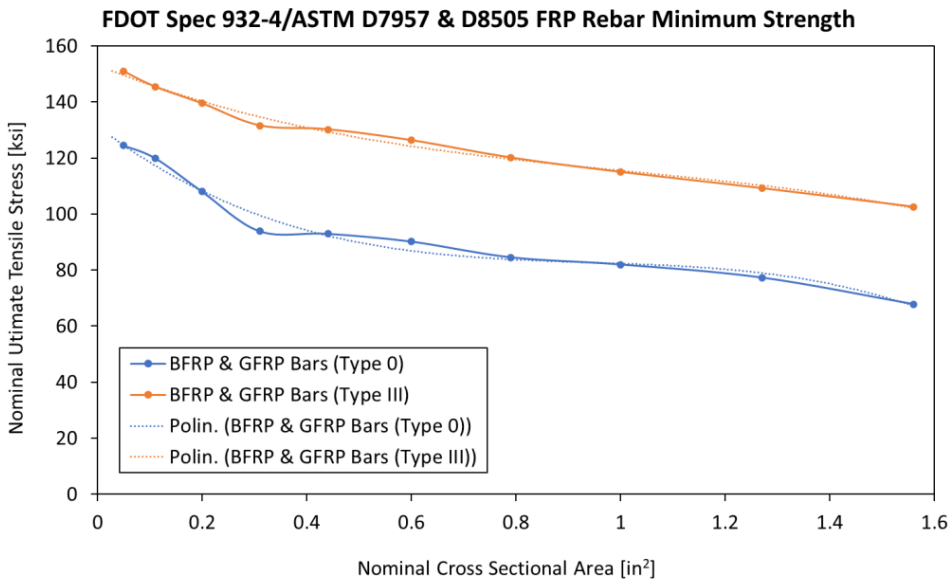

Figure 65. Ultimate stress trend vs. FRP bars area

For all the other bar sizes used in the design, the mechanical properties are in accordance with ASTM D8505.

932-4.2 Bar Sizes and Loads: The sizes and loads of FRP reinforcing bars shall meet the requirements in Table 932-8. The measured cross-sectional area, including any bond enhancing surface treatments, shall be determined according to Materials Manual Section 12.1 Volume II.

Table 932-8
Sizes and Tensile Loads of FRP Reinforcing Bars

Bar Size Designation	Nominal Bar Diameter (in)	Nominal Cross Sectional Area (in^2)	Measured Cross-Sectional Area (in^2)		Minimum Guaranteed Tensile Load (kips)			
			Minimum	Maximum	BFRP & GFRP Bars (Type 0)	BFRP & GFRP Bars (Type III)	CFRP (Type II) Single & 7-Wire Strands	CFRP (Type I) Bars
2.1-CFRP	0.21	0.028	0.026	0.042	-	-	7.1	-
2	0.250	0.049	0.046	0.085	6.1	7.4	-	10.3
2.8-CFRP	0.280	0.051	0.048	0.085	-	-	13.1	-
3	0.375	0.11	0.104	0.161	13.2	16.0	-	20.9
3.8-CFRP	0.380	0.09	0.087	0.134	-	-	23.7	-
4	0.500	0.20	0.185	0.263	21.6	27.9	-	33.3
5	0.625	0.31	0.288	0.388	29.1	40.8	-	49.1
6	0.750	0.44	0.415	0.539	40.9	57.3	-	70.7
6.3-CFRP	0.630	0.19	0.184	0.242	-	-	49.8	-
7	0.875	0.60	0.565	0.713	54.1	75.8	-	-
7.7-CFRP	0.770	0.29	0.274	0.355	-	-	74.8	-
8	1.000	0.79	0.738	0.913	66.8	94.9	-	-
9	1.128	1.00	0.934	1.159	82.0	115.0	-	-
10	1.270	1.27	1.154	1.473	98.2	138.7	-	-
11	1.410	1.56	1.500	1.700	105.8	160.0	-	-

Figure 66. Table 932-8 FDOT FY2024-25 – Sizes and tensile loads of FRP reinforcing bars

The elastic modulus of GFRP bars is assumed to be $E_f = 8700\ [\text{psi}] = 60[\text{GPa}]$ according to ASTM D8505.

6.3.1. Ultimate Limit State (ULS) verification criteria

6.3.1.1. Flexure

To calculate the balanced reinforcement ratio, the GFRP is considered to rupture and the concrete being compressed at maximum strain of $\varepsilon_{cu} = 0.003$. The reinforcement ratio computed $\rho_{f.bal}$ corresponds to the Balanced Failure Mode I-II (BFM I-II) shown in Figure 67.

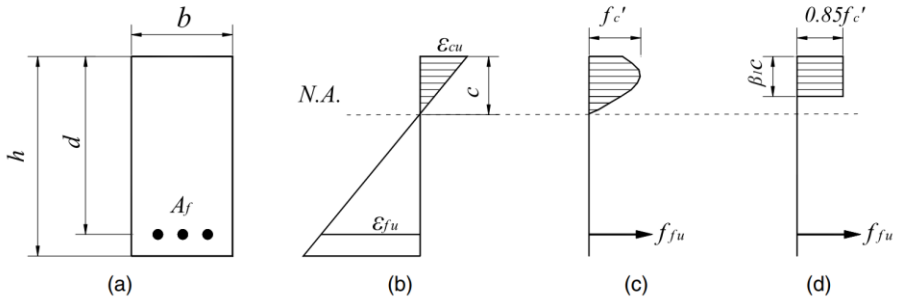

Figure 67. Balanced failure mode: strain and stress conditions: (a) cross section; (b) strain; (c) stress; (d) stress (equivalent)

The geometric percentage of tensioned reinforcement is:

$$\rho_f = \frac{A_f}{b \cdot d_f} \tag{34}$$

where:

- A_f = area of the longitudinal tension GFRP reinforcement within width b (typically taken as 12-in.);

The balanced configuration is:

$$\rho_{f.bal} = \frac{0.85 \cdot \beta_1 \cdot f_c'}{f_{fd}} \cdot \frac{\varepsilon_{cu} \cdot E_f}{f_{fd} + \varepsilon_{cu} \cdot E_f} \tag{35}$$

where:

- β_1 = ratio of depth of equivalent rectangular stress block to depth of neutral axis;
- E_f = elastic modulus for GFRP;
- f_{fd} = ultimate tensile strength of GFRP;

$$f_{fd} = C_e \cdot f_{fu} \tag{36}$$

- C_e= environmental reduction factor as specified

- f_c' = cylinder compressive strength of concrete;
- $\varepsilon_{cu} = 0.003$ = ultimate compressive strain of concrete.

Table 2.4.2.1-1—Environmental Reduction Factors

Exposure Condition	Environmental Reduction Factor, C_E
Concrete not exposed to earth or weather	0.80
Concrete exposed to earth or weather	0.70

Figure 68. Table 2.4.2.1-1 – Environmental Reduction Factors AASHTO LRFD GFRP

A GFRP-RC section subjected to flexure ULS has two Failure Modes (FM) shown in Figure 69:

I. Tension control (FM-I) if $\rho_f < \rho_{f.bal} \rightarrow \varepsilon_f = \varepsilon_{ffd}$ and $\varepsilon_c < \varepsilon_{cu}$;
II. Compression control (FM-II) if $\rho_f > \rho_{f.bal} \rightarrow \varepsilon_c = \varepsilon_{cu}$ and $\varepsilon_f < \varepsilon_{ffd}$.

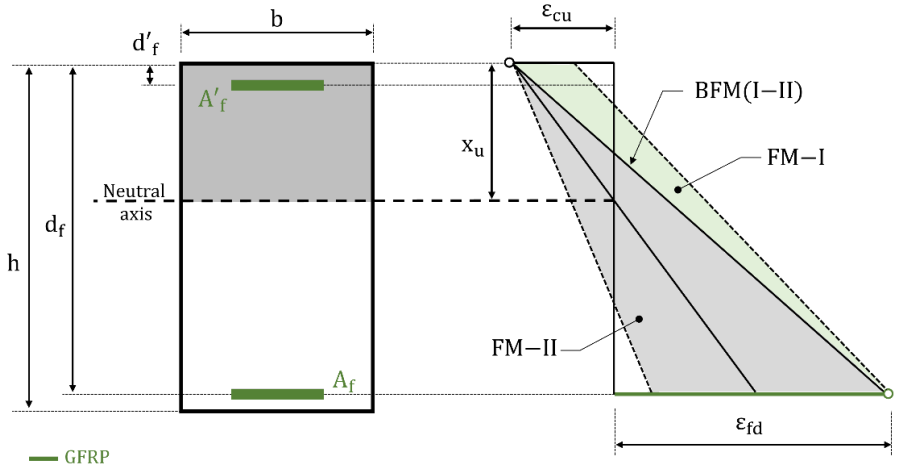

Figure 69. ULS failure modes of a rectangular GFRP-RC section

Through strain compatibility assuming that sections remain plain after deformations, is possible to calculate the balanced neutral axis depth:

$$c_{bal} = \frac{\varepsilon_{cu}}{\varepsilon_{cu} + \varepsilon_{fd}} \cdot d_f \qquad (37$$

Where:

- d_f = distance from extreme compression fiber to centroid of tensile reinforcement;
- ε_{fd} = design tensile strain at rupture of GFRP reinforcing bars.

$$\varepsilon_{fd} = C_e \cdot \varepsilon_{fu} \qquad (38)$$

The stress distribution in concrete can be approximated with an equivalent rectangular stress block using two strain-dependent and stress-dependent parameters α and β as shown in Figure 70. To compute the equivalent stress block parameters α and β, the stress-strain relationship in concrete needs to be determined.

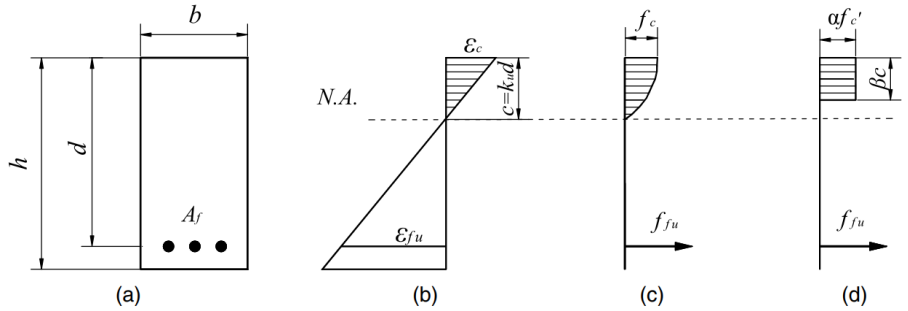

Figure 70. Tension failure mode –strain and stress conditions: (a) cross section; (b) strain; (c) stress; (d) stress (equivalent)

One of the commonly used models is the Todeschini model [56]. The equivalent stress block parameters for the Todeschini model are given as [3]:

$$\beta = 2 - \frac{4 \cdot \left[\frac{\varepsilon_c}{\varepsilon_{c0}} - tan^{-1}\left(\frac{\varepsilon_c}{\varepsilon_{c0}}\right)\right]}{\frac{\varepsilon_c}{\varepsilon_{c0}} \cdot ln\left(1 + \frac{{\varepsilon_c}^2}{{\varepsilon_{c0}}^2}\right)}; \qquad \alpha = \frac{0.9 \cdot ln\left(1 + \frac{{\varepsilon_c}^2}{{\varepsilon_{c0}}^2}\right)}{\beta \cdot \frac{\varepsilon_c}{\varepsilon_{c0}}} \tag{39}$$

where:

- ε_c= compressive concrete strain depending on the GFRP-RC configuration;
- ε_{c0}= concrete strain at maximum strength as determined from cylinder tests calibrated based on the results reported by Todeschini et al. 1964 [56];

$$\varepsilon_{c0} = \frac{f_c'}{E_c} \tag{40}$$

- E_c= concrete modulus, according to the AASHTO LRFD GFRP 5.4.2.4, is equal to:

$$E_c = 1820\ [ksi] \cdot \sqrt{f_c'[ksi]} \tag{41}$$

Adopting the rectangular stress block distribution equivalent to the real stress distribution of the compressed concrete it is possible to define:

$$a = \beta c \quad \text{and} \quad \alpha {f'}_c \tag{42}$$

- the rectangular stress block depth $a = \beta c$;
- the uniform equivalent rectangular stress block stress $\alpha {f'}_c$.

Following an iterative procedure based on the equilibrium, varying the neutral axis depth c (actual depth of the compression zone), it is possible to calculate the resultant forces in concrete:

$$C = \alpha {f'}_c \cdot \beta c \cdot b \tag{43}$$

the tensioned GFRP reinforcement:

$$F = A_f \cdot f_{ft} \quad (44)$$

and the convergence is reached when the resultant axial force N is null:

$$N = F + C = 0 \quad (45)$$

From the equilibrium state, the nominal resistant moment is derived:

$$M_n = A_f \cdot f_{fd} \cdot \left(d_f - \frac{u}{2}\right) \quad (46)$$

Where:

- d_e = depth of the tensioned reinforcement from the extreme fiber of concrete in compression.

Finally, the resisting design moment $\phi_f M_n$ should be computed and ensured is greater than the ULS action:

$$\phi_f \cdot M_n > M_u \quad (47)$$

Where:

- M_u = the design flexural moment at ULS;
- M_n = the nominal flexural resistance;
- ϕ_f = the flexural resistance (strength reduction) factor, for tension-controlled GFRP-RC section (*AASHTO LRFD BDS GFRP 2.5.5.2*).

As shown in Figure 71 ϕ_f varies depending on the GFRP-RC tensile strain in extreme tension GFRP at nominal resistance ε_{ft}, thus on the failure mode and on the provided geometric percentage of tensioned reinforcement ρ_f:

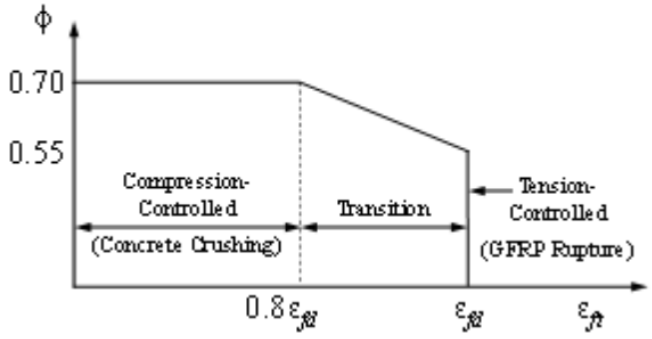

Figure 71. Figure C2.5.5.2-1—Variation of ϕ_f with tensile strain at failure ε_{ft} in GFRP Reinforcement

The law of variation of ϕ_f is the following:

$$\phi_f = \begin{cases} 0.55 & \text{for } \varepsilon_{ft} = \varepsilon_{fd} \\ 1.55 - \dfrac{\varepsilon_{ft}}{\varepsilon_{fd}} & \text{for } 0.8\varepsilon_{fd} < \varepsilon_{ft} < \varepsilon_{fd} \\ 0.75 & \text{for } \varepsilon_{ft} < 0.8\varepsilon_{fd} \end{cases} \quad (48)$$

6.3.1.2. Shear

The resistant design shear $\phi_s V_n$ must be greater than the ULS shear action V_u:

$$V_u < \phi_s V_{1w.n} \quad (49)$$

where:

- $\phi_s = 0.75$ is the resistance factor, shear and torsion normal weight concrete section (AASHTO LRFD BDS GFRP 2.5.5.2).
- V_u = the design shear at ULS.

The nominal one-way shear is calculated as follow:

$$V_{1w.n} = V_{1w.c} + V_f \quad (50)$$

Where transverse reinforcement is required as specified in AASHTO LRFD GFRP 2.7.2.2, the area of GFRP A_{fv} shall satisfy:

$$A_{fv} \geq 0.05 \frac{b_v \cdot s}{f_{fv}} \quad (51)$$

where:

- b_v = effective web width taken as the minimum web width, measured parallel to the neutral axis, between the resultants of the tensile and compressive forces due to flexure, or for circular sections, the diameter of the section, modified for the presence of ducts where applicable [in].

The nominal shear resistance provided by the transverse reinforcement V_f as specified in AASHTO LRFD GFRP 2.7.3.5 shall satisfy:

$$V_f \leq 0.25 \sqrt{f'_c} \cdot b_v \cdot d_v \quad (52)$$

The resistant design shear $\phi_s V_n$ must be greater than the ULS shear action V_u:

$$V_u < \phi_s V_{2w.n} \quad (53)$$

where:

- $\phi_s = 0.75$ is the resistance factor, shear and torsion normal weight concrete section (AASHTO LRFD BDS GFRP 2.5.5.2).

The nominal <u>two-way shear</u> [kips] is:

$$V_{2w.c} = 0.316 \cdot k \cdot \sqrt{f'_c} \cdot b_0 \cdot d_v \quad (54)$$

where:

- β_c is the ratio of long side to short side of the rectangle through which the concentrated load or reaction force is transmitted:

$$\beta_c = \begin{cases} \dfrac{X + b_{pile} + edge}{Y + b_{pile} + edge} & (X > Y) \\ \dfrac{Y + b_{pile} + edge}{X + b_{pile} + edge} \end{cases}$$

$$X = \begin{cases} 0.5d_v & spa_T \geq d_v + b_{pile} \\ \dfrac{spa_T - b_{pile}}{2} \end{cases} \quad (55)$$

$$Y = \begin{cases} 0.5d_v & spa_L \geq d_v + b_{pile} \\ \dfrac{spa_L - b_{pile}}{2} \end{cases}$$

- b_0 is the perimeter of critical section

$$b_0 = 2\left(X + b_{pile} + edge\right) + 2\left(Y + b_{pile} + edge\right) \quad (56)$$

where:

- V_c = nominal shear resistance of the concrete [kip];
- V_f = nominal shear resistance provided by transverse GFRP reinforcement [kip].

The nominal shear resistance of the concrete V_c shall be calculated as:

$$V_c = 0.0316 \cdot \beta \cdot \sqrt{f'_c} \cdot b \cdot d_v \quad (57)$$

where:

- $\beta = 5k$ is the factor indicating ability of diagonally cracked concrete to transmit tension and shear with $\theta = 45°$ as specified in AASHTO LRFD BDS GFRP 2.7.3.6;
- k ratio of depth of neutral axis to depth of flexural reinforcement in AASHTO LRFD BDS GFRP 2.5.3:

$$k = \sqrt{2 \cdot \rho \cdot n_f + (\rho \cdot n_f)^2} - \rho \cdot n_f \quad (58)$$

- n_f = modular ratio

$$n_f = \frac{E_f}{E_c} \quad (59)$$

- d_v = effective shear depth [in] as determined in AASHTO LRFD BDS GFRP 2.7.2.8;
- b = effective web width [in] taken as the minimum web width within the depth d_v.

AASHTO LRFD BDS GFRP C2.7.3.4: "Compared *with a steel-RC sections with equal areas of longitudinal reinforcement, a cross section reinforced with GFRP flexural reinforcement after cracking has a smaller depth to the neutral axis because of the lower GFRP axial stiffness. As a result, the shear resistance provided by both aggregate interlock and compressed concrete is reduced. Research on the shear resistance of flexural members without shear reinforcement has indicated that the concrete shear strength is influenced by the longitudinal stiffness of the tension (flexural) reinforcement. Because of the lower strength and stiffness of GFRP bars in the transverse direction, it is assumed that their dowel action contribution is less than that of a steel bar of equivalent area."*

The nominal shear resistance provided by the transverse reinforcement:

$$V_f = \frac{A_{fv} \cdot f_{fv} \cdot d_v \cdot cot\theta}{s} \quad (60)$$

Where:

- A_{fv} = area of transverse reinforcement within distance s [in^2];
- s = spacing of transverse reinforcement measured in a direction parallel to the longitudinal reinforcement [in];
- θ = angle of inclination of diagonal compressive stresses as determined in Article 2.7.3.6 [°].
- f_{fv} = design tensile strength of transverse reinforcement [ksi]:

$$f_{fv} = 0.004\, E_f \leq f_{fb} \quad (61)$$

- f_{fb} = design tensile strength of bent portion of GFRP reinforcing bar [ksi]:

$$f_{fb} = \left(0.05 \frac{r_b}{d_b} + 0.3\right) f_{fd} \leq f_{fd} \quad (62)$$

- r_b = design tensile strength of bent portion of GFRP reinforcing bar [ksi] as determined in AASHTO BDS GFRP 6.6.4:

Table 6.6.4-1—Minimum Diameter of Prefabricated GFRP Bends

Bar Size Designation	Minimum Inside Bend Diameter
No. 2 through 8	3 bar diameters
No. 9 and 10	4 bar diameters

Figure 72. Table 6.6.4-1 – Minimum diameter of prefabricated GFRP bends

- d_b = GFRP reinforcing bar diameter [in];
- f_{fd} = design tensile strength of GFRP reinforcing bars considering reductions for service environment [ksi].

6.4. Serviceability Limit State (SLS) verification criteria

The tension reinforcement in flexural bending must be sufficient to ensure crack control at the SLS.

Creep rupture occurs when the sustained stress exceeds the creep rupture factor times the design tensile strength of GFRP bars. To avoid creep rupture of GFRP reinforcing bars, the sustained stress level shall be limited by the creep rupture stress. Because these stress levels will be within the elastic range of the member, the stresses can be computed through an elastic analysis.

The maximum sustained tensile stress in the GFRP reinforcement f_{fs} shall be calculated using the dead loads and live loads included in the Service I load combination specified in the AASHTO LRFD 3.4.1, where the live load factor shall be reduced from 1.0 to 0.2. Using the full live load in determining the applied stress is prohibitively conservative. Therefore, the load factor applied to live load is reduced from 1.0 to 0.2 as a means to account for the sustained portion of the live load [3].

f_{fs} shall satisfy the following equation:

$$f_{fs} \leq C_c \cdot f_{fd} \quad (63)$$

Where:

$$f_{fs} = \frac{n_f \cdot d_f \cdot (1-k)}{I_{cr}} \cdot M_{s.s} \quad (64)$$

- $M_{s.s}$ = moment due to dead loads and sustained portion of live loads included in Service I load combination [kip-in];
- I_{cr} = moment of inertia of transformed moment of inertia of transformed [in^4];

$$I_{cr} = \frac{b \cdot d_f}{3} k^3 + n_f \cdot A_f \cdot \left(d_f - k \cdot d_f\right) \quad (65)$$

- C_c = creep reduction factor equal to 0.3 [-].

6.4.1. Fatigue limit state

The maximum tensile stress in the GFRP reinforcement f_{ff} resulting from the dead loads included in the Service I load combination and the factored live loads included in the Fatigue I load combination, as specified in Table 3.4.1-1 and Article 3.6.1.4 of the AASHTO LRFD Bridge Design Specifications, shall satisfy the following equation:

$$f_{ff} \leq C_f \cdot f_{fd} \quad (66)$$

Where:

$$f_{ff} = \frac{n_f \cdot d_f \cdot (1-k)}{I_{cr}} \cdot M_{s.f} \quad (67)$$

- $M_{s.f}$ = moment due to dead loads included in Service I load combination and factored live loads included in Fatigue I load combination [kip-in];
- I_{cr} = moment of inertia of transformed moment of inertia of transformed [in^4];

$$I_{cr} = \frac{b \cdot d_f}{3} k^3 + n_f \cdot A_f \cdot \left(d_f - k \cdot d_f\right) \quad (68)$$

- C_c = creep reduction factor equal to 0.25.

6.5. Detailing Requirements

For cast-in-place concrete, the clear distance between parallel bars in a layer shall not be less than the largest of the following:

$$s_{min} = min\left(1.5\ \emptyset_{bar};\ 1.5\ \emptyset_{aggr};\ 1.5[\text{in}]\right) \quad (69)$$

Where:

- $\emptyset_{bar}$ = nominal diameter of the bars;
- $\emptyset_{aggr}$ = maximum size of the coarse aggregate.

It is necessary that the resistant design moment $\phi_f M_n$ developed by the cross section is at least 1/3 greater than the design bending moment at the ULS M_u and that the collapse condition does not occur just after cracking of the section when the cracking moment M_{cr} is reached:

$$\phi_f M_n < min(1.33\ M_u; 1.6\ M_{cr}) \quad (70)$$

The cracking moment of the cross section M_{cr} is calculated as follow:

$$M_{cr} = f_r \cdot \frac{I_g}{y_t} \quad (71)$$

Where:

- y_t is the neutral axis depth, distance from neutral axis to the extreme tension fiber:

$$y_t = \frac{h_{ftg}}{2} \quad (72)$$

- I_g is the gross moment of inertia of the uncracked sections:

$$I_g = \frac{1}{12} \cdot b_{ftg} \cdot h_{ftg}^3 \quad (73)$$

- f_r Limit tensile stress of concrete exceeded which results in the formation of the first crack (AASHTO LRFD 5.4.2.6):

$$f_r = 0.24\sqrt{f'_c} \quad (74)$$

The reinforcement to be installed vertically along the sides base section should be the maximum between the skin reinforcement A_{SK} and temperature and shrinkage reinforcement A_{TS}:

$$A_{face.min} = max(A_{SK};\ A_{ST}) \quad (75)$$

And the spacing shall be greater than the minimum between the skin reinforcement s_{SK} and temperature and shrinkage reinforcement s_{TS}:

$$s_{face.max} = min(s_{SK.max};\ s_{ST.max}) \quad (76)$$

All reinforced concrete members are subject to cracking under any load condition, including thermal effects and restraint of deformations, which produces tension in the gross section in excess of the cracking strength of the concrete.

The skin reinforcement, additional to the reinforcing contributing to flexural resistance and controls flexural cracking, must be provided if:

$$d_e > 3[\text{ft}] \quad (77)$$

The maximum spacing of the skin reinforcement shall not exceed the lesser of:

$$s_{SK.max} = min\left(\frac{d_f}{6}; 12[\text{in}]\right) \quad (78)$$

The area of skin reinforcement distributed along each side faces $A_{sk}\left[\frac{\text{in}^2}{\text{ft}}\right]$ of height:

$$A_{sk} \geq A_{SK.min} = 0.012\left[\frac{\text{in}}{\text{ft}}\right](d_f - 30[\text{in}]) \quad (79)$$

However, the total area of longitudinal skin reinforcement (per face) need not exceed:

$$A_{sk} < A_{SK.max} = \frac{A_f}{4} \quad (80)$$

Reinforcement for shrinkage and temperature stresses shall be provided near surfaces of concrete exposed to daily temperature changes and in structural mass concrete. Temperature and shrinkage reinforcement shall be sufficient to ensure that the total reinforcement on exposed surfaces is not less than that specified herein. The area of shrinkage and temperature reinforcement, divided between each face and in each direction, shall not be less than the area associated with the ratio of GFRP shrinkage and temperature reinforcement area to gross concrete area given by below equation:

$$\rho_{ST.min} = max\left(\frac{3132}{E_f \cdot f_{fd}};\ 0.0014\right) \leq 0.0036 \quad (81)$$

The area of GFRP reinforcement for shrinkage and temperature $A_{ST.min}\left[\frac{\text{in}^2}{\text{ft}}\right]$ is calculated referring to the cross-section area $A_{section}$ and the perimeter of the section $p_{section}$:

$$A_{ST.min} = \rho_{ST.min} \cdot \frac{p_{section}}{A_{section}} \quad (82)$$

Area of provided shrinkage and temperature reinforcement per each length of the side faces of the section L_i :

$$A_{ST.i} = \frac{n_{bar} \cdot A_{bar}}{L_i}\left[\frac{\text{in}^2}{\text{ft}}\right] \quad (83)$$

The spacing of GFRP reinforcing bars used as shrinkage and temperature reinforcement shall not exceed:

$$s_{ST.max} = min(3\,h_{section};\ 12\ [\text{in}]) \quad (84)$$

The tension development length l_d shall satisfy the following equation:

$$l_d \geq max\left(\frac{31.6 \cdot \alpha \cdot \frac{f_{fr}}{\sqrt{f'_c}} - 340}{13.6 + \frac{C}{\emptyset_{bar}}}\emptyset_{bar};\ 20\ \emptyset_{bar}\right) \quad (85)$$

Where:

- α = bar location modification factor that shall be set equal to 1.0 except for bars with more than 12 in. of concrete cast below the reinforcement, for which a value of 1.5 shall be adopted;
- C = lesser of the cover to the center of the bar or one-half of the center-to-center spacing of the bars being developed [in];
- f_{fr} = required GFRP reinforcing bar stress as determined in AASHTO BDS GFRP 2.7.3.7 [ksi]:

$$f_{fr} = \min(f_f; f_{fd}) \quad (86)$$

- f_r = design tensile strength of GFRP reinforcing bars considering reductions for service environment at nominal flexural resistance [ksi] see AASHTO BDS GFRP 2.6.3.1:
- $\frac{C}{\emptyset_{bar}}$ shall not be taken larger than 3.5.

GFRP reinforcing bars are typically manufactured without end bends. When hooks are provided, the development length l_{dh} shall not be less than

$$l_{dh} = \begin{cases} 63.2\ \dfrac{\emptyset_{bar}}{\sqrt{f'_c}} & \text{for } f_{fd} \leq 75\ [\text{ksi}] \\ \dfrac{f_{fd}}{1.2} \cdot \dfrac{\emptyset_{bar}}{\sqrt{f'_c}} & \text{for } f_{fd} \leq 75\ [\text{ksi}] < f_{fd} \leq 150\ [\text{ksi}] \\ 126.4\ \dfrac{\emptyset_{bar}}{\sqrt{f'_c}} & \text{for } f_{fd} \geq 75\ [\text{ksi}] \end{cases} \quad (87)$$

The development length l_{dh} shall be:

$$l_{dh} \geq \max(12\ \emptyset_{bar}; 9\ [\text{in}]) \quad (88)$$

The minimum required tail length $l_{d.end}$ shall be specified in AASHTO BDS GFRP 2.7.2.7.2 for anchorage of reinforcement:

$$l_{d.tail} \geq 12\ \emptyset_{bar} \quad (89)$$

It is important to point out that by adopting the ACI 440.11-22 and AASHTO BDS GFRP 2nd edition (2018) standards, the GFRP bar strength changes as shown below in Table 62.

Table 62. Comparison between ACI and AASHTO LRFD BDS for GFRP

GFRP bars #11		**AASHTO GFRP 2nd Ed. (2018) [50]**	**ACI 440.11-22 [48]**	
Reduction Factor GFRP failure	$\phi_{M.f}$	0.55	0.55	[-]
Reduction Factor Concrete failure	$\phi_{M.c}$	0.75	0.65	[-]
Reduction Factor for shear	ϕ_S	0.75	0.75	[-]
Environmental Reduction Factor	C_e	0.70	0.85	[-]
Creep Reduction Factor	C_c	0.30	0.30	[-]
Fatigue Reduction Factor	C_f	0.25	0.30	[-]
Bond Reduction Factor	C_b	0.80	0.70	[-]
Crack width limit	w	0.028	0.028	[in]
Clear cover	$C_{c.stirrups}$	1.50	2.00	[in]
Clear cover	$C_{c.slab}$	1.00	0.75 to 2.0	[in]

The entire design procedure for pier 24 footing is documented in a separate file with this report.

The following are the results from Altair S-Foundation® software.

The utilization coefficient (Demand/Capacity ratio) for “GFRP-RC foundation (2b)” with 4.5” bottom concrete cover are given in Figure 73. The flexural and shear verifications at ULS are largely satisfied.

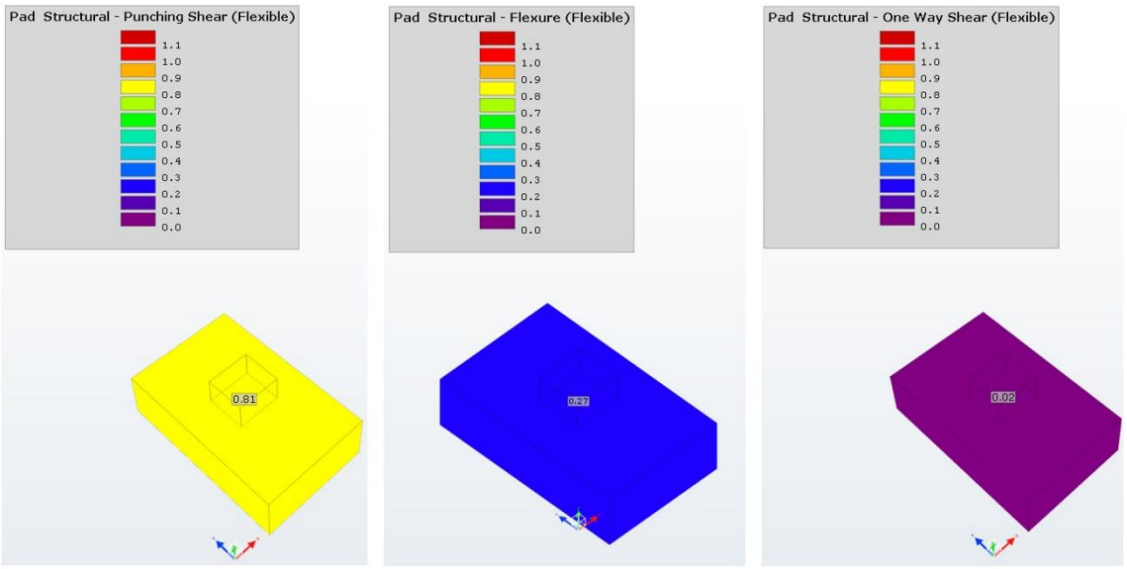

Figure 73. Utilization coefficient GFRP-RC (2b) – ULS moment and shear

The utilization coefficient (Demand/Capacity ratio) for "GFRP-RC foundation (2c)" with 12" bottom concrete cover are given in Figure 74. In this case by decreasing the cover by 3 times, the utilization factor increases but the verifications at ULS are always satisfied.

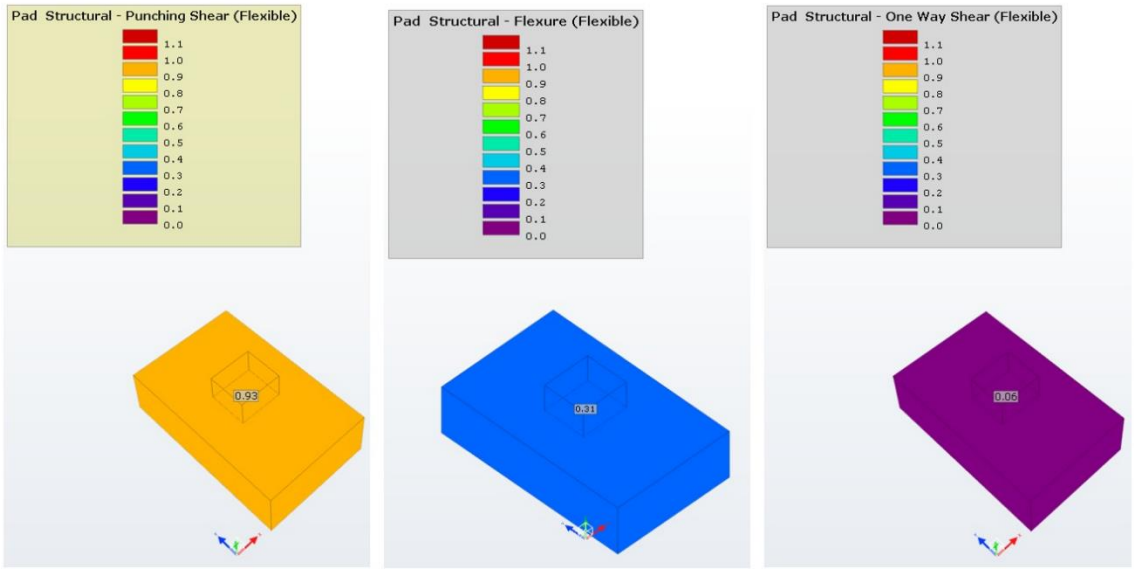

Figure 74. Utilization coefficient GFRP-RC (2c) – ULS moment and shear

7. Conclusions

The research and testing conducted throughout this project provide significant insights into the feasibility and application of large-diameter FRP bars in waterline pile cap footings for bridges. The findings underscore the potential benefits of utilizing #11 GFRP bars while also addressing the challenges associated with their adoption in structural applications. The conclusions drawn from each task contribute to a comprehensive understanding of the behavior, performance, and design considerations necessary for successfully implementing large-diameter FRP reinforcement in bridge foundations.

The literature review conducted in Task 1 highlighted the limited experimental studies available on FRP bars exceeding #8 in diameter. While some manufacturers have begun producing #11 FRP bars, peer-reviewed publications and standardized testing data remain scarce. Key challenges identified include testing complexities, size-dependent mechanical properties such as the shear-lag effect, and reductions in bond strength to concrete. Additionally, accelerated aging and long-term durability studies on large-diameter FRP bars are insufficient, making it difficult to extrapolate existing data on smaller bars to larger diameters. Despite these challenges, the review confirmed that large-diameter FRP bars exhibit slower strength degradation and greater resistance to environmental factors due to their thicker resin layers, suggesting their viability for long-term structural applications. The need for updated design specifications tailored to large-diameter FRP bars is critical, as current codes primarily rely on extrapolated data from smaller bars rather than empirical results.

Task 2 established a comprehensive testing plan to evaluate the physico-mechanical properties of #11 GFRP bars, ensuring compliance with ASTM standards and Florida Department of Transportation (FDOT) specifications. Task 3 then implemented this testing plan, confirming that the tested GFRP bars met most of the material requirements outlined in FDOT Materials Manual Section 12.1. The bars demonstrated satisfactory tensile strength, shear strength, and environmental durability, reinforcing their potential for use in harsh marine environments. These findings validate the structural integrity of large-diameter GFRP bars under typical loading conditions and highlight their suitability for bridge applications.

The case study analysis in Task 4 focused on redesigning an Eastbound Bridge foundation, originally reinforced with carbon steel, using large-diameter GFRP bars. The study adhered to the AASHTO LRFD Bridge Design Guide Specifications for GFRP-Reinforced Concrete [1] and the FDOT Structures Manual (2024). Verification of the ultimate and serviceability limit states (ULS and SLS) was conducted, and design considerations for pier cap foundations were evaluated. The analysis confirmed that GFRP bars could effectively replace traditional steel reinforcement while maintaining structural integrity, though adjustments in detailing and design philosophy were necessary due to the lower shear strength of GFRP-reinforced concrete.

Building on these findings, Task 5 further refined the GFRP-RC pile cap footing design, incorporating numerical modeling through Altair® software. The analysis accounted for shear stresses within shell elements, pile cap flexibility, and pile-column spacing. The results demonstrated that GFRP reinforcement required modifications in shear detailing compared to steel reinforcement. Specifically, the absence of shear reinforcement in certain GFRP-RC configurations was feasible due to adjustments in shear strength assumptions. Additionally, the analytical MathCAD approach, which considers axial force transfer from piles as shear, was found to be highly conservative for GFRP-reinforced footings. The key distinction between steel and GFRP reinforcement lies in shear design requirements rather than bending capacity, emphasizing the need for revised shear strength provisions in GFRP-RC design.

Overall, this project confirms that large-diameter GFRP bars can be successfully implemented in waterline pile cap footings for bridges, offering corrosion resistance and durability advantages over traditional steel reinforcement. However, addressing challenges such as size-dependent mechanical properties, bond strength variations, and shear design considerations is crucial for widespread adoption. The research underscores the necessity for further experimental testing, refinement of existing design codes, and the development of specifications tailored specifically to large-diameter FRP bars. Continued collaboration between researchers, manufacturers, and transportation agencies will be essential in optimizing the structural use of GFRP reinforcement in marine bridge foundations.

References

CSA Group, *Specification for Fibre-Reinforced Polymers*, CSA S807:19. Canadian Standards Association, 2019.

ASTM International, *Standard Test Method for Tensile Properties of Fiber Reinforced Polymer Matrix Composite Bars*, ASTM D7205/D7205M-06. ASTM International, 2006. doi: 10.1520/D7205_D7205M-06

American Association of State Highway and Transportation Officials, *AASHTO LRFD Bridge Design Specifications*, 7th ed. AASHTO, 2014.

American Association of State Highway and Transportation Officials, *AASHTO LRFD Bridge Design Specifications*, 9th ed. AASHTO, 2020. ISBN: 978-1-56051-738-2.

American Association of State Highway and Transportation Officials, *AASHTO LRFD Bridge Design Guide Specifications for GFRP-Reinforced Concrete*, 2nd ed. AASHTO, 2018.

[1] AASHTO (2018) AASHTO LRFD, *Bridge design guide specifications for GFRP-reinforced concrete, 2nd Edn*. American Association of State Highway and Transportation Officials, Washington, DC, 2018.

[2] "Elium by Arkema (https://www.arkema.com/usa/en/product-range/incubator/elium_resins/)."

[2] A. Nanni, A. De Luca, H. J. Zadeh, *Reinforced Concrete with FRP Bars*. London: CRC Press, 2014. doi: 10.1201/b16669.

[3] L. C. Bank, *Composites for Construction: Structural Design with FRP Materials*. Wiley, 2006. doi: 10.1002/9780470121429.

[4] B. Başaran, İ. Kalkan, A. Beycioğlu, and I. Kasprzyk, "A Review on the Physical Parameters Affecting the Bond Behavior of FRP Bars Embedded in Concrete," *Polymers (Basel)*, vol. 14, no. 9, p. 1796, Apr. 2022, doi: 10.3390/polym14091796.

[5] H. Liu *et al.*, "Experimental Study of Dimensional Effects on Tensile Strength of GFRP Bars," *Buildings*, vol. 14, no. 5, p. 1205, Apr. 2024, doi: 10.3390/buildings14051205.

[6] L. S. Sutherland, R. A. Shenoi, and S. M. Lewis, "Size and scale effects in composites: I. Literature review," *Compos Sci Technol*, vol. 59, no. 2, pp. 209–220, Feb. 1999, doi: 10.1016/S0266-3538(98)00065-7.

[7] N. Van Vo, “Assessing Shear-Lag Effect on Pultruded FRP Rods Based on a Numerical Simulation,” *International Journal of GEOMATE*, vol. 21, no. 84, Aug. 2021, doi: 10.21660/2021.84.j2163.

[8] O. I. Abdelkarim, E. A. Ahmed, H. M. Mohamed, and B. Benmokrane, “Flexural strength and serviceability evaluation of concrete beams reinforced with deformed GFRP bars,” *Eng Struct*, vol. 186, pp. 282–296, May 2019, doi: 10.1016/j.engstruct.2019.02.024.

[9] O. H. Zinkaah and A. Ashour, “Load capacity predictions of continuous concrete deep beams reinforced with GFRP bars,” *Structures*, vol. 19, pp. 449–462, Jun. 2019, doi: 10.1016/j.istruc.2019.02.007.

[10] H. E. Daniels and H. Jeffreys, “The statistical theory of the strength of bundles of threads. I,” *Proc R Soc Lond A Math Phys Sci*, vol. 183, no. 995, pp. 405–435, 1945, doi: 10.1098/rspa.1945.0011.

[11] S.-Z. Feng *et al.*, “Accelerated aging tests of large-diameter GFRP bars in alkaline environment,” *Composites Part C: Open Access*, vol. 14, p. 100486, Jul. 2024, doi: 10.1016/j.jcomc.2024.100486.

[12] A. H. Ali, H. M. Mohamed, and B. Benmokrane, “Bar size effect on long-term durability of sand-coated basalt-FRP composite bars,” *Compos B Eng*, vol. 195, p. 108059, Aug. 2020, doi: 10.1016/j.compositesb.2020.108059.

[13] G. B. Maranan, A. C. Manalo, W. Karunasena, B. Benmokrane, and D. Lutze, “Flexural Behaviour of Glass Fibre Reinforced Polymer (GFRP) Bars Subjected to Elevated Temperature,” 2014. [Online]. Available: https://www.researchgate.net/publication/271545120

[14] L. C. Hollaway, “A review of the present and future utilisation of FRP composites in the civil infrastructure with reference to their important in-service properties,” *Constr Build Mater*, vol. 24, no. 12, pp. 2419–2445, Dec. 2010, doi: 10.1016/j.conbuildmat.2010.04.062.

[15] G. Wu, X. Wang, Z. Wu, Z. Dong, and Q. Xie, “Degradation of basalt FRP bars in alkaline environment,” *Science and Engineering of Composite Materials*, vol. 22, no. 6, pp. 649–657, Nov. 2015, doi: 10.1515/secm-2014-0040.

[16] G. Feng, D. Zhu, S. Guo, M. Z. Rahman, Z. Jin, and C. Shi, “A review on mechanical properties and deterioration mechanisms of FRP bars under severe environmental and loading conditions,” *Cem Concr Compos*, vol. 134, p. 104758, Nov. 2022, doi: 10.1016/j.cemconcomp.2022.104758.

[17] D. G. Schesser, “Mechanics of Expanding Grout Based Grips for Large Scale Composites Testing,” 2011. [Online]. Available: https://scholarship.miami.edu/esploro/outputs/graduate/Mechanics-of-Expanding-Grout-Based-Grips/

[18] V. Carvelli, G. Fava, and M. A. Pisani, “Anchor System for Tension Testing of Large Diameter GFRP Bars,” *Journal of Composites for Construction*, vol. 13, no. 5, pp. 344–349, Oct. 2009, doi: 10.1061/(ASCE)CC.1943-5614.0000027.

[19] G. Li, J. Wu, and W. Ge, “Effect of loading rate and chemical corrosion on the mechanical properties of large diameter glass/basalt-glass FRP bars,” *Constr Build Mater*, vol. 93, pp. 1059–1066, Sep. 2015, doi: 10.1016/j.conbuildmat.2015.05.044.

[20] J. Alves, A. El-Ragaby, and E. El-Salakawy, “Durability of GFRP Bars’ Bond to Concrete under Different Loading and Environmental Conditions,” *Journal of Composites for Construction*, vol. 15, no. 3, pp. 249–262, Jun. 2011, doi: 10.1061/(ASCE)CC.1943-5614.0000161.

[21] W. Li, M. Zhou, F. Liu, Y. Jiao, and Q. Wu, “Experimental Study on the Bond Performance between Fiber-Reinforced Polymer Bar and Unsaturated Polyester Resin Concrete,” *Advances in Civil Engineering*, vol. 2021, pp. 1–12, Apr. 2021, doi: 10.1155/2021/6676494.

[22] Z. Achillides and K. Pilakoutas, “Bond Behavior of Fiber Reinforced Polymer Bars under Direct Pullout Conditions,” *Journal of Composites for Construction*, vol. 8, no. 2, pp. 173–181, Apr. 2004, doi: 10.1061/(ASCE)1090-0268(2004)8:2(173).

[23] B. Di, J. Wang, H. Li, J. Zheng, Y. Zheng, and G. Song, “Investigation of Bonding Behavior of FRP and Steel Bars in Self-Compacting Concrete Structures Using Acoustic Emission Method,” *Sensors*, vol. 19, no. 1, p. 159, Jan. 2019, doi: 10.3390/s19010159.

[24] E. Nepomuceno, J. Sena-Cruz, L. Correia, and T. D’Antino, “Review on the bond behavior and durability of FRP bars to concrete,” *Constr Build Mater*, vol. 287, p. 123042, Jun. 2021, doi: 10.1016/j.conbuildmat.2021.123042.

[25] K. M. A. Hossain, “Bond Strength of GFRP Bars Embedded in Engineered Cementitious Composite using RILEM Beam Testing,” *Int J Concr Struct Mater*, vol. 12, no. 1, p. 6, Dec. 2018, doi: 10.1186/s40069-018-0240-0.

[26] F. Yan, Z. Lin, and M. Yang, “Bond mechanism and bond strength of GFRP bars to concrete: A review,” *Compos B Eng*, vol. 98, pp. 56–69, Aug. 2016, doi: 10.1016/j.compositesb.2016.04.068.

[27] R. J. Gravina, J. Li, S. T. Smith, and P. Visintin, “Environmental Durability of FRP Bar-to-Concrete Bond: Critical Review,” *Journal of Composites for Construction*, vol. 24, no. 4, Aug. 2020, doi: 10.1061/(ASCE)CC.1943-5614.0001016.

[28] S. Solyom and G. L. Balázs, “Bond of FRP bars with different surface characteristics,” *Constr Build Mater*, vol. 264, p. 119839, Dec. 2020, doi: 10.1016/j.conbuildmat.2020.119839.

[29] M. Harajli and M. Abouniaj, “Bond Performance of GFRP Bars in Tension: Experimental Evaluation and Assessment of ACI 440 Guidelines,” 2010, doi: 10.1061/ASCECC.1943-5614.0000139.

[30] R. Tepfers and L. De Lorenzis, “Bond of FRP reinforcement in concrete-a challenge,” *Mechanics of Composite Materials*, vol. 39, no. 4, pp. 315–328, 2003, doi: 10.1023/A:1025642411103.

[31] M. R. Ehsani, H. Saadatmanesh, and S. Tao, “Design Recommendations for Bond of GFRP Rebars to Concrete,” *Journal of Structural Engineering*, vol. 122, no. 3, pp. 247–254, Mar. 1996, doi: 10.1061/(ASCE)0733-9445(1996)122:3(247).

[32] A. Veljkovic, V. Carvelli, M. M. Haffke, and M. Pahn, “Concrete cover effect on the bond of GFRP bar and concrete under static loading,” *Compos B Eng*, vol. 124, pp. 40–53, Sep. 2017, doi: 10.1016/j.compositesb.2017.05.054.

[33] T. D’Antino and M. A. Pisani, “Long-term behavior of GFRP reinforcing bars,” *Compos Struct*, vol. 227, p. 111283, Nov. 2019, doi: 10.1016/j.compstruct.2019.111283.

[34] D. Hiesch, T. Proske, C. Graubner, L. Bujotzek, and R. El Ghadioui, “Theoretical and experimental investigation of the time-dependent relaxation rates of GFRP and BFRP reinforcement bars,” *Structural Concrete*, vol. 24, no. 2, pp. 2800–2816, Apr. 2023, doi: 10.1002/suco.202200212.

[35] L. Guo-wei, P. Hua-Fu, and H. Cheng-yu, “Study on the Stress Relaxation Behavior of Large Diameter B-GFRP Bars Using FBG Sensing Technology,” *Int J Distrib Sens Netw*, vol. 9, no. 10, p. 201767, Oct. 2013, doi: 10.1155/2013/201767.

[36] G. Li, S. K. Bakarr, J. Wang, X. Liu, and C. Hong, “Effect of Stress Corrosion on Relaxation of Large Diameter BGFRP Bars,” *International Journal of Corrosion*, vol. 2018, pp. 1–8, Dec. 2018, doi: 10.1155/2018/3418596.

[37] D. Schesser, Q. D. Yang, A. Nanni, and J. W. Giancaspro, “Expansive Grout-Based Gripping Systems for Tensile Testing of Large-Diameter Composite Bars,” *Journal of Materials in Civil Engineering*, vol. 26, no. 2, pp. 250–258, Feb. 2014, doi: 10.1061/(asce)mt.1943-5533.0000807.

[38] S. Telikapalli and A. Ruiz Emparanza, “The Effect of the Free Specimen Length on the Tensile Strength of Basalt FRP Rebars,” 2019. [Online]. Available: https://www.researchgate.net/publication/354856690

[39] “ATP GFRP rebars (http://www.atp-frp.com/html/gfrp_rebar.html).”

[40] “MST GFRP rebars (https://www.mstrebar.com/).”

[41] ASTM D7957/D7957M-22, *"Standard Specification for Solid Round Glass Fiber Reinforced Polymer Bars for Concrete Reinforcement."* ASTM International, West Conshohocken, PA, 2022.

[42] ASTM D8505/D8505M-23, "'Standard Specification for Basalt and Glass Fiber Reinforced Polymer (FRP) Bars for Concrete Reinforcement'", doi: 10.1520/D8505_D8505M-23.

[43] FDOT Design Manual 2024 V.4, "Fiber Reinforced Polymer Guidelines, 2024 Structures Manual, Florida Department of Transportation (FDOT)." [Online]. Available: http://www.fdot.gov/construction/DesignBuild/DBRules/DB-

[44] FDOT FY2024-25, "Florida Department of Transportation Standard Specifications for Road and Bridge Construction," (https://www.fdot.gov/programmanagement/implemented/specbooks/default.shtm), Mar. 2024.

[45] CSA 807-19, "National Standard of Canada - 'Specification for fibre-reinforced polymers,'" 2019. [Online]. Available: www.csagroup.org/legal

[46] AC454, "0543 A Subsidiary of the International Code Council ® ACCEPTANCE CRITERIA FOR FIBER-REINFORCED POLYMER (FRP) BARS FOR INTERNAL REINFORCEMENT OF CONCRETE MEMBERS AC454," 2022. [Online]. Available: www.icc-es.org

[47] AC521, "A Subsidiary of the International Code Council ® ACCEPTANCE CRITERIA FOR FIBER-REINFORCED POLYMER (FRP) BARS AND MESHES FOR INTERNAL REINFORCEMENT OF NON-STRUCTURAL CONCRETE MEMBERS AC521," 2020. [Online]. Available: www.icc-es.org

[48] ACI Committee 440, *"Building Code Requirements for Structural Concrete Reinforced with Glass Fiber-Reinforced Polymer (GFRP) Bars - Code and Commentary (ACI CODE-440.11-22)."* American Concrete Institute, Farmington Hills, MI, 2023.

[49] ACI PRC-440.1-15, *Guide for the design and construction of structural concrete reinforced with fiber-reinforced polymer FRP bars*. American Concrete Institute, 2015.

[51] CSA_S806-12, "Design and construction of building structures with fibre-reinforced polymers," 2021.

[52] CSA S6-19, "Canadian Highway Bridge Design Code," 2019. [Online]. Available: www.ShopCSA.ca

[53] ACI 440-508, "'Specification for Construction with Fiber-Reinforced Polymer Reinforcing Bars'".

[54] ASTM International. "ASTM D2584-18, Standard Test Method for Ignition Loss of Cured Reinforced Resins." West Conshohocken, PA: ASTM International, 2018.

[55] ASTM International. "ASTM D570-22, Standard Test Method for Water Absorption of Plastics. Section 8.1 for short term and Section 8.4 for long term." West Conshohocken, PA: ASTM International, 2022.

[56] ASTM International. "ASTM E1356-23, Standard Test Method for Assignment of the Glass Transition Temperatures by Differential Scanning Calorimetry." West Conshohocken, PA: ASTM International, 2023.

[57] ASTM International. "ASTM D7028-07(2015), Standard Test Method for Glass Transition Temperature (DMA) of Polymer Matrix Composites by Dynamic Mechanical Analysis (DMA)." West Conshohocken, PA: ASTM International, 2015.

[58] ASTM International. "ASTM E2160-04 (2018), Standard Test Method for Heat of Reaction of Thermally Reactive Materials by Differential Scanning Calorimetry." West Conshohocken, PA: ASTM International, 2018.

[59] ASTM International. "ASTM D792-20, Standard Test Methods for Density and Specific Gravity (Relative Density) of Plastics by Displacement." West Conshohocken, PA: ASTM International, 2020.

[60] ASTM International. "ASTM D7205/D7205M-21, Standard Test Method for Tensile Properties of Fiber Reinforced Polymer Matrix Composite Bars." West Conshohocken, PA: ASTM International, 2021.

[61] ASTM International. "ASTM D7705/D7705M-12(2019), Standard Test Method for Alkali Resistance of Fiber Reinforced Polymer (FRP) Matrix Composite Bars used in Concrete Construction, Procedure A." West Conshohocken, PA: ASTM International, 2019.

[62] ASTM International. "ASTM D7617/D7617M-11(2017), Standard Test Method for Transverse Shear Strength of Fiber–Reinforced Polymer Matrix Composite Bars." West Conshohocken, PA: ASTM International, 2017.

[63] ASTM International. "ASTM D4475-21, Standard Test Method for Apparent Horizontal Shear Strength of Pultruded Reinforced Plastics Rods by Short-Beam Method." West Conshohocken, PA: ASTM International, 2021.

[64] ASTM International. "ASTM D7913/D7913M – 14(2020), Standard Test Method for Bond Strength of Fiber-Reinforced Polymer Matrix Composite Bars to Concrete by Pullout Testing." West Conshohocken, PA: ASTM International, 2020.

[65] ASTM International. "ASTM C39-20, Standard Test Method for Compressive Strength of Cylindrical Concrete Specimens." West Conshohocken, PA: ASTM International, 2020.

[66] C.E. Todeschini, A.C. Bianchini, and C.E. Kesler. Behavior of concrete columns reinforced with high strength steels. In *Journal Proceedings* (Vol. 61, No. 6, pp. 701-716), 1964.

[67] B. Abdeldjelil, “Guidelines for the Design of Prestressed Concrete Bridge Girders Using FRP Auxiliary Reinforcement.” National Cooperative Highway Research Program (NCHRP) Transportation Research Board of The National Academies of Sciences, Engineering, and Medicine. Project No. 12-121, Interim Report No. 2. University of Houston, Houston, TX, 2022.

Appendix A – Tabulated Test Results

Tabulated test results are presented in this appendix.

Table 63. Certified Test Results per Materials Manual Section 12.1 Volume II

Standard Test Reference	Property	Unit	Bar Size & Properties*	
		SI US	V-Rod/Pultrall	MST-Bar
ASTM D2584	Fiber Mass Content	%	84	81
ASTM E1356	Glass Transition Temperature (DSC)	°C	118	114
		°F	244	238
ASTM E2160	Degree of Cure	%	99	98
ASTM D7205	Measured Cross-Sectional Area	mm^2	1108	1118
ASTM D792		in^2	1.717	1.734
ASTM D7205	Guaranteed Ultimate Tensile Force	kN	1098	824
		kip	246.9	185.3
	Nominal Ultimate Tensile Strength	MPa	1202	918.1
		ksi	174.3	133.2
	Nominal Tensile Modulus of Elasticity	GPa	59.9	57.8
		Msi	8.7	8.4
	Nominal Ultimate Strain	%	2.0	1.6
ASTM D7705-Procedure A	Alkaline Resistance (with no load): Tensile Retention[a]	%	90	88
ASTM D7913	Bond Strength[a]	MPa	4.9	9.2
		ksi	0.71	1.33
ASTM D7617	Transverse Shear Strength	MPa	163	172
		ksi	23.6	25.0
ASTM D4475	Horizontal Shear Strength	MPa	40.6	39.5
		ksi	5.9	5.7
ASTM D570	Moisture Absorption in 24 hrs.	%	0.14	0.17
	Moisture Absorption to Saturation		0.48	0.67

*Refer to Section 1.4 and 2 of report for bar description and identification. [a]Partial testing.

Fiber content – ASTM D2584

Table 64. Tabulated results for fiber content by mass per ASTM D2584 (Pultrall)

Specimen ID	W_1	W_2	RC	FC*
	g	g	%	%
PUL_11S_FC_01	59.536	50.055	15.9	84.1
PUL_11S_FC_02	57.987	49.007	15.5	84.5
PUL_11S_FC_03	55.882	47.141	15.6	84.4
PUL_11S_FC_04	54.552	45.972	15.7	84.3
PUL_11S_FC_05	58.772	49.580	15.6	84.4
Average				**84.3**
S_{n-1}				0.2
CV (%)				0.2

Table 65. Tabulated results for fiber content by mass per ASTM D2584 (MST)

Specimen ID	W_1	W_2	RC	FC*
	g	g	%	%
MST-11S_FC_01	56.228	45.277	19.5	80.5
MST-11S_FC_02	54.731	44.136	19.4	80.6
MST-11S_FC_03	58.296	47.037	19.3	80.7
MST-11S_FC_04	61.483	49.606	19.3	80.7
MST-11S_FC_05	57.209	45.908	19.8	80.2
Average				**80.6**
S_{n-1}				0.2
CV (%)				0.2

**Condition of acceptance is equivalent to FC≥ 70%*

Glass transition temperature – ASTM E1356

Table 66. Tabulated results for glass transition temperature per ASTM E1356 (Pultrall)

Specimen ID		Glass Transition Temperature T_g*	
		°C	°F
PUL_11S_TG_01		119.7	247.4
PUL_11S_TG_02		117.8	244.0
PUL_11S_TG_03		119.1	246.3
PUL_11S_TG_04		116.0	240.8
PUL_11S_TG_05		115.7	240.3
	Average	**117.7**	**243.8**
	S_{n-1}	1.8	3.2
	CV (%)	1.5	1.3

Table 67. Tabulated results for glass transition temperature per ASTM E1356 (MST)

Specimen ID		Glass Transition Temperature T_g*	
		°C	°F
MST_11S_TG_01		115.2	239.3
MST_11S_TG_02		115.9	240.5
MST_11S_TG_03		113.2	235.7
MST_11S_TG_04		115.1	239.2
MST_11S_TG_05		113.0	235.4
	Average	**114.5**	**238.0**
	S_{n-1}	1.3	2.3
	CV (%)	1.1	1.0

**Condition of acceptance is equivalent to T_g > 100°C (212°F)*

Degree of cure – ASTM E2160

Table 68. Tabulated results for glass transition temperature per ASTM E2160 (Pultrall)

Report Specimen ID	**Mass M**	**Normalized heat of reaction H**	**Total heat of reaction[a] Ht**	**Degree of Cure DC***
	mg	**J/g**	**J/g**	**%**
PUL_11S_DC_01	21.73	0.50	100.0	99.5
PUL_11S_DC_02	29.60	0.62		99.4
PUL_11S_DC_03	22.13	0.54		99.5
PUL_11S_DC_04	19.18	0.61		99.4
PUL_11S_DC_05	15.20	0.58		99.4
Average				**99.4**
S_{n-1}				0.1
CV (%)				0.1

Table 69. Tabulated results for glass transition temperature per ASTM E2160 (MST)

Report Specimen ID	**Mass M**	**Normalized heat of reaction H**	**Total heat of reaction[a] Ht**	**Degree of Cure DC***
	mg	**J/g**	**J/g**	**%**
MST_11S_DC_01	26.65	0.89	100.0	99.1
MST_11S_DC_02	10.67	1.97		98.0
MST_11S_DC_03	13.48	1.35		98.7
MST_11S_DC_04	24.84	2.83		97.2
MST_11S_DC_05	27.33	2.29		97.7
Average				**98.1**
S_{n-1}				0.8
CV (%)				0.8

[a]Conservatively assumed value of 100 J/g to compute the degree of cure.
**Condition of acceptance is equivalent to DC≥ 95%*

Cross-sectional area – ASTM D7205/D792

Table 70. Tabulated results for measured cross-sectional area per ASTM D792 (Pultrall)

Specimen ID	Average Length L		Density ρ_s		Volume V		Measured Area* A		Weight/unit length	
	mm	in.	kg/m³	lb./ft³	mm³	in³	mm²	in²	Kg/m	lb./ft
PUL_11S_MXA_01	19.09	0.752	2084	130	21281	1.30	1114.90	1.728	2.323	1.561
PUL_11S_MXA_02	18.05	0.711	2090	130	19816	1.21	1098.02	1.702	2.295	1.542
PUL_11S_MXA_03	18.67	0.735	2069	129	20770	1.27	1112.54	1.724	2.302	1.547
PUL_11S_MXA_04	18.92	0.745	2085	130	20915	1.28	1105.52	1.714	2.305	1.549
PUL_11S_MXA_05	18.45	0.726	2081	130	20434	1.25	1107.62	1.717	2.305	1.549
Average			**2082**	**130**	**20643**	**1.26**	**1107.72**	**1.717**	**2.306**	**1.550**
S_{n-1}			8	0	554	0.03	6.59	0.010	0.011	0.007
CV (%)			0.4	0.4	2.7	2.7	0.6	0.6	0.5	0.5

Table 71. Tabulated results for measured cross-sectional area per ASTM D792 (MST)

Specimen ID	Average Length L		Density ρ_s		Volume V		Measured Area* A		Weight/unit length	
	mm	in.	kg/m³	lb./ft³	mm³	in³	mm²	in²	Kg/m	lb./ft
MST_11S_MXA_01	18.92	0.745	1991	124	21084	1.29	1114.19	1.727	2.218	1.491
MST_11S_MXA_02	18.52	0.729	2000	125	20726	1.26	1119.07	1.735	2.238	1.504
MST_11S_MXA_03	18.30	0.721	2013	126	20450	1.25	1117.17	1.732	2.249	1.511
MST_11S_MXA_04	18.77	0.739	2014	126	20965	1.28	1116.63	1.731	2.249	1.511
MST_11S_MXA_05	19.66	0.774	2000	125	22119	1.35	1125.32	1.744	2.251	1.512
Average			**2004**	**125**	**21069**	**1.29**	**1118.48**	**1.734**	**2.241**	**1.506**
S_{n-1}			10	1	635	0.04	4.21	0.007	0.014	0.009
CV (%)			0.5	0.5	3.0	3.0	0.4	0.4	0.6	0.6

**Condition of acceptance, Rebar [#11]: area range within 968 to 1097 mm² (1.500 to 1.700 in²)*

Tensile Properties – ASTM D7205

Table 72. Tabulated results for tensile test per ASTM D7205 (Pultrall)

Specimen ID	Tensile Force P_{max}		Nominal Area A_{nom}		Ultimate Strength F^{tu}_{nom}		Modulus of Elasticity* E_{nom}		Ultimate Strain* $\varepsilon_{u\text{-}nom}$	Coefficient of determination
	kN	kips	mm^2	in^2	MPa	r^2	GPa	Msi	%	
PUL_11S_TNS_01	1131.7	254.4			1124.5	163.1	59.1	8.57	1.90	1.0000
PUL_11S_TNS_02	1190.6	267.6			1182.9	171.6	59.9	8.69	1.97	1.0000
PUL_11S_TNS_03	1199.0	269.6			1191.4	172.8	60.3	8.74	1.98	1.0000
PUL_11S_TNS_04	1238.7	278.5			1230.7	178.5	60.0	8.71	2.05	1.0000
PUL_11S_TNS_05	1234.6	277.6	1006	1.56	1226.7	177.9	59.9	8.69	2.05	1.0000
PUL_11S_TNS_06	1186.4	266.7			1178.8	171.0	59.1	8.58	1.99	1.0000
PUL_11S_TNS_07	1240.4	278.8			1232.4	178.7	60.8	8.82	2.03	1.0000
PUL_11S_TNS_08	1215.6	273.3			1207.8	175.2	59.6	8.65	2.02	1.0000
PUL_11S_TNS_09	1247.8	280.5			1239.8	179.8	60.4	8.76	2.05	1.0000
Average	**1209.4**	**271.9**			**1201.7**	**174.3**	**59.9**	**8.69**	**2.01**	
S_{n-1}	37.1	8.3			36.8	5.3	0.6	0.08	0.05	
CV (%)	3.1	3.1			3.1	3.1	0.9	0.9	2.4	
P_G, Guaranteed Tensile Load[1]	**1098.2**	**246.9**								

**Condition of acceptance: P_G > 470 kN (108.8 kip) for #11 Type 0 bars; and E > 44.8 GPa (6.5 Msi).*

**Condition of acceptance: P_G > 712 kN (160.0 kip) for #11 Type III bars; and E > 58.6 GPa (8.5 Msi).*

1 Guaranteed is not derived from three different production lots as per specification, reported guaranteed values is based only on the results reported herein

Table 73. Tabulated results for tensile test per ASTM D7205 (MST)

Specimen ID	Tensile Force P_{max}		Nominal Area A_{nom}		Ultimate Strength F^{tu}_{nom}		Modulus of Elasticity* E_{nom}		Ultimate Strain* $\varepsilon_{u\text{-}nom}$	Coefficient of determination
	kN	kips	mm^2	in^2	MPa	ksi	GPa	Msi	%	r^2
MST_11S_TNS_01	944.06	212.2	1006	1.56	938.0	136.0	58.2	8.44	1.61	0.9999
MST_11S_TNS_02	945.48	212.6			939.4	136.3	57.2	8.30	1.64	1.0000
MST_11S_TNS_03	872.76	196.2			867.2	125.8	56.9	8.26	1.52	1.0000
MST_11S_TNS_04	865.74	194.6			860.2	124.8	58.3	8.46	1.47	1.0000
MST_11S_TNS_05	935.00	210.2			929.0	134.7	59.5	8.64	1.56	0.9995
MST_11S_TNS_06	932.96	209.7			927.0	134.4	57.1	8.28	1.62	0.9999
MST_11S_TNS_07	897.92	201.9			892.2	129.4	58.4	8.48	1.53	0.9999
MST_11S_TNS_08	948.58	213.2			942.5	136.7	57.6	8.36	1.64	1.0000
MST_11S_TNS_09	935.32	210.3			929.3	134.8	58.1	8.44	1.60	1.0000
MST_11S_TNS_10	962.22	216.3			956.1	138.7	56.7	8.22	1.69	1.0000
Average	**924.00**	**207.7**			**918.1**	**133.2**	**57.8**	**8.39**	**1.59**	
S_{n-1}	33.26	7.5			33.1	4.8	0.9	0.13	0.07	
CV (%)	3.6	3.6			3.6	3.6	1.5	1.5	4.1	
P_G, Guaranteed Tensile Load[1]	**824.21**	**185.3**								

**Condition of acceptance: P_G > 470 kN (108.8 kip) for #11 Type 0 bars; and E > 44.8 GPa (6.5 Msi).*

**Condition of acceptance: P_G > 712 kN (160.0 kip) for #11 Type III bars; and E > 58.6 GPa (8.5 Msi).*

[1] Guaranteed is not derived from three different production lots as per specification, reported guaranteed values is based only on the results reported herein

Transverse shear strength – ASTM D7617

Table 74. Tabulated results for transverse shear strength per ASTM D7617 (Pultrall)

Specimen ID		Peak Transverse Force, P_{max}		Nominal Area A_{nom}		Shear Strength τ_u	
		kN	lb.	mm^2	in^2	MPa	ksi
PUL_11S_TSS_01		326.63	73400			162.27	23.53
PUL_11S_TSS_02		325.74	73200			161.83	23.46
PUL_11S_TSS_03		331.53	74500	1006	1.560	164.70	23.88
PUL_11S_TSS_04		327.52	73600			162.71	23.59
PUL_11S_TSS_05		327.97	73700			162.93	23.62
	Average	**327.88**	**73680**			**162.89**	**23.62**
	S_{n-1}	2.21	497			1.10	0.16
	CV (%)	0.7	0.7			0.7	0.7

Table 75. Tabulated results for transverse shear strength per ASTM D7617 (MST)

Specimen ID		Peak Transverse Force, P_{max}		Nominal Area A_{nom}		Shear Strength τ_u	
		kN	lb.	mm^2	in^2	MPa	ksi
MST_11S_TSS_01		315.95	71000			156.96	22.76
MST_11S_TSS_02		369.35	83000			183.49	26.60
MST_11S_TSS_03		361.34	81200	1006	1.560	179.51	26.03
MST_11S_TSS_04		319.51	71800			158.73	23.01
MST_11S_TSS_05		366.24	82300			181.94	26.38
	Average	**346.48**	**77860**			**172.13**	**24.96**
	S_{n-1}	26.43	5939			13.13	1.90
	CV (%)	7.6	7.6			7.6	7.6

**Condition of acceptance: τ_u >151 MPa (22 ksi)*

Horizontal shear strength – ASTM 4475

Table 76. Tabulated results for Horizontal shear strength per ASTM D4475 (Pultrall)

Specimen ID	Peak Force, P_{max}		Nominal Diameter $ø_{nom}$		Horizontal Strength S	
	kN	lb.	mm	in	MPa	ksi
PUL_11S_HSS_01	58.40	13123			40.63	5.89
PUL_11S_HSS_02	58.05	13046			40.39	5.86
PUL_11S_HSS_03	58.21	13082	34.9	1.375	40.50	5.87
PUL_11S_HSS_04	58.23	13085			40.51	5.88
PUL_11S_HSS_05	58.59	13166			40.76	5.91
Average	**58.30**	**13100**			**40.56**	**5.88**
S_{n-1}	0.20	46			0.14	0.02
CV (%)	0.3	0.3			0.3	0.3

Table 77. Tabulated results for Horizontal shear strength per ASTM D4475 (MST)

Specimen ID	Peak Force, P_{max}		Nominal Diameter $ø_{nom}$		Horizontal Strength S	
	kN	lb.	mm	in	MPa	ksi
MST_11S_HSS_01	57.44	12908			39.96	5.80
MST_11S_HSS_02	58.21	13081			40.50	5.87
MST_11S_HSS_03	58.22	13083	34.9	1.375	40.51	5.88
MST_11S_HSS_04	54.79	12312			38.12	5.53
MST_11S_HSS_05	54.98	12354			38.25	5.55
Average	**56.73**	**12748**			**39.47**	**5.72**
S_{n-1}	1.71	385			1.19	0.17
CV (%)	3.0	3.0			3.0	3.0

**Condition of acceptance: S >38 MPa (5.5 ksi)*

Bond strength – ASTM 7913

Table 78. Tabulated results for bond tests per ASTM D7913 (Pultrall)

Specimen ID	Nominal Diameter d_b		Nominal Circumference C_b		Bonded length l		Nominal Bonded Area A_L		Peak Load F_u		Maximum Bond Strength* τ	
	mm	in.	mm	in.	mm	in.	mm^2	in^2	kN	kip	MPa	ksi
PUL-11S_BS_01									70.73	15.90	3.69	0.54
PUL-11S_BS_02									84.81	19.07	4.43	0.64
PUL-11S_BS_03	34.9	1.375	109.7	4.320	174.6	6.875	19160	29.7	118.85	26.72	6.20	0.90
PUL-11S_BS_04									107.12	24.08	5.59	0.81
PUL-11S_BS_05									89.80	20.19	4.69	0.68
Average									**94.26**	**21.19**	**4.92**	**0.71**
S_{n-1}									18.93	4.26	0.99	0.14
CV (%)									20.1	20.1	20.1	20.1

**Condition of acceptance is equivalent to average bond strength > 9.7 MPa (1.4 ksi) for Type III bars and bond strength > 7.6 MPa (1.1 ksi) for Type 0 and Type II bars.*

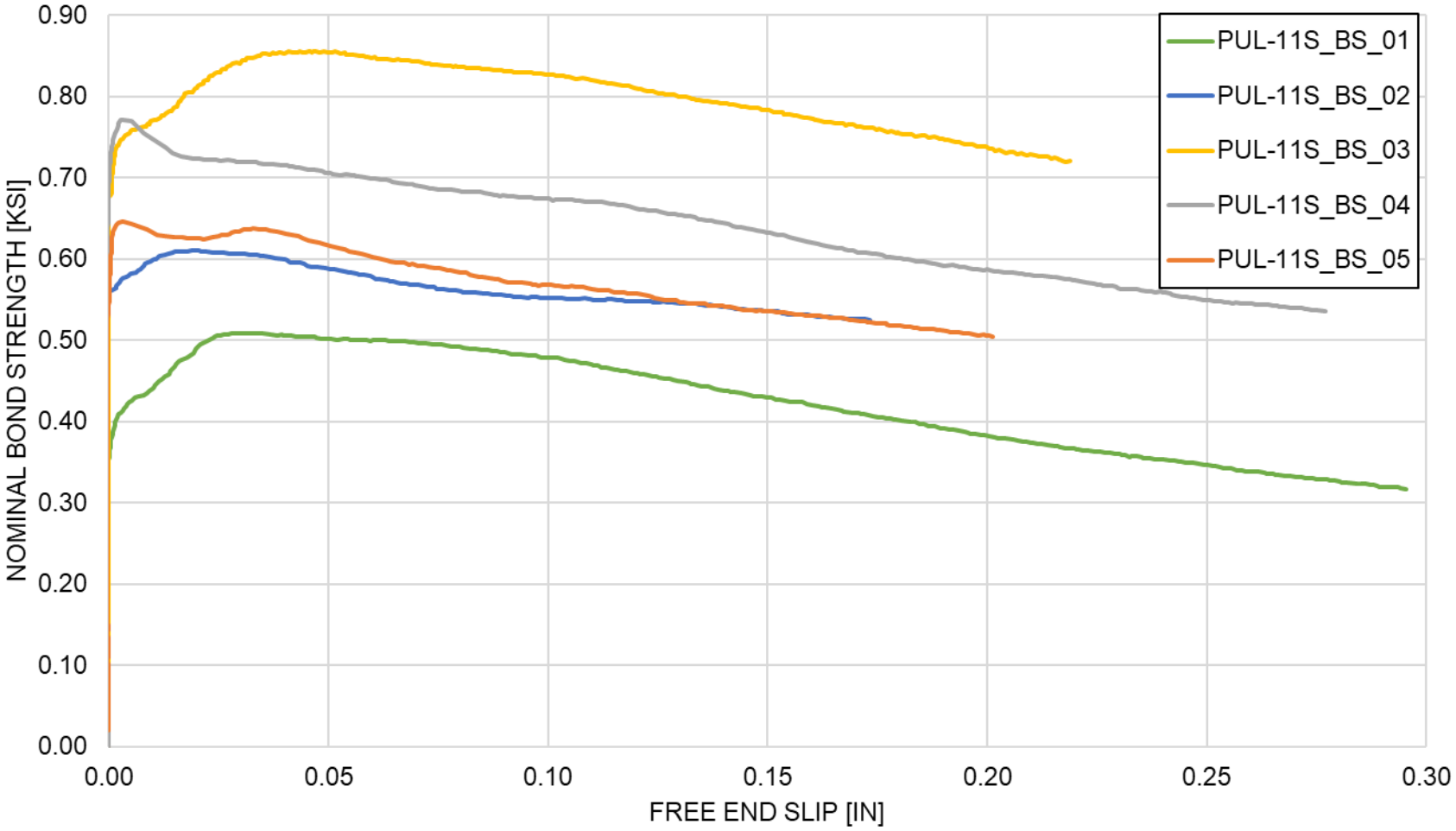

Figure 75. Nominal bond strength vs. free-end slip for Pultrall #11 bars

Table 79. Tabulated results for bond tests per ASTM D7913 (MST)

Specimen ID	Nominal Diameter d_b		Nominal Circumference C_b		Bonded length l		Nominal Bonded Area A_L		Peak Load F_u		Maximum Bond Strength* τ	
	mm	in.	mm	in.	mm	in.	mm^2	in^2	kN	kip	MPa	ksi
MST-11S_BS_01									140.82	31.66	7.35	1.07
MST-11S_BS_02									160.28	36.03	8.37	1.21
MST-11S_BS_03	34.9	1.375	109.7	4.320	174.6	6.875	19160	29.7	214.42	48.20	11.19	1.62
MST-11S_BS_04									207.19	46.58	10.81	1.57
MST-11S_BS_05									156.48	35.18	8.17	1.18
Average									**175.84**	**39.53**	**9.18**	**1.33**
S_{n-1}									32.84	7.38	1.71	0.25
CV (%)									18.7	18.7	18.7	18.7

**Condition of acceptance is equivalent to average bond strength > 9.7 MPa (1.4 ksi) for Type III bars and bond strength > 7.6 MPa (1.1 ksi) for Type 0 and Type II bars.*

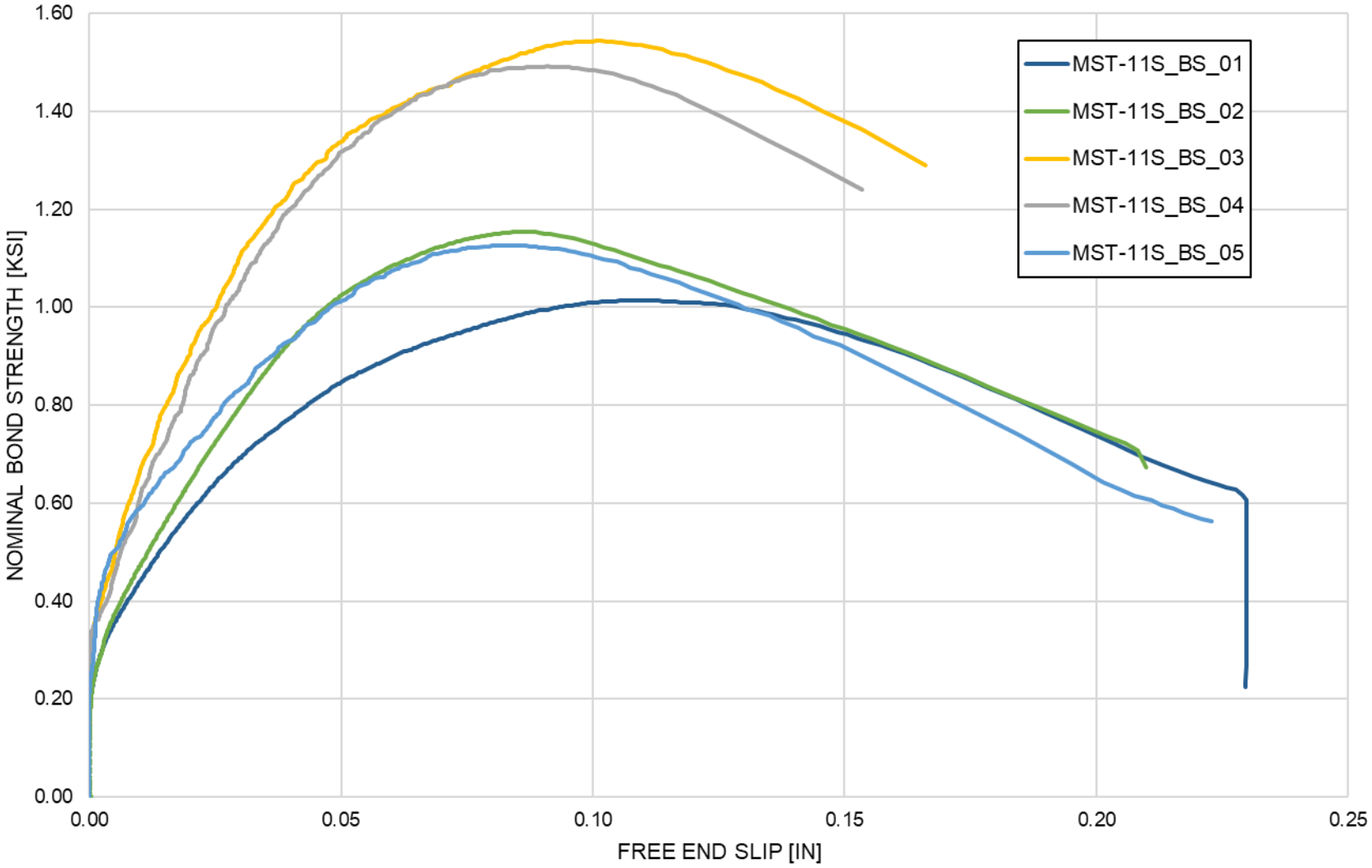

Figure 76. Nominal bond strength vs free-end slip for MST-Bar #11 bars

Moisture absorption – ASTM D570

Table 80. Tabulated results for water/moisture absorption per ASTM D570 (Pultrall)

Specimen ID	W_d g	W_{24} g	W_{24}^* %	W_s g	W_s^* %
PUL_11S_MA_01	27.894	27.934	0.14	28.023	0.46
PUL_11S_MA_02	28.814	28.855	0.14	28.950	0.47
PUL_11S_MA_03	28.948	28.990	0.14	29.089	0.49
PUL_11S_MA_04	31.342	31.383	0.13	31.480	0.44
PUL_11S_MA_05	30.808	30.849	0.13	30.979	0.55
Average			**0.14**		**0.48**
S_{n-1}			0.01		0.04
CV (%)			4.2		9.1

**Condition of acceptance for $W_{24} < 0.25\%$, and for $W_s < 1.00\%$*

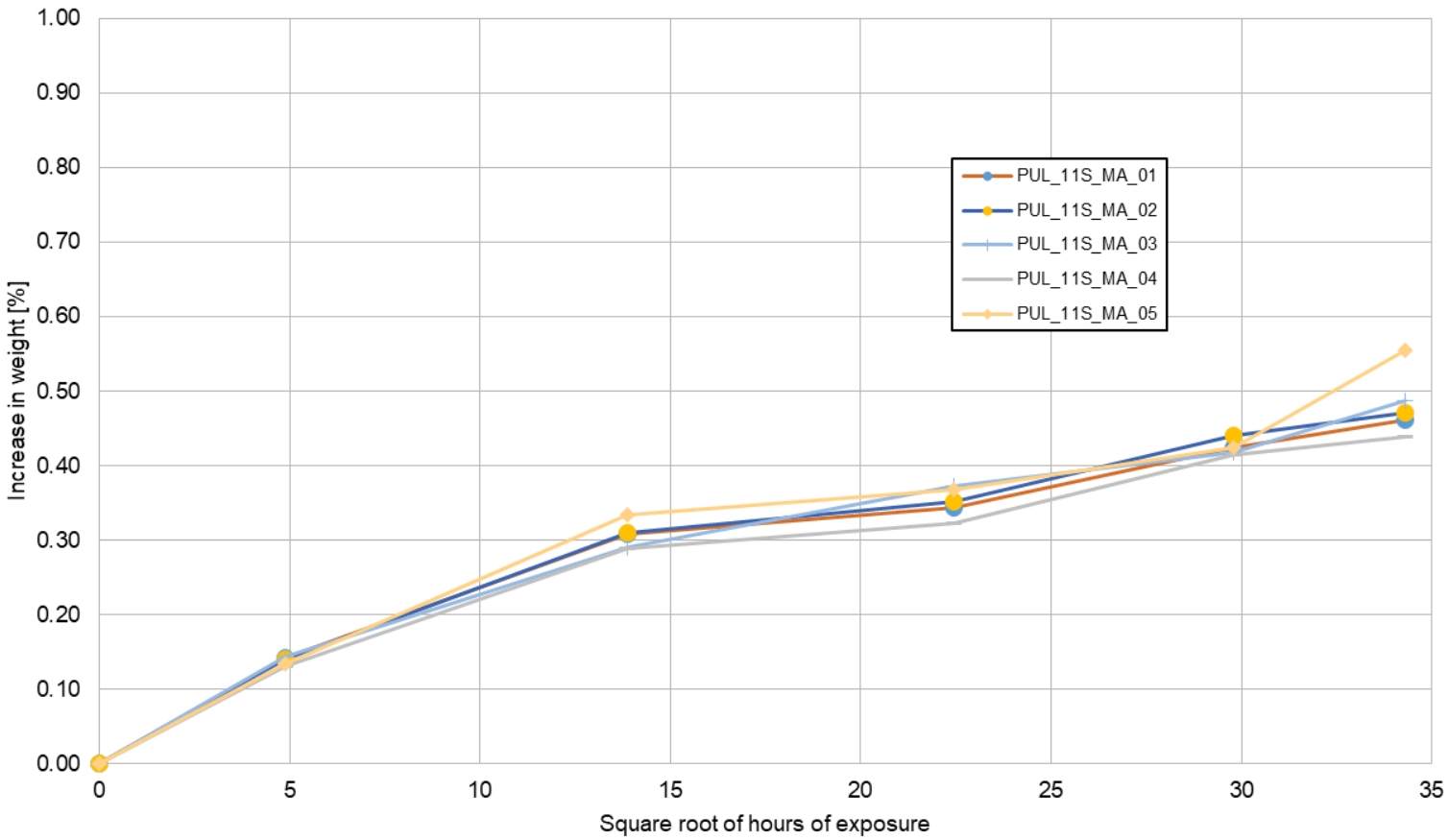

Figure 77. Square root of hours vs. increase in weight for Pultrall #11 bars

Table 81. Tabulated results for water/moisture absorption per ASTM D570 (MST)

Specimen ID	W_d g	W_{24} g	W_{24}^* %	W_s g	W_s^* %
MST_11S_MA_01	30.341	30.391	0.16	30.520	0.59
MST_11S_MA_02	28.886	28.940	0.19	29.090	0.71
MST_11S_MA_03	30.670	30.719	0.16	30.875	0.67
MST_11S_MA_04	29.763	29.811	0.16	29.962	0.67
MST_11S_MA_05	30.958	31.009	0.16	31.184	0.73
Average			**0.17**		**0.67**
S_{n-1}			0.01		0.05
CV (%)			6.9		7.8

**Condition of acceptance for $W_{24} < 0.25\%$, and for $W_s < 1.00\%$*

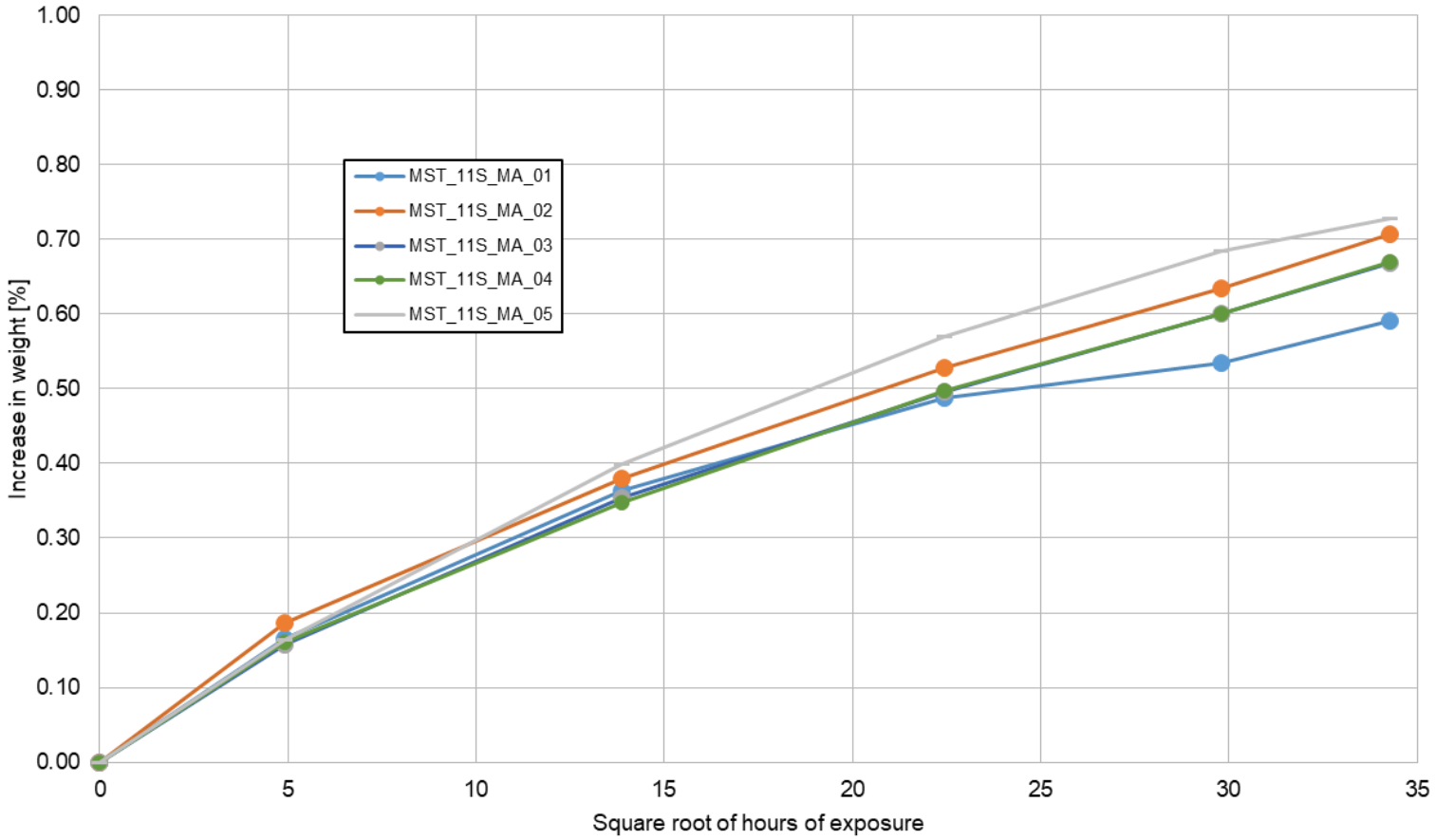

Figure 78. Square root of hours vs. increase in weight for MST #11 bars

Alkaline resistance (with no load) – ASTM D7705-A

Table 82. Tabulated results for tensile test per ASTM D7205 post Alkaline resistance per ASTM D7705, Procedure-A (Pultrall)

Specimen ID	Tensile Force P_{max}		Nominal Area A_{nom}		Ultimate Strength F^{tu}_{nom}		Modulus of Elasticity E_{nom}		Ultimate Strain $\varepsilon_{u\text{-}nom}$	Tensile Capacity Retention*
	kN	kips	mm^2	in^2	MPa	ksi	GPa	Msi	%	%
PUL_11S_TNS-AR_01	1096.60	246.5			1089.6	158.0	60.4	8.77	1.80	90.50
PUL_11S_TNS-AR_02	1072.40	241.1			1065.5	154.5	62.5	9.07	1.70	88.50
PUL_11S_TNS-AR_03	1092.42	245.6	1006	1.560	1085.4	157.4	63.8	9.25	1.70	90.15
PUL_11S_TNS-AR_04	1100.56	247.4			1093.5	158.6	61.7	8.95	1.77	90.82
PUL_11S_TNS-AR_05	1110.06	249.6			1102.9	160.0	62.5	9.07	1.76	91.61
Average	**1094.41**	**246.0**			**1087.4**	**157.7**	**62.2**	**9.02**	**1.75**	**90.31**
S_{n-1}	13.93	3.1			13.8	2.0	1.2	0.18	0.04	
CV (%)	1.3	1.3			1.3	1.3	2.0	2.0	2.5	

Table 83. Tabulated results for tensile test per ASTM D7205 post Alkaline resistance per ASTM D7705, Procedure-A (MST)

Specimen ID	Tensile Force P_{max}		Nominal Area A_{nom}		Ultimate Strength F^{tu}_{nom}		Modulus of Elasticity E_{nom}		Ultimate Strain $\varepsilon_{u\text{-}nom}$	Tensile Capacity Retention*
	kN	kips	mm^2	in^2	MPa	ksi	GPa	Msi	%	%
MST_11S_TNS-AR_01	808.32	181.7			803.1	116.5	56.6	8.21	1.42	87.48
MST_11S_TNS-AR_02	853.98	192.0			848.5	123.1	57.4	8.33	1.48	92.42
MST_11S_TNS-AR_03	812.70	182.7	1006	1.560	807.5	117.1	55.6	8.06	1.45	87.95
MST_11S_TNS-AR_04	807.30	181.5			802.1	116.3	57.3	8.31	1.40	87.37
MST_11S_TNS-AR_05	801.80	180.3			796.7	115.5	57.1	8.28	1.40	86.77
Average	**816.82**	**183.6**			**811.6**	**117.7**	**56.8**	**8.24**	**1.43**	**88.40**
S_{n-1}	21.13	4.8			21.0	3.0	0.7	0.11	0.04	
CV (%)	2.6	2.6			2.6	2.6	1.3	1.3	2.5	

**Condition of acceptance is a Tensile Capacity Retention ≥ 70% of average ultimate tensile force.*

Appendix B – Pile Cap Design of the Eastbound Bridge

The pile cap design of the Eastbound Bridge along with its detailing with GFRP reinforcement is presented in this appendix.

In this report, several solutions for the reinforcement layout of the selected pile cap of stack #24 were analyzed:

- **Steel-RC (1a)**: is the foundation of the original steel design;
- **GFRP-RC (1b)**: is the foundation with the same amount of reinforcement as the Steel-RC (1a) case but in GFRP instead of steel. This solution does not meet the SLE and detailing verifications of the AASHTO BDS GFRP 2nd edition [1];
- **GFRP-RC (2a)**: is the foundation with designed with MathCad software that satisfies AASHTO BDS GFRP 2nd edition [1] verifications;
- **GFRP-RC (2b)**: is the foundation, equal to GFRP-RC (2a) and designed Altair® software and based on ACI 440.11-22 provisions;
- **GFRP-RC (2c)**: is the foundation with designed analytically with Altair® software based on ACI 440.11-22 provisions and bottom reinforcement concrete cover equal to 12", instead of 4.5", which means to place the lower longitudinal and transverse reinforcement above the piles for ease of installation.

In all cases, the overall geometry and loads are unchanged from the original design. The most relevant steel (Steel-RC (1a) case) and GFRP (GFRP-RC (1b) and (2a)) reinforcement quantitative design parameters are listed in Table 84.

Table 84. Pile cap reinforcement of the selected pier n.24 of the Eastbound Bridge

FLEXURAL REINFORCEMENT					
		Steel-RC (1a) GFRP-RC (1b)	**GFRP-RC (2a)**	**GFRP-RC (2b-2c)**	
BOTTOM - Longitudinal Direction					
Bars	$\#_{bars}$	#11	#11	#11	[-]
Number of bars	n_{bars}	13	13	13	[-]
Spacing	s_{bars}	12	7	7	[in]
Total area	A_{tot}	20.28	20.28	20.28	[in^2]
BOTTOM - Transverse Direction					
Bars	$\#_{bars}$	#11	#11	#11	[-]
Number of bars	n_{bars}	22	24	24	[-]
Spacing	s_{bars}	12	7	7	[in]
Total area	A_{tot}	34.32	37.44	37.44	[in^2]
TOP - Longitudinal Direction					
Bars	$\#_{bars}$	#8	#8	#8	[-]
Number of bars	n_{bars}	14	22	22	[-]
Spacing	s_{bars}	12	7	7	[in]

FLEXURAL REINFORCEMENT					
		Steel-RC (1a) GFRP-RC (1b)	**GFRP-RC (2a)**	**GFRP-RC (2b-2c)**	
Total area	A_{tot}	11.06	17.38	17.38	[in^2]
TOP - Transverse Direction					
Bars	$\#_{bars}$	#8	#8	#8	[-]
Number of bars	n_{bars}	21	35	35	[-]
Spacing	s_{bars}	12	7	7	[in]
Total area	A_{tot}	16.59	27.65	27.65	[in^2]
FACE REINFORCEMENT					
		Steel-RC (1a) GFRP-RC (1b)	**GFRP-RC (2a)**	**GFRP-RC (2b)**	
Bars	$\#_{bars}$	#6	#8	N/A	[-]
Number of bars	n_{bars}	7	9		[-]
Spacing	s_{bars}	6.25	6"		[in]
Total area	A_{tot}	3.08	7.11		[in^2]
SHEAR REINFORCEMENT					
		Steel-RC (1a) GFRP-RC (1b)	**GFRP-RC (2a)**	**GFRP-RC (2b)**	
Longitudinal Direction					
Bars	$\#_{bars}$	-	#6	N/A	[-]
Number of bars	n_{bars}	-	2		[-]
Spacing	s_{bars}	-	24		[in]
Total area	A_{tot}	-	0.88		[in^2]
Transverse Direction					
Bars	$\#_{bars}$	-	#6	N/A	[-]
Number of bars	n_{bars}	-	3		[-]
Spacing	s_{bars}	-	12		[in]
Total area	A_{tot}	-	1.32		[in^2]

The bidirectional GFRP reinforcement arrangement of the 6-pile cap group “A” (pier 24) is shown in Figure 79 to Figure 82**.** Due to conservative design provisions [57] for non-prestressed transverse shear resistance in both AASHTO LRFD GFRP and ACI 440.11-22 (see Figure 83 and Figure 84), a limited number of shear stirrups are required to satisfy the ULS. Recent changes adopted in the Canadian Standards Association Bridge Code S6:2025 could provide a more efficient shear design approach. The position of the stirrups was selected to intercept potential shear cracks connecting pile to column.

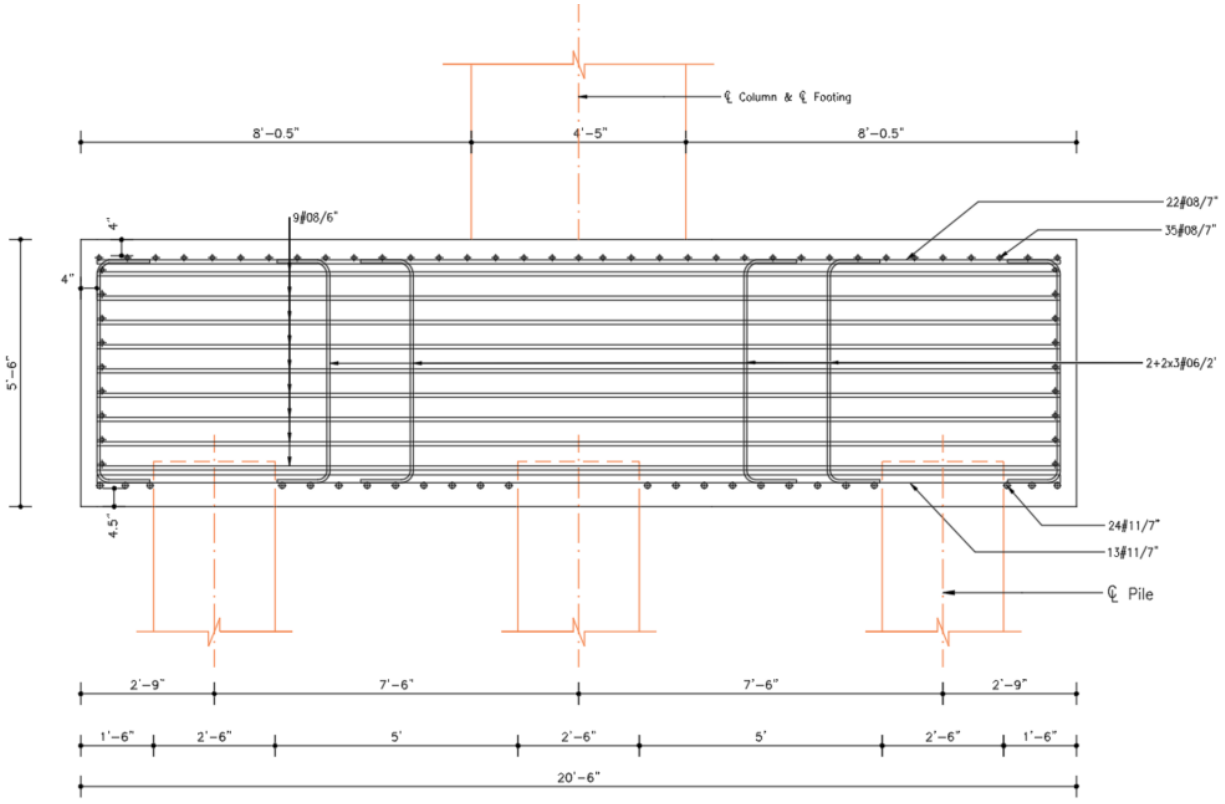

Figure 79. GFRP reinforcement layout (longitudinal view) – Pile cap 6-pile group "B" of the selected Pier n.24 of the Eastbound Bridge

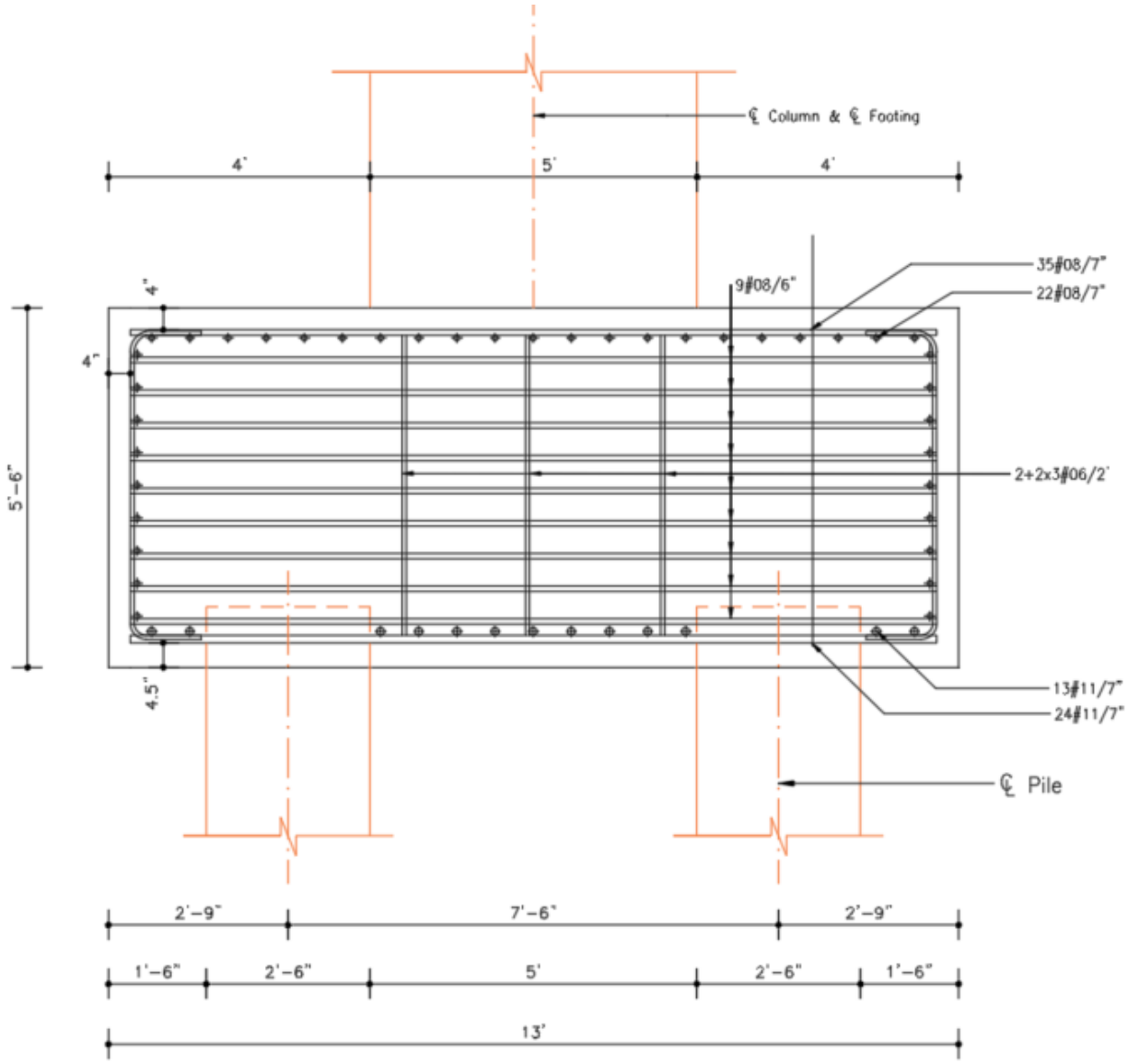

Figure 80. GFRP reinforcement layout (transversal view) – Pile cap 6-pile group "B" of the selected Pier n.24 of the Eastbound Bridge

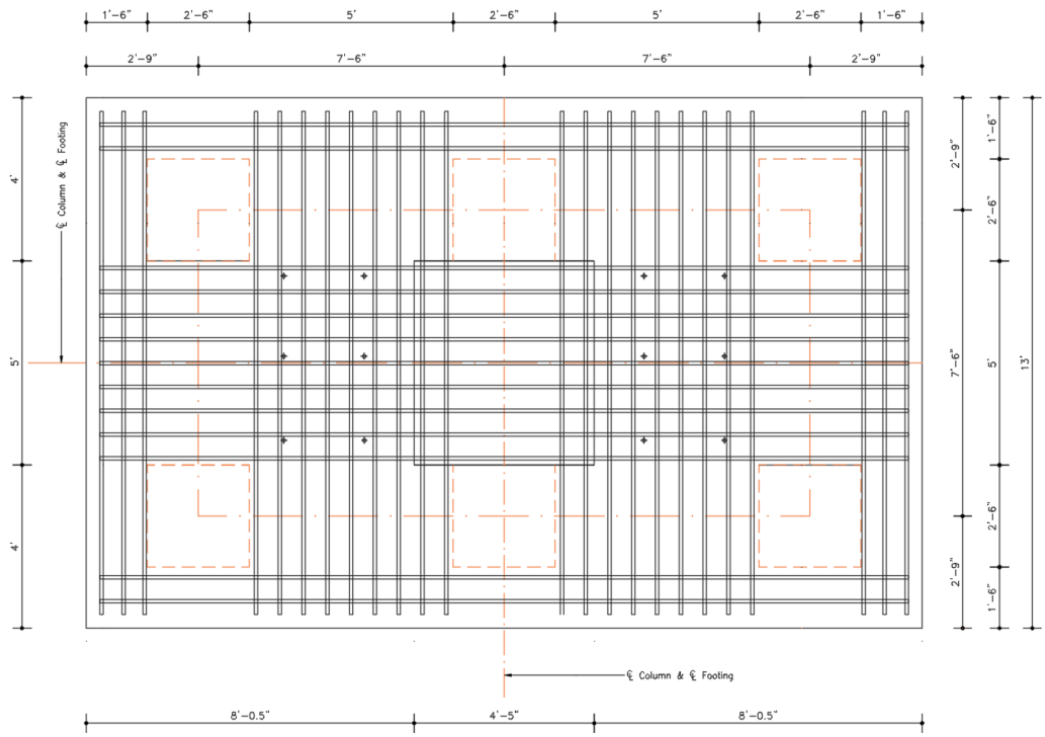

Figure 81. GFRP reinforcement layout (bottom reinforcement) – Pile cap 6-pile group "B" of the selected Pier n.24 of the Eastbound Bridge

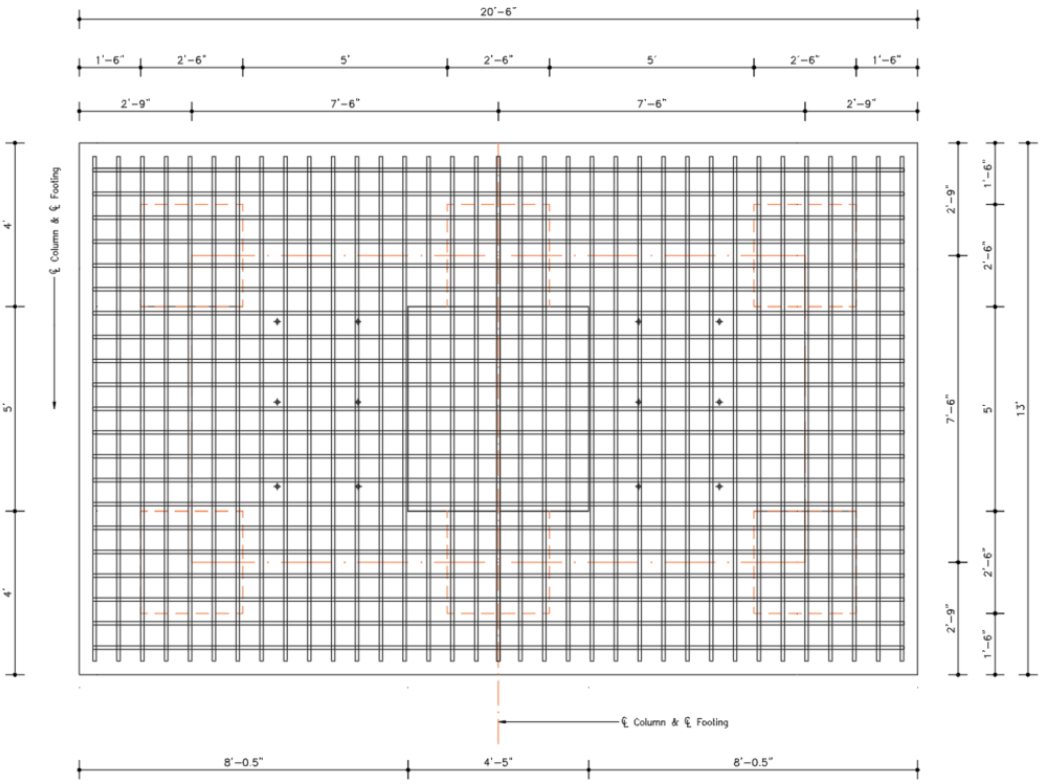

Figure 82. GFRP reinforcement layout (top reinforcement) – Pile cap 6-pile group "B" of the selected Pier n.24 of the Eastbound Bridge

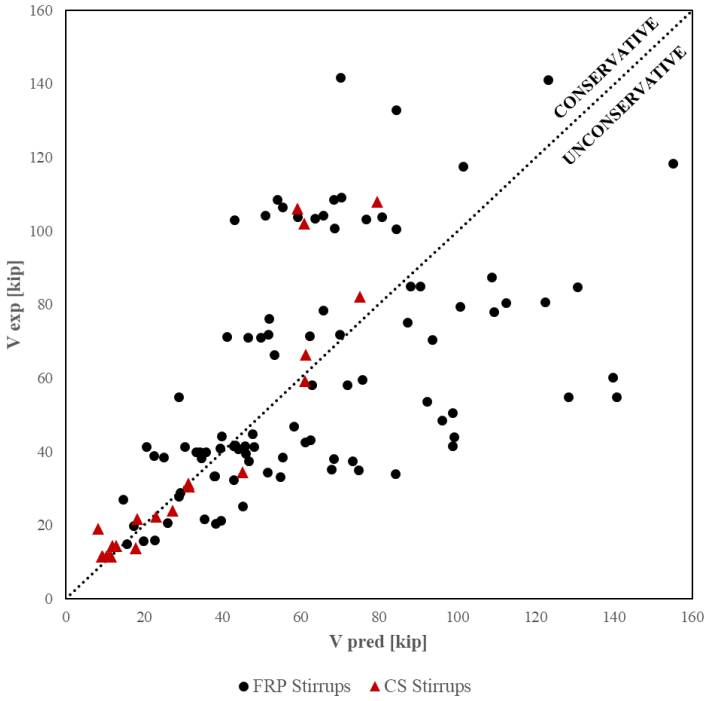

Figure 83. V_{exp}/V_{pred} computed according (ACI 440.4R-04, 2015) for specimen with transverse reinforcement [57]

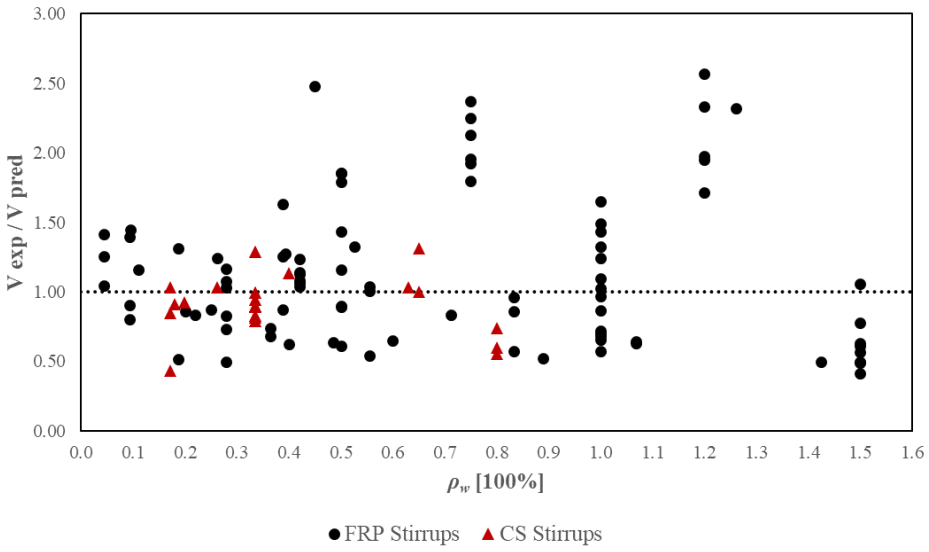

Figure 84. Shear reinforcement ratio vs V_{exp}/V_{pred} computed according (ACI 440.4R-04, 2015) [57]